SINGLE AND MULTIPLE ANTENNA COMMUNICATION SYSTEMS: PERFORMANCE ANALYSIS AND JOINT SOURCE-CHANNEL CODING

by

Firouz Behnamfar

A thesis submitted to the

Department of Electrical and Computer Engineering

in conformity with the requirements for

the degree of Doctor of Philosophy

Queen's University

Kingston, Ontario, Canada

September 2004

Abstract

Performance analysis plays a central role in the design of reliable communication systems. It helps to reduce the probability of error in the transmission of digital data or to improve the quality of the recovered signals when analog signals are communicated. In this dissertation, we first address the problem of performance analysis by presenting analytical methods to derive upper and lower bounds for the error rates of various systems. We then design a joint source-channel coding system for the transmission of analog sources over a multiple antenna communication link.

We begin by considering a single-antenna system with additive white Gaussian noise as well as block Rayleigh fading channels. It is shown that one can reduce the complexity of some of the existing methods and, at the same time, obtain tighter results, which is very favorable particularly when the complexity of the problem (i.e., the codebook size) is prohibitive. Closed-form formulas for the block pairwise error probabilities are derived everywhere.

We then consider a multi-antenna communication link with space-time orthogonal block coding and establish tight upper and lower bounds on the symbol and bit error rates of the system. The signaling scheme and the mapping between the signals and bits can be arbitrary.

We next consider the case where the input bit-stream has a non-uniform distribution, which allows the use of maximum *a posteriori* (MAP) decoding. We derive the MAP decoding rule, calculate a closed-form formula for the symbol pairwise error probability, and establish tight upper and lower bounds for the symbol and bit error rates. Another

contribution is to demonstrate that systems with MAP decoding, which is a form of joint source-channel coding, can outperform those with separate source and channel coding (i.e., tandem systems) at all error rates of interest.

Finally, we propose a joint source-channel coding system for the transmission of analog sources over multiple-antenna links. The proposed setup uses soft-decision decoding channel-optimized vector quantization (COVQ) to achieve a large portion of the soft-decoding gain with reduced complexity. Two COVQs with fixed encoders and adaptive decoders are also designed. The superiority of the proposed COVQ over tandem systems is also demonstrated.

Acknowledgments

I would like to express my sincere thanks to my supervisors, Professor Fady Alajaji and Professor Tamás Linder, for their support, continuous encouragement, and thoughtful suggestions and comments throughout the completion of this work. I am also grateful to my committee members Professor Steve Blostein, Professor Lorne Campbell, Professor Amir Khandani, and Professor Shahram Yousefi, for spending valuable time to read my thesis, attending my defense, and providing detailed and constructive comments. I am also thankful to Professor Martin Guay for chairing my defense session.

I would also like to gratefully acknowledge the financial support received from the Natural Sciences and Engineering Research Council (NSERC), the Ontario Premier's Research Excellence Award (PREA), the Department of Electrical and Computer Engineering, the Department of Mathematics and Statistics, and the School of Graduate Studies.

I am greatly indebted to my best friend and loving wife, Arezou, whose patience, understanding, and sacrifices enabled me to pursue my studies. I cannot thank her enough. I have been fortunate to have wonderful parents, brother, and sisters; I thank them all for their constant love and stimulation.

Contents

List of Figures

Chapter 1

Introduction

The next generation of wireless communication systems faces the demand for increased data rates, higher mobility, larger carrier frequencies, and more link reliability. Wireless channels are characterized by fading, multipath, limited bandwidth, and frequency and time selectivity which make system design a challenge. It is therefore crucial to have an understanding of the behavior of wireless channels in order to know their performance limits and to be able to design efficient communication systems for them. This dissertation considers the analysis of the performance of wireless systems with single or multiple antennas at the transmit and the receive sides. It addresses both of the cases where the transmitted data is or is not protected against channel noise (i.e., channel coded). An application of the analysis results is presented by designing a robust communication system for the transmission of analog data such as speech over a multiple antenna communication link.

This chapter begins with a short description of conventional communications systems. Two methods to improve the performance of the general system are then described. The

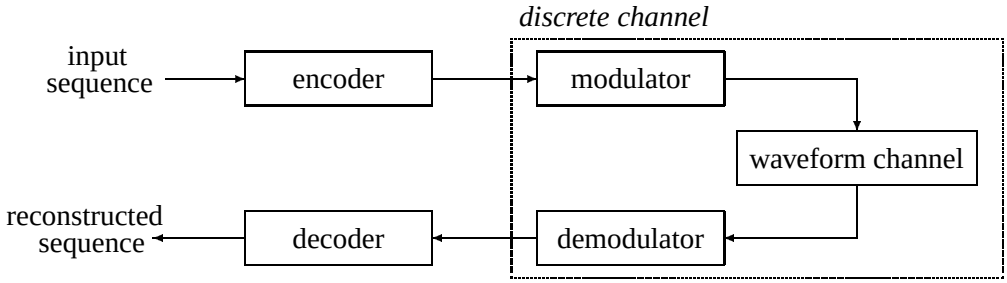

Figure 1.1: Block diagram of a digital communication system.

two problems considered in this thesis, i.e., performance analysis and system design, are next introduced. The chapter ends with a review of the related literature.

1.1 The Communication System Model

A typical communication system is depicted in Figure 1.1. We consider the transmission of discrete-time (discrete or continuous-amplitude) sequences over noisy waveform channels. The assumption that the input is discrete in time is justified by the sampling theorem which states that any band-limited signal can be represented by its samples without loss of information provided that it is sampled at a rate which is at least twice the signal bandwidth [143, 162]. In practice, the signals to be transmitted by a communication system are first low-pass filtered, and hence it is reasonable to consider band-limited signals.

The encoder and decoder are signal processing blocks. The encoder aims to represent the source in an efficient form (source encoding) and to protect the information against channel noise (channel encoding). The decoder exploits the error detection structure to cancel the effect of channel noise and reconstruct the input message.

The use of source coding is inevitable due to restrictions on channel bandwidth or storage space. Source encoding aims to remove the redundancy of the input and represent it with as low a bit rate and inaccuracy as possible. In effect, the source encoder maps the input sequence to a string of binary symbols. For analog sources, this mapping incorporates quantization, which causes partial loss of information. The encoder also inserts controlled redundancy to help error detection and correction at the receiver, which is known as channel coding. The modulator maps blocks of certain length from the encoder output to multidimensional waveforms, so that the data sequence can be transmitted over the analog channel. We assume that pulse shaping is also included in the modulator block. By pulse shaping, we mean using a modified waveform instead of the rectangular pulse, such as the raised cosine pulse, in order to reduce inter-symbol interference (ISI) at the receiver [150]. Amplitude attenuation and noise addition are the two main effects of the waveform channel. While both of these phenomena occur in channels with a frequency response not equal to unity, such as the Rayleigh fading channel, the sole effect of the additive white Gaussian noise (AWGN) channel is the addition of a constant power density noise to the waveform at the channel input. The demodulator estimates what waveform was transmitted over the analog channel. The output of the demodulator is a discrete-time stream which is passed through the decoder so that the errors caused by the channel are detected and corrected. The decoder also maps its input sequence to symbols that are in a subset of the original input alphabet to reconstruct the transmitted message. Note that the input and output of the concatenation of the modulator, the waveform channel, and the demodulator are discrete sequences and hence these three blocks may be regarded as a discrete (in terms of time and alphabet) channel as indicated in Figure 1.1.

1.2 The Source-Channel Separation Theorem

The design of the encoder-decoder pairs can be performed based on results from information theory. The results state that, for a given distortion D, there exists a rate $R(D)$ – called the rate-distortion function – below which the source cannot be compressed with a distortion less than D. In the positive direction, the rate $R(D)$ is asymptotically achievable at distortion level D by encoding large blocks of the source together. The results further state that, for every communication channel, there exists a quantity called channel capacity C, which is the maximum rate that information can be transmitted over the channel with arbitrarily small probability of error. The rate-distortion function depends on the source statistics. The capacity of a single-antenna waveform channel depends on the channel frequency response and noise distribution. For discrete channels, channel capacity depends on the channel crossover probabilities.

Let us assume that a source-channel code with transmission rate r source symbols/channel symbols is used at the encoder. From the lossy joint source-channel coding theorem [160, 161, 63, 31], it follows that as long as

$$R(D)r < C$$

holds, communication within distortion D is asymptotically possible.

Many communication systems are designed according to the following interpretation of the first two results: "communication with distortion D can be achieved by designing two *independent* codes: a source code with rate r_s and a channel code with rate r_c. The only constraint is that $R(D)r_c/r_s < C$; there is no performance penalty associated with the separate independent design." This result is called the source-channel separation principle. For

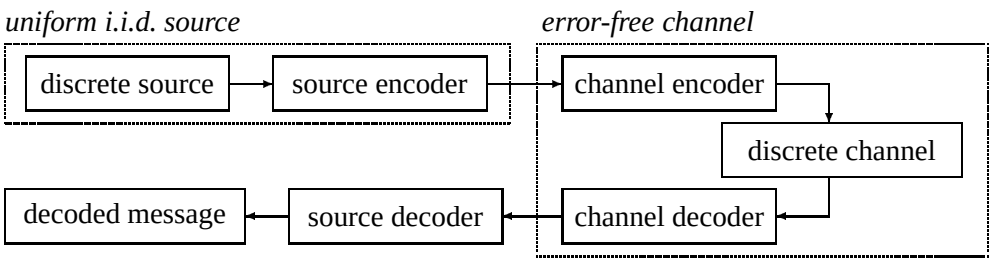

Figure 1.2: The idea of the source-channel separation principle for discrete sources.

discrete memoryless sources, if we require lossless bit error rate performance (this results in the Hamming distance distortion measure), then we replace $R(D)$ by source entropy $H(X)$ to require $H(X)r_c/r_s < C$. This result has given rise to the communication system model of Figure 1.2. According to this model, channel coding will correct all channel errors, no matter what the source statistics are, and hence the source encoder/decoder pair should be designed as if the channel was error-free, no matter what the channel conditions are.

1.3 Performance Enhancement

In this section, we describe two methods which lead to performance gains over the communication system of Figure 1.2. The first scheme reconsiders the separation of the source and channel codes and the second method changes the physical setup by deploying multiple antennas at the transmit and receive sides to obtain performance gains.

1.3.1 Improvement via Joint Source-Channel Coding

The source-channel separation principle simplified the theory and technology by dividing a difficult problem into two less challenging problems which may be solved independently. In agreement with the literature, we use the term "tandem systems" for systems designed based on this principle. There are numerous successful theoretical results and practical systems available today which are based on tandem systems. In fact, the performance of some tandem systems is becoming very close to the theoretical limits for simple channels, such as single-user Gaussian noise linear channels [29, 151]. However, there are a number of facts about the separation approach which merit attention. The first point is that in order for this result to hold, the source and channel code lengths need to grow without bound. As a result, communication systems built from independently designed source and channel codes may require greater computational resources and cause more delay than jointly designed systems. Separation-based codes may be far from the optimal design for systems with critical constraints on delay and complexity, such as wireless communication systems. Joint source-channel coding was shown in [123] to outperform tandem coding for systems having delay or complexity below a certain threshold. It was further proved in [216] that given a probability of block error, optimal joint source-channel coding may require half of the encoding/decoding delay of optimal tandem coding.

Secondly, the separation principle ignores the imperfections in real systems. In particular, source codes are designed assuming that the channel codes will correct all errors introduced by the channel. Knowing that this is not always the case even for the most powerful channel codes, one is not informed by this theorem how to modify the source codes

to deal with noisy channels. Similarly, channel codes are usually designed assuming that all bits created by the source code are of equal importance [31]. This assumption, which results from the assumption of a perfect source code, leads to the design of channel codes that protect all bits equally. In a large number of applications the source output bit-stream is the binary expansion of some decimal numbers or it is related to more "sensitive" parts of the data (as in the case where transform coefficients are encoded) and hence allocating more protection to the more significant bits than the less significant bits is a better way to use the bit rate. Indeed, equal error protection causes performance degradation in such conditions.

The third point is that there are channels for which the separation principle does not hold. An example of such channels is the multiuser channel whose capacity depends on the length of the source code [31]. Clearly, joint design of the source and channel codes is a more viable way to design codes for such systems.

Several methods have been proposed for joint source-channel coding. They are briefly described and reviewed in Subsection 1.5.2.

1.3.2 Improvement via Diversity in Space and Time

Diversity provides the receiver with several replicas of the transmitted signal. Therefore, it is a powerful technique to mitigate fading and interference from other users, thereby improving link reliability. Depending on the domain where diversity is created, diversity techniques may be divided into three main categories; i.e., temporal, frequency, and spatial. The first two techniques normally introduce redundancy in the time and/or frequency

domain, causing loss in transmission efficiency. Spatial diversity techniques employ multiple antennas for transmission and/or reception without necessarily sacrificing bandwidth or power. Therefore, it is natural to consider channels with multiple input (transmit) and multiple output (receive) antennas, often referred to as MIMO channels, to obtain improved reliability and/or increased data rates wherever possible.

Higher data rates and more reliable communication over MIMO channels are promised by information theoretic results. For the coherent case; i.e., when the receiver knows the channel fading coefficients perfectly, and for independent Rayleigh fading, channel capacity at a high channel signal-to-noise ratio (CSNR) is approximately equal to [196]

$$C \approx \min(K, L) \log \gamma_s \qquad \text{bits/sec/Hz},$$

where K and L are the numbers of transmit and receive antennas and γ_s is the CSNR. For the non-coherent case, which is the scenario that the channel is not known at the transmitter or the receiver, channel capacity at high CSNR approximately equals [215]

$$C \approx K^* \left(1 - \frac{K^*}{T_c}\right) \log \gamma_s \qquad \text{bits/sec/Hz},$$

where $K^* = \min(K, L, T_c/2)$ and T_c is the coherence time of the channel, that is the number of symbol intervals over which the channel is static.

Both of the above results are very significant, because they show that the capacity increases *linearly* in the minimum of the number of receive and transmit antennas (provided that T_c is large enough for the non-coherent case) and therefore it can be much larger than the single-antenna case. To increase channel capacity in the single-antenna scenario, one has two options: increasing the bandwidth, for which the capacity is asymptotically upper bounded by a constant, or increasing the transmit power which leads to a logarithmic

growth in capacity. Linear increase in channel capacity is therefore very attractive for wireless applications.

For the coherent case, channel capacity is plotted in Figure 1.3 for three cases; namely, for a system with a single transmit antenna but multiple receive antennas, a system with a single receive element but multiple transmit antennas, and a system with the same number of transmit and receive antennas. It is observed that the gain of having multiple antennas at both sides is much larger than having a number of antennas at only one side. If one is constrained to have a single antenna at one side of the channel, then receive diversity is more promising. Transmit diversity is the choice when the mobile has limited processing resources.

One signal processing approach to exploit the larger capacity of MIMO channels is spatial multiplexing. In this approach, which is typically known as the BLAST architecture [56], the input bit-stream is de-multiplexed to a number of branches where conventional channel coding may be employed. The information at each branch is then transmitted in a certain order over the transmit antennas. At the receiver side, the signals are estimated in a step-by-step fashion according to the CSNR of the received signals. Another approach which combines coding and modulation is known as space-time coding. Space-time codes introduce temporal and spatial correlation into the signals transmitted from different antennas without increasing the total transmit power and often without extra bandwidth. There is a diversity gain that results from multiple paths between the transmit and the receive terminals, and a coding gain that results from the correlation among the symbols across the transmit antennas[1].

[1]In this work, we are interested in point-to-point communications. Therefore, cooperative diversity [158, 103, 114], in which the mobiles relay each other's messages to obtain diversity gains, is not considered.

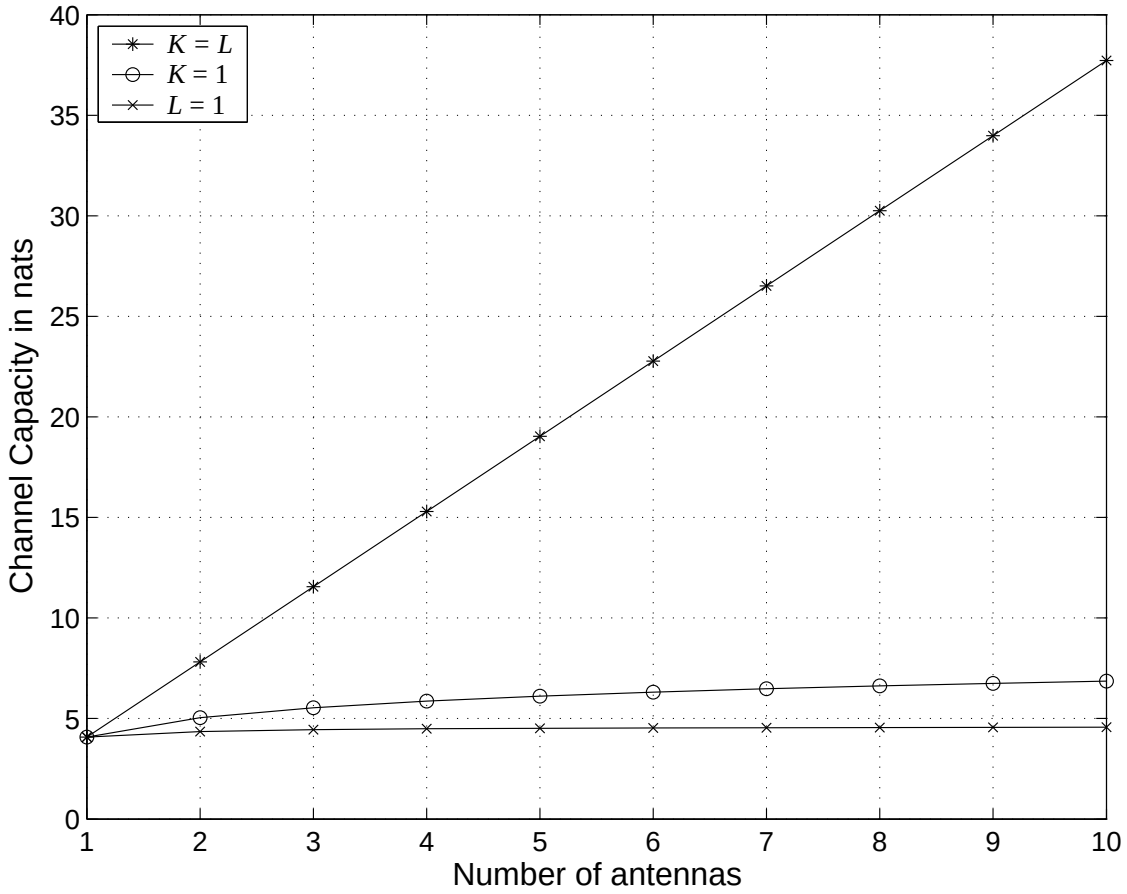

Figure 1.3: Improvement of channel capacity when multiple antennas are used. The CSNR is 20 dB.

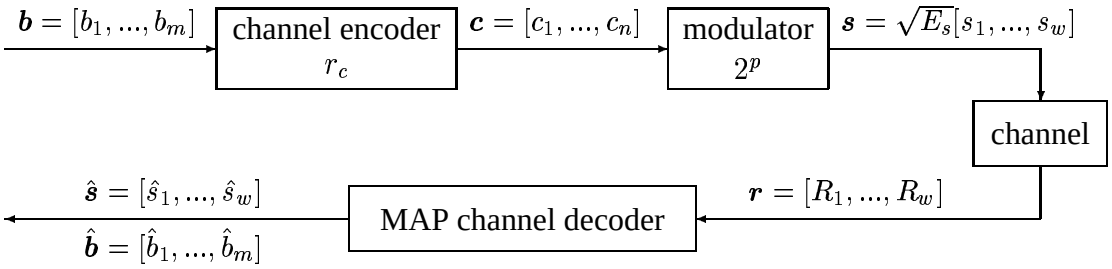

Figure 1.4: Block diagram of a communication system with MAP sequence estimation.

1.4 Summary of the Thesis

1.4.1 Problem Statement

Error Analysis of Communication Systems

Let us consider the communication system in Figure 1.4, which encodes a group of data bits $\boldsymbol{b} = [b_1, ..., b_m]$ at a time and maps them to a sequence of baseband signals. The above mapping may include any kind of channel coding with rate r_c, such as linear block codes, for which the coded bits are denoted by $\boldsymbol{c} = [c_1, ..., c_n]$ with $n = m/r_c$, or trellis coded modulation. Each of the signal sequences will be called a "frame" and denoted by $\boldsymbol{s}_i = [s_1^i, ..., s_w^i], i = 1, \cdots, M$, where $M = 2^m$, $w = m/(r_c p)$ is the frame length in symbols, and 2^p is the constellation size to which s_t^i belongs. We assume that s_t^i is selected from a unit-energy constellation and weighted later at the modulator. When s_t^i is transmitted and for a transmit power of $E_s = r_c p E_b$, where E_b is the power per an uncoded (information) bit, the input-output relationship of the channel is represented by

$$R_t = \sqrt{E_s} H s_t^i + N_t,$$

where R_t and N_t are the channel output and additive noise, respectively, and H is the channel gain. We assume that N_t, H, and s_t^i are independent. The additive noise is assumed to be complex Gaussian with independent and identically distributed (i.i.d.) real and imaginary parts, each having distribution $\mathcal{N}(0, N_0/2)$. We denote such a distribution by $\mathcal{CN}(0, N_0)$. We herein consider three cases: $H = 1 = const.$, which indicates the AWGN channel, H being i.i.d. $\mathcal{CN}(0, 1)$ among frames, which is the block Rayleigh fading model, and H following an i.i.d. chi square distribution, which models the block Rayleigh fading channel with diversity reception and also the space-time orthogonal block coded channels (see Chapter 3). In the fading cases, we assume coherent detection, which is the case where the receiver can accurately estimate the channel gain H.

We are interested in finding upper and lower bounds on the error rates of the above system. More precisely, we want to derive upper and lower bounds on the frame error rate, which is the probability that a frame is detected in error; i.e.,

$$\text{FER} = \Pr\left(\hat{\boldsymbol{s}} \neq \boldsymbol{s}\right),$$

where $\boldsymbol{s}$ and $\hat{\boldsymbol{s}}$ are the transmitted and decoded frames, respectively, as well as the probability that a bit is detected wrongly, which is given by

$$\text{BER} = \frac{1}{m} \sum_{u=1}^{M} p(\boldsymbol{s}_u) \sum_{j \neq u} D_H(u, j) P(\hat{\boldsymbol{s}} = \boldsymbol{s}_j | \boldsymbol{s} = \boldsymbol{s}_u),$$

where $D_H(u, j)$ is the number of bit differences between the data bits corresponding to $\boldsymbol{s}_u$ and $\boldsymbol{s}_j$ and $P(\hat{\boldsymbol{s}} = \boldsymbol{s}_j | \boldsymbol{s} = \boldsymbol{s}_u)$ is the conditional probability that $\hat{\boldsymbol{s}} = \boldsymbol{s}_j$ is detected given that $\boldsymbol{s} = \boldsymbol{s}_u$ is transmitted.

We are interested in both uniform and non-uniform i.i.d. binary input sequences. Therefore, we consider maximum *a posteriori* (MAP) decoding.

Quantization for MIMO Wireless Channels

Unlike the previous system in which the input is a bit-stream, in many applications the problem at hand is to transmit an analog source, such as the speech or image signals, over a digital communication system. In such cases, it is required to quantize the source; i.e., to approximate it with a source which has a finite alphabet.

The performance of a quantizer is expressed by its signal-to-distortion ratio (SDR). Therefore, when an analog source is transmitted, it is reasonable to choose to minimize the end-to-end distortion of the system as the design goal, as opposed to approaches which opt to minimize the system bit, symbol, codeword, or frame error rate. We measure the inaccuracy by a distortion measure, such as the squared error between the original and the decoded sequences.

Let $\boldsymbol{x}$ and $\hat{\boldsymbol{x}}$ be, respectively, the original and reconstructed source vectors, i.e., the system input and output. We are interested in this case to transmit analog sources over communication links with multiple transmit and possibly multiple receive antennas. Our objective is to minimize the mean-square error; namely, we want to minimize

$$D = E\left\{\|\boldsymbol{x} - \hat{\boldsymbol{x}}\|^2\right\}$$

subject to constraints on the average transmit power and channel bandwidth. The bandwidth constraint can simply be met by fixing the quantization rate and dimension, the modulation scheme, and the constellation size as described in [150, 200].

1.4.2 Thesis Organization and Contributions

This dissertation is divided into eight chapters. Relevant upper and lower bounds on the probability of a union of a finite number of events are reviewed in Chapter 2. We present these bounds in their general form and employ them throughtout this thesis to establish upper and lower bounds on the error rates of various communication systems. In Chapter 3, we briefly review the space-time orthogonal block codes. These codes are frequently used in the following chapters of the thesis. The maximum likelihood (ML) decoding rule and the symbol pairwise error probability of space-time orthogonal block codes are also reviewed. As a contribution, an alternate derivation of the codeword pairwise error probability of general space-time codes is presented.

In Chapter 4, we derive upper and lower bounds on the error rates of channel coded single input-single ouput (SISO) AWGN as well as block Rayleigh fading channels with arbitrary signaling schemes and under ML decoding. In this chapter, we show how to use the Hunter and Kounias upper and lower bounds, which are Bonferroni-type bounds, to bound the error rates of such systems and also improve an already existing lower bound, known as the KAT bound. We also devise a way to make the computation of the above bounds feasible when the codebook size is large. Furthermore, we find a closed-form expression for the probability of the intersection of two pairwise error events under Rayleigh fading.

MIMO systems which use space-time orthogonal block codes and ML decoding are considered in Chapter 5. As such MIMO channels are equivalent to a number of parallel SISO channels with chi square fading, a similar approach to that in Chapter 4 is used to

derive tight upper and lower bounds on the symbol and bit error rates of the system. A closed-form expression for the probability of the intersection of two pairwise error events is also derived.

We consider the error rates for orthogonal space-time coded channels under MAP decoding in Chapter 6. We derive the MAP decoding rule and show that, similar to ML decoding, symbol detection is decoupled in this case. The main contribution of this chapter is that we derive a closed-form expression for the symbol pairwise error probability. Signal mapping and comparison with tandem systems, which perform source and channel coding independently, are also presented.

In Chapter 7, we design a communication system for the transmission of analog sources over MIMO channels. The contribution is to show how to use space-time soft-decoding and soft-decision decoding channel-optimized vector quantization (COVQ) to achieve performance gains over tandem systems comprising vector quantization, channel coding, and space-time coding and also over systems which employ COVQ with hard decoding. Two COVQs which do not assume the knowledge of the CSNR at the transmitter are also designed.

Chapter 8 presents a summary of the thesis.

1.5 Literature Review

In what follows, we mention the major work on the subject of this thesis; namely, performance analysis, joint source-channel coding, and space-time codes. For an overview on

the fundamental problems in information theory, one can refer to Shannon's original papers [160, 161], further descriptions on rate distortion theory in [163], and Gallager's tutorial on Shannon's contributions in [64].

1.5.1 Error Analysis of Channel Coded SISO Systems

The most common estimate of the error rate of a communication system is the union bound which only depends on the pairwise error probabilities (see, e.g., [150]). The union bound, which presents an upper bound to the codeword error rate, is loose particularly at low CSNR values. Shannon presented a lower bound to the codeword error rate of systems with AWGN channel and M-ary modulation in [164] using a sphere packing approach. Shannon's lower bound is tight at low CSNR, but it becomes loose as the CSNR grows. An upper bound to the codeword error rate of BPSK-modulated AWGN channels was derived in [149], extended to PSK-modulated channels in [84], and tightened for some long binary block codes in [211]. A lower bound to de Caen's lower bound on the probability of a union [39] was derived in [156] and applied to BPSK-modulated AWGN channels with linear block codes. Although the lower bound in [156] is poor even at moderately low error rates, it is significant because it is asymptotically tight and converges to the union upper bound at high CSNR [156] and it only depends on the weight enumeration of the code. The lower bound in [39] was improved in [109], where the KAT bound was introduced by solving the same optimization problem as in [39], but using stronger analysis. Since the lower bounds in [39, 109] are stronger than the bound in [156], they also converge to the union upper bound as the CSNR grows to infinity when applied to the same communication system as

in [156]. The lower bounds in [39, 156, 109] are all in terms of sums of ratios. Another improvement of the bound in [39] is given in [30], where the lower bound is expressed in terms of a weighted sum of ratios and tightened via careful selection of the weights (as well as exhaustive search). These methods are described in detail in Chapter 2.

1.5.2 Joint Source-Channel Coding Methods

We categorize joint source-channel coding approaches as unequal error protection, channel-optimized vector quantization, optimization of index assignment, and exploitation of the (residual) redundancy at the source encoder output via MAP decoding. COVQ and MAP decoding are reviewed here with more emphasis since these two methods are used in the following chapters.

Unequal error protection (UEP) trades off source resolution and channel error protection to allocate the available bit rate. The rate of the channel code depends on the channel conditions, such as the bit error rate. As the channel becomes more noisy, the number of bits used for channel coding increases. The aim in UEP is to find the optimal balance between the source and channel code rates. Most UEP systems are implemented using rate-compatible punctured convolutional (RCPC) codes for error protection [76], often with a measure of parity checking, such as cyclic redundancy check (CRC) [205], for detection of errors in the channel-decoded sequence. Good examples of UEP systems include the work in [187] – where entropy-coded subband coding together with packetization and RCPC channel coding were used for image transmission over memoryless noisy channels – and the work in [165] which follows [187], but instead of ad hoc source coding, it uses

the strong image coder SPIHT introduced in [152]. A different approach to UEP can be found in [4], where larger energy levels and smaller signaling schemes were assigned to the more sensitive transform coefficients in image transform coding using the discrete cosine transform (DCT). A major source of complexity in UEP methods is the allocation of the available bit rate between the source and channel codes. An adaptive source and channel coding rate allocation scheme for finite state channels, including the Gilbert channel model [68, 48], was examined in [94]. In [142], the logarithm of the channel code block error rate was assumed to have a linear relation with the channel code rate. Rate allocation was next done using iterative optimization.

Channel optimized scalar/vector quantization is another alternative to joint source-channel coding. In this approach, channel conditions in the form of COVQ index crossover probabilities are incorporated in quantizer design. As a result, the source is compressed depending on the channel conditions. The optimality conditions of a general digital communication system with noisy channels and real-valued input and output were studied in [54]. Later, the necessary conditions for optimality of scalar quantization for binary symmetric channels given a fixed index assignment were derived in [113]. In [50], it was shown that the algorithm in [113] need not converge and a realizability constraint on the codewords was imposed to guarantee convergence. The generalized Lloyd algorithm (GLA) [66] for joint source-channel coding over noisy channels was studied in [14] for trellis and predictive coding and it was shown that the considered schemes outperformed tandem systems. The approaches toward vector quantization for noisy channels began with the work in [43] where the optimality conditions of the encoder were found. Finally, in [111], COVQ optimality conditions were formulated. Among the various algorithms that are proposed for

COVQ design, we cite the modified GLA initialized by simulated annealing [49], noisy channel relaxation [60, 61], stochastic relaxation [214], deterministic annealing [136], and COVQ design using fuzzy logic [92]. Theoretical studies on vector quantization were done in [125, 126, 213]. For example, it was shown in [126] that, as expected, the distortion of a quantizer approaches to what is predicted by the rate distortion function as the quantizer dimension increases. In [125], the rate of convergence of a quantizer in the presence of channel noise was studied. In [147], COVQ design for the Polya channel with finite memory [5] was addressed and it was shown that significant gains can be achieved through exploiting the memory of the channel (instead of interleaving). The work in [25] used subband coding, all-pass filtering, and COSQ for subband image transmission over memoryless noisy channels. This method is similar in spirit to the approach in [20, 21, 22], where channel memory is exploited and discrete wavelet transform (DWT)-based subband coding, which is substantially less complex due to reduced filter lengths, is used. Soft decoding COVQ was introduced in [200, 179] and applied to image coding in [177]. Soft-decoding COVQ is computationally demanding due to the need for matrix inversion and evaluation of trigonometric functions. In an effort to reduce the computational complexity of the decoder, COVQ with soft-decision decoder was developed in [6] for non-coherent Rayleigh fading channels and used in [146] for channels with additive Gaussian noise with inter-symbol interference.

Another approach to joint source-channel coding assigns indices to the quantizer codevectors according to channel conditions. The source is coded for a noiseless channel and no explicit channel coding is applied. Then, taking the channel crossover probabilities into account, indices are assigned to source (scalar or vector) samples such that the end-to-end

distortion is minimized. The index assignment approach to joint source-channel coding was studied in [212], where closer codevectors in the Euclidean distance sense were assigned to closer indices in the Hamming distance sense in an iterative manner. The simulated annealing algorithm was applied in [49] to find the best assignment of indices via perturbing the index assignment and accepting the labeling which could increase distortion according to a probabilistic measure. In [106], the codevectors were written as a linear summation of the index bits and the Hadamard transform was used to find the best index assignment.

The fourth method of joint source-channel coding considers source *a priori* probabilities in channel decoding. Ideally, a source coder would compress any discrete-alphabet sequence into an i.i.d. bit-stream having a rate equal to the source entropy rate [31]. Nevertheless, no source encoder is ideal. The output of the source encoder would then contain redundancy in the form of memory and/or non-uniform distribution. A MAP detector may exploit this residual redundancy to gain performance improvements over ML detection. MAP decoding was first used in [154] for scalar quantization. This work was later extended to the vector case in [148]. In [145], the characteristics of the arithmetic source coder and the source were modeled by a Markov source of order one and MAP decoding was employed using the model statistics. A similar approach was taken in [52], where MELP-compressed speech was modeled as a first-degree Markov chain. Sequence MAP decoding for various trellis coding systems and channel conditions, including the Rayleigh fading channel, was studied in [13, 75]. MAP decoding was used for channels with memory in [7, 178] and, later, in [182], where the Gilbert channel model was used. Robust speech transmission via MAP decoding was developed in [8] and application of MAP decoding to image communication over noisy channels was studied in [210].

1.5.3 Multi-antenna Systems

Communication systems with receive antenna diversity have attracted a lot of attention since relatively long ago. In fact, in current cellular applications, receive diversity is already in use for improving reception from mobiles. A few general ideas on receive diversity are explained in [150]. A more advanced study can be found, for example, in [16]. In the following, we cite the major references on the studies on channels with multiple transmit and multiple receive antennas. This subsection is divided into four parts which address the information theoretic issues, code design, performance analysis/evaluation, and other issues which are important in MIMO channels but are not directly related to this thesis.

Let us consider a multiple-antenna system which employs K transmit and L receive antennas as depicted in Figure 1.5. The encoder converts a block of m input bits $\boldsymbol{b}$ into matrix codewords of size $K \times w$ symbols denoted by $\boldsymbol{S} = (\boldsymbol{s}_1, \boldsymbol{s}_2, ..., \boldsymbol{s}_w)$, where $\boldsymbol{s}_t = (s_{1,t}, s_{2,t}, ..., s_{K,t})^T$ with $s_{i,t}$ being the signal assigned to transmit antenna i at time index t and ^{T} denoting transposition. At time index t, the entries of $\boldsymbol{s}_t$ are transmitted simultaneously from the transmit antennas. At the receiver, the L receive antennas collect the incoming signals attenuated by fading and perturbed by additive noise. The received signals are then demodulated and decoded.

In this thesis, we consider Rayleigh flat fading, so that the complex path gain from transmit antenna i to receive antenna j, denoted by $H_{j,i}$, has a zero-mean unit-variance complex Gaussian distribution, denoted by $\mathcal{CN}(0, 1)$, with i.i.d. real and imaginary parts. In many scenarios, it is assumed that the channel is quasi-static, which means that the path gains remain constant during a codeword transmission, but vary in an i.i.d. fashion

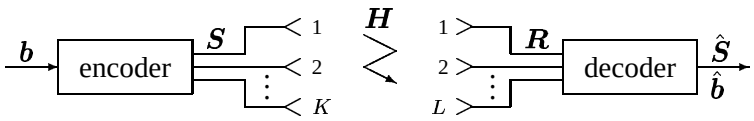

Figure 1.5: Block diagram of a typical multi input-multi output system, where $\boldsymbol{b} = [b_1, ..., b_m]$ is encoded to $\boldsymbol{S} = (\boldsymbol{s}_1, \boldsymbol{s}_2, ..., \boldsymbol{s}_w)$, attenuated by $\boldsymbol{H}$, received as $\boldsymbol{R}$, and decoded to $\hat{\boldsymbol{S}}$ which corresponds to $\hat{\boldsymbol{b}} = [\hat{b}_1, ..., \hat{b}_m]$.

from one codeword interval to the other. The additive noise at receiver j at time t, $N_{j,t}$, is assumed to be $\mathcal{CN}(0, 1)$ distributed with i.i.d. real and imaginary parts. We assume that the input, fading coefficients, and channel noise are independent from each other. Based on the above, for a CSNR of γ_s at each receive branch and at time t, the signal at receive antenna j can be written as $R_{j,t} = \sqrt{\frac{\gamma_s}{K}} \sum_{i=1}^{K} H_{j,i} s_{i,t} + N_{j,t}$, or in matrix form,

$$\boldsymbol{r}_t = \sqrt{\frac{\gamma_s}{K}} \boldsymbol{H} \boldsymbol{s}_t + \boldsymbol{n}_t, \tag{1.1}$$

where $\boldsymbol{r}_t = (R_{1,t}, ..., R_{L,t})^T$, $\boldsymbol{n}_t = (N_{1,t}, ..., N_{L,t})^T$, and $\boldsymbol{H} = [H_{j,i}]$.

Information Theoretic Studies

Research on systems with multiple transmit antennas began in the late 1980s and early 1990s. The potential for lower error rates at no extra bandwidth and transmit power with multiple transmit antennas was demonstrated via simulations in [206, 207, 208, 209] using delay elements, transmit-antenna diversity, and equalization. It was shown in [196, 57] that the capacity of fast fading MIMO channels scales linearly in the minimum of the number of the transmit and receive antennas assuming independent fading between each

transmit-receive antenna pair. This potential increase was shown to hold also for block Rayleigh fading channels in [134]. In [87], it was shown that temporal diversity can be replaced with transmit antenna diversity to gain non-zero capacity in a single coherence interval if the number of transmit antennas and the coherence time can grow without bound. Capacity reduction due to spatial correlation was investigated through Monte-Carlo simulations in [169] and theoretically in [26], where it was shown that the reduction in outage and Shannon capacity is not significant when the correlation coefficient between the fading coefficients is less than 0.5. In [27] some degenerate channel models to account for spatial correlation and keyhole (where each entry in the channel matrix is a product of two complex Gaussian random variables) were investigated and validated through physical measurements. Using the idea of [72], tight upper bounds for the capacity of spatially correlated and double-scaterring MIMO channels were developed in [168] which can be used together with the lower bound derived in [144]. The capacity of keyhole MIMO channels was calculated in closed form in [168]. Using random matrix theory [93] and Gaussian approximation of the unaveraged channel capacity, asymptotic behavior of MIMO outage capacity was studied in [72, 138, 159]. Finally, in [59], sphere packing bounds were derived for codeword error rate of space-time codes over block Rayleigh fading channels. It was shown that the codeword error rate significantly improves as the codewords span a larger number of fading blocks.

Code Design for Multi-Antenna Systems with Coherent Detection

The step next to information theoretic studies is to design codes to achieve a performance as close as possible to the information theoretic limits. In this subsection, we consider code

design methods for coherent scenarios; namely, the methods in which the channel matrix is assumed to be known at the receiver. This assumption is due to the fact that the channel fading coefficients need to be estimated at the receiver for synchronization purposes.

We divide code design approaches into three groups: spatial multiplexing, space-time coding, and ad hoc methods. Spatial multiplexing contains mostly the schemes which add little (or no) redundancy at the transmitter, and use signal processing techniques for detection. Spatial multiplexing was introduced in [56], where the diagonal Bell Laboratories layered space-time (D-BLAST) architecture was developed. In D-BLAST, the input data bits are first de-multiplexed into K sub-sequences, each of which may be channel coded by a conventional (SISO) encoder. The coded bits are then modulated and sent via antennas in turn; for example, modulator 1 sends its first symbol via antenna 1, its second symbol via antenna 2, and so on. At the receiver, the symbols are detected in an iterative manner via "nulling and cancelling" which detects and removes the effect of the symbols with the highest signal-to-noise ratio at each iteration. The D-BLAST decoder suffers from being too computationally intensive. A simplified version of D-BLAST, called the vertical BLAST (V-BLAST) was proposed in [58], where modulator i sends K symbols over the K transmit antennas at the i^{th} symbol period. Typical variations of BLAST are the work in [129, 157], where interleaving, BLAST, and iterative decoding were used to improve the BLAST performance. The major drawback of BLAST is its complexity as the number of transmit and/or receive antennas grows.

In order to design space-time codes, the codeword pairwise error probability (PEP) was considered in [194]. The codeword PEP is the probability of the event that when $\boldsymbol{S}$ was sent and between $\boldsymbol{S}$ and $\hat{\boldsymbol{S}}$, $\hat{\boldsymbol{S}}$ is detected. We shall denote this probability by $\Pr(\boldsymbol{S} \rightarrow \hat{\boldsymbol{S}})$.

Using the Chernoff bound, it was shown in [194] that the codeword PEP is upper bounded by

$$\Pr(\boldsymbol{S} \rightarrow \hat{\boldsymbol{S}}) \leq (\Lambda \gamma_s / 4)^{Lr} ,$$

where r is the rank of the matrix $\boldsymbol{S} - \hat{\boldsymbol{S}}$ and Λ, also known as the coding advantage, is given by

$$\Lambda = |(\boldsymbol{S} - \hat{\boldsymbol{S}})(\boldsymbol{S} - \hat{\boldsymbol{S}})^{\dagger}|^{1/r},$$

where † denotes complex conjugate transpose and $|\mathbf{A}|$ for a matrix $\mathbf{A}$ is the determinant of $\mathbf{A}$. The product Lr is known as the diversity order. The code design criteria proposed in [194] is to maximize the worse-case (minimum) rank r and determinant of the codeword differences. The maximum value that r can take on is K. Codes for which $r = K$ are called full-rank (or full diversity) codes.

The first coding scheme for multiple transmit antennas was designed in [9], where a rate-1 full-diversity space-time code with orthogonal columns was designed for a dual transmit antenna system. Using a generalization of the theory of orthogonal designs, the work of [9] was extended to any number of transmit antennas in [192], where codes for two to eight transmit antennas were given. The codewords of such codes had orthogonal columns and were hence known as space-time orthogonal block (STOB) codes. Such codes do not depend on the number of receive antennas. The key advantage of space-time orthogonal block codes is that decoding of the STOB coded symbols is decoupled. In other words, one can perform scalar ML decoding instead of vector decoding and hence have polynomial as opposed to exponential decoding complexity. An important result in [192] is that rate-1 space-time orthogonal block codes exist only for two transmit anten-

nas with complex signaling schemes. Space-time orthogonal codes were also studied in [82, 120, 121, 185]. An interesting result in [121] is that the maximum rate of space-time orthogonal codes with complex signaling and $K = 2m$ or $K = 2m-1$ transmit antennas is $(m+1)/2m$. Space-time orthogonal block codes are reviewed in more detail in Chapter 3.

Space-time orthogonal block codes achieve full diversity gain, but they fail to have a large coding gain. In order to achieve a coding gain (at the price of increased decoding – and possibly encoding – complexity), one may use a concatenation of conventional channel coding and either space-time orthogonal codes (see, for example, [10]) or BLAST (such as the work in [132]). Other choices are space-time trellis coding [194, 95] (and their design via computer search [18, 73, 189]), using iterative (turbo) coding ideas (with parallel [34, 98, 98, 184] and serial [23, 70, 124, 127, 183] encoder concatenation), and non-orthogonal block coding. An important class of high-rate non-orthogonal block codes was introduced in [80] and called the linear dispersion (LD) code. Every entry of an LD codeword is a weighted sum of the baseband signals with the weights chosen such that the mutual information between the channel input and output codewords is maximized given the number of transmit and receive antennas. Other major space-time code design methods include the work in [35, 36], where constellation rotation and the Hadamard transform were used, and in [46, 77] and their extension in [47], where a connection between the rank criterion of [194] with binary fields to design space-time codes for PSK constellations using Algebraic tools was created. Among ad hoc methods, we cite the work in [118] that used conventional channel coding to obtain coding gain followed by random constellation mapping of the same data at every transmit branch to achieve diversity gain.

Performance Evaluation/Analysis

Our main focus in this thesis (except for Chapter 7) is performance analysis of digital communication systems. Many conventional methods for analysis of SISO communication systems become infeasible in multi-antenna systems (e.g., due to their large codebooks). Therefore, it is required to find ways to either extend the existing methods to MIMO channels or to come up with new analysis strategies.

Early papers on space-time code design derived the Chernoff upper bound on the pairwise error probability between codewords [194, 74]. Chernoff upper bounds for channels with correlated Rician fading and correlated noise can be found in [41]. The pairwise error probability under fast fading was considered in [173], where an integral solution was found, and in [199] where the solution was in terms of a derivative. In [190] a form of the moment generating function of the ML metric was derived which was simpler to evaluate for block fading channels, and the PEPs were found numerically. The exact expression and a lower bound for the pairwise error probability of arbitrary space-time codewords under quasi-static fading were found in [131] (we will present an alternative derivation in Chapter 3). For a land-mobile to satellite link, the pairwise error probability was found in [197] for Rician-lognormal fading and in [198] for Rician-Nakagami-m fading. A moment-generating function approach was used in [176], where the pairwise error probability of the so-called super-orthogonal space-time trellis codes was found, and in [222], where upper bounds on the symbol error rate of D-BLAST systems without channel coding were evaluated. The transfer function method can be used to derive upper bounds on the bit error rate of space-time trellis codes as was the case in [173, 223], but the bounds are often over

an order of magnitude larger than simulation results even at high signal-to-noise ratios and they become too complex to evaluate for large diversity orders.

For standard M-ary PSK and QAM constellations with Gray signal mapping [150], the standard approach for performance analysis in [175], which is widely adopted in many references, is to use the exact conditional symbol error rate and approximate conditional bit error rate formulas of [175] which are conditioned on the channel fading coefficients. For example, the conditional symbol error rate $P_s(\mathcal{E})$ of standard M-ary PSK is given by

$$P_s(\mathcal{E}|H=h) = \frac{1}{\pi}\int_0^{(M-1)\pi/M} \exp\left\{-\frac{\gamma_s \sin^2(\pi/M)h^2}{\sin^2\theta}\right\} d\theta, \tag{1.2}$$

and the conditional SER of standard square M-ary QAM is given by

$$P_s(\mathcal{E}|H=h) = \frac{4q}{\pi}\int_0^{\pi/2} \exp\left\{-\frac{\gamma_s g_{\text{QAM}} h^2}{\sin^2\theta}\right\} d\theta - \frac{4q^2}{\pi}\int_0^{\pi/4} \exp\left\{-\frac{\gamma_s g_{\text{QAM}} h^2}{\sin^2\theta}\right\} d\theta, \tag{1.3}$$

where $q = 1 - 1/\sqrt{M}$ and $g_{\text{QAM}} = 3/2(M-1)$. Similar expressions hold for the BER, which we do not report here for brevity. To derive the error rates, one needs to find the distribution of the equivalent fading coefficients based on which the symbol error rate and approximate bit error may be evaluated. An example of such an approach is the work in [53], in which an approximate expression for the bit error rate of space-time orthogonal block coded channels with correlated Nakagami-m fading was derived. In [19] and [166], the symbol error rate for space-time orthogonal coded channels with i.i.d. Rayleigh and keyhole Nakagami-m fading were found, respectively (although the results of the latter reference are complex to evaluate). An interesting result in the latter paper is that the symbol error rate of keyhole space-time orthogonal coded channels with a growing number

of receive antennas approaches that of the i.i.d. channels with a single receive antenna, which is expected because keyhole channels have only one degree of freedom (i.e., their diversity gain in one). Note that the above results hold only for standard signaling schemes and Gray signal mapping.

Miscellaneous Issues

We have left out many areas which are applied in MIMO systems, because they are not directly related to this thesis. Many of these issues are important by themselves. An important issue is space-time code design for non-coherent detection. Differential and non-coherent techniques in communications do not require an explicit carrier phase reference. These techniques are specially needed for wireless radio communication systems, where carrier phase synchronization is difficult due to fading, high mobility, severe interference, and the use of short data packets. Non-coherent detection is required also when there are a lot of antennas in the system and training sequences become too large to be possible. The ideas for communication over non-coherent SISO channels can be applied to MIMO channels as well. These solutions include frequency shift keying (FSK) [117] and differential transmission.

It was shown in [86] that for asymptotically large channel signal-to-noise ratios or when the channel coherence time T_c and the number of transmit antennas K grow without bound but the ratio of T_c/K is fixed, capacity-achieving codewords are the product of an isotropically distributed unitary matrix with an independent real non-negative diagonal matrix. A systematic method to design unitary constellations was proposed in [88], but decoding complexity of such constellations remained exponential. Design of differential space-time

codes based on the orthogonal designs was addressed in [191, 96], but these codes exist only for certain rates and certain numbers of transmit antennas. In order to design non-coherent space-time codes with some structure (so that decoding complexity is reduced), space-time codes which form a group under matrix multiplication were studied and developed in [85, 89, 90, 170, 171, 170, 172, 99, 81]. As group codes do not exist for arbitrary rates, other strategies such as code concatenation [12, 15, 155, 188] need to be devised. An interesting code design method proposed in [79] (and its extension to non-square codewords in [100]), considered the design of unitary space-time codes based on the Cayley transform. The key advantage of the Cayley transform is that it makes it possible to do code design in a linear vector space over the reals instead of the non-linear and non-concave space of complex unitary matrices, significantly reducing encoding and decoding complexity.

Many algorithms have been proposed to reduce the complexity of encoding/decoding in multi-antenna communication systems. We categorize these algorithms in three groups: algorithms which are aimed to reduce the decoding complexity through sub-optimal methods (such as [37, 78]), those that use fewer antennas to reduce computations, and combinations of spatial multiplexing and space-time coding. The algorithm in [37] applied the sphere decoding algorithm of [202] to multi-antenna applications. The key advantage of this algorithm is that it does not depend on the transmission rate. Although it has exponential complexity [97], it has a smaller exponent as compared with ML decoding. Antenna selection for space-time orthogonal block codes was addressed in [193] (and extended in [104]), where, among the receive antennas, the one with the highest channel signal-to-noise ratio was chosen. An optimal algorithm for receive antenna selection from a capacity-

maximizing perspective was given in [69], where, at each iteration, the antenna which had the least effect on channel capacity was removed until the desired number of antennas remained. In [67], a sub-optimal algorithm was given which had a reduced complexity by an order of magnitude as compared with the algorithm in [69] by adding the antenna with the largest increase in channel capacity at each step. The third approach is to combine spatial multiplexing and space-time coding. In such methods, the transmit antennas are divided into a number of groups among which the incoming bit-stream is de-multiplexed. A form of space-time coding is then applied to each group; for example, in [38, 45] the diagonal space-time codes are used with this method, while in [195] space-time trellis codes, in [105] space-time orthogonal block codes, and in [203] V-BLAST were applied.

An important issue is the estimation of the channel fading coefficients at the receiver, which is made for coherent detection. Channel estimation methods can be found, for example, in [133, 32, 153, 24]. As the transmission bandwidth increases beyond the coherence bandwidth of the channel, equalization becomes indispensable. An overview of practical equalization techniques for space-time coded systems can be found in [11]. When the channel is frequency selective, it may be divided into a number of sub-channels which can be assumed frequency flat and multiple tones can be used. This method is known as orthogonal frequency division multiplexing (OFDM). OFDM for MIMO channels was studied, for example, in [17, 119, 139]. Note that as shown in [219], frequency selectivity can be exploited to obtain diversity gains. If, at least, the channel covariance matrix can be fed back to the transmitter, optimal power allocation via water-filling [31] and also beamforming can be employed to increase the throughput. The main result in beamforming is that the optimal beamformer should have multiple beams pointing along the eigenvectors of the

channel correlation matrix with proper power loading across beams [218]. Other issues include multiuser MIMO communication [130, 141, 204], broadcast MIMO channels [115], and MIMO channel modeling [2, 28, 65, 102, 122, 137].

Chapter 2

Bounds on the Probability of a Finite Union of Events

2.1 The Lower and Upper Bounds

2.1.1 Introduction

Let $\{A_1, A_2, ..., A_M\}$ be a finite set of events and let $P(A_i)$ be the probability that the outcome of the experiment is A_i. In this section, we review a number of upper and lower bounds on $P(\cup_i A_i)$, which is the probability of the union of A_i. The upper and lower bounds that we consider in this chapter require the knowledge of the probability of the individual events $P(A_i), i = 1, ..., M$, which we herein refer to as the first order probabilities, and the second order probabilities $P(A_i \cap A_j), i, j = 1, ..., M$ (which is the probability of the intersection of a pair of events A_i and A_j). These bounds hold for any probability space.

We are interested in such bounds because, as is demonstrated in the following chapters, the error rates of communication systems can be expressed in terms of sums of probabilities of the union of error events. Therefore, establishing upper and lower bounds on the probability of a finite union helps to establish bounds on the error rates.

We mention two types of bounds. The first two bounds are Bonferroni-type bounds [62] which are expressed in terms of sums of the first and second order probabilities. The second group of bounds are in terms of ratios.

2.1.2 The Hunter Upper Bound

A Bonferroni-type upper bound, due to Hunter, for the probability of the union of a finite number of events is given by [91]

$$P\left(\bigcup_{i=1}^{M} A_i\right) \leq \sum_{i=1}^{M} P(A_i) - \max_{T_0 \in \mathcal{T}} \sum_{(i,j)\in T_0} P(A_i \cap A_j), \tag{2.1}$$

where $\mathcal{T}$ is the set of all spanning trees of the M indices, i.e., the trees that include all indices as nodes.

The computational complexity of finding the optimal spanning tree via exhaustive search is exponential making it infeasible for most of the applications. In [91, 110], it is noted that the problem of finding the optimal spanning tree can be recast into determining the maximal spanning tree of a completely connected weighted graph whose nodes are the indices of the events and the weight of the edge between a pair of nodes i and j is the probability of the joint event $A_i \cap A_j$. This idea makes it possible to use Kruskal's greedy algorithm [3] which finds the optimal spanning tree for a weighted graph. This algorithm is described in Subsection 2.2.1.

2.1.3 The Kounias Lower Bound

For the set of events $A_1, ..., A_M$, the Kounias lower bound, which is a Bonferroni-type bound, is given by [108]

$$P\left(\bigcup_{i=1}^{M} A_i\right) \geq \max_{\mathcal{I}} \left\{ \sum_{i \in \mathcal{I}} P(A_i) - \sum_{\substack{i,j \in \mathcal{I} \\ i<j}} P(A_i \cap A_j) \right\}, \tag{2.2}$$

where $\mathcal{I}$ is a subset of the set of indices $\mathcal{S} \stackrel{\triangle}{=} \{1, 2, ..., M\}$. The computational complexity of direct search to perform the above maximization is exponential. Unlike the Hunter upper bound, there is no algorithmic solution (or otherwise) to find the optimal index set in this problem. Nevertheless, a sub-optimal algorithm with complexity $O(M^2)$ is proposed in [110]. This algorithm is described in Subsection 2.2.2.

2.1.4 The de Caen Lower bound

In [39], a lower bound on the probability of a union of events is derived. This lower bound, which is due to de Caen, is given by

$$P\left(\bigcup_{i=1}^{M} A_i\right) \geq \sum_{i=1}^{M} \frac{P(A_i)^2}{\sum_{j=1}^{M} P(A_i \cap A_j)}. \tag{2.3}$$

Notice that the above bound is different from the two previous ones in that it is in terms of a ratio. In the following, we review two other lower bounds which are also expressed in terms of a sum of ratios and improve over de Caen's lower bound.

2.1.5 The KAT Lower Bound

A lower bound on the probability of the union of a finite number of events is derived in [109]. This bound, to which we refer as the KAT lower bound, is given by

$$P\left(\bigcup_{i=1}^{M} A_i\right) \geq \sum_{i=1}^{M}\left(\frac{\theta_i P(A_i)^2}{\sum_{j=1}^{M} P(A_i \cap A_j) + (1-\theta_i)P(A_i)} + \frac{(1-\theta_i)P(A_i)^2}{\sum_{j=1}^{M} P(A_i \cap A_j) - \theta_i P(A_i)}\right), \tag{2.4}$$

where

$$\theta_i = \frac{\beta_i}{\alpha_i} - \left\lfloor \frac{\beta_i}{\alpha_i} \right\rfloor,$$

with $\lfloor x \rfloor$ being the largest integer smaller than x,

$$\alpha_i = P(A_i) \qquad \text{and} \qquad \beta_i = \sum_{j:j\neq i} P(A_i \cap A_j)\cdot$$

Note that the above bound reduces to de Caen's lower bound if we set $\theta_i = 0$ for all i. The KAT bound is tighter than de Caen's lower bound by a factor of at most 9/8 [40].

2.1.6 The Cohen and Merhav Lower bound

Another lower bound for the probability of a finite union is derived in [30]. Similar to the KAT bound, this lower bound is an improvement over the de Caen lower bound although it requires more information than just the knowledge of $P(A_i)$ and $P(A_i \cap A_j)$. For a finite event set, Cohen and Merhav's lower bound is given by

$$P\left(\bigcup_{i=1}^{M} A_i\right) \geq \sum_{i=1}^{M} \frac{\left(\sum_{x\in A_i} p(x) m_i(x)\right)^2}{\sum_{j=1}^{M} \sum_{x\in A_i\cap A_j} p(x) m_i^2(x)}, \tag{2.5}$$

where $m_i(x) \geq 0$ is an arbitrary real function which can be chosen so that the lower bound is tightened. It is noted in [30] that equality in (2.5) is achieved when $m_i(x) = 1/\deg(x)$, where $\deg(x)$ is the number of events to which x belongs; in other words,

$$\deg(x) \stackrel{\triangle}{=} |\{i \in \mathcal{S} : x \in A_i\}|.$$

Finally, note that for $m_i(x) = 1$, Cohen and Merhav's lower bound reduces to de Caen's lower bound. Therefore, by including $m_i(x) = 1$ in the possible choices for $m_i(x)$, one is guaranteed to get a lower bound which is at least as tight as de Caen's lower bound.

2.2 Algorithmic Implementation of the Hunter and Kounias Bounds

2.2.1 The Hunter Upper Bound

A greedy algorithm, known as Kruskal's algorithm, is given in [3] to find the optimal spanning tree that maximizes the sum on the right hand side of (2.1). The algorithm is described as follows. First, all nodes i and j are connected via edges of weight $P(A_i \cap A_j)$ to form a fully connected graph. To form the tree T_0, the algorithm starts from the edge with the largest weight (the (i, j) with the largest $P(A_i \cap A_j)$). Then, at each step, the edge with the largest weight is added to T_0, subject to the constraint that no cycle is formed in T_0. This step is executed until all of the nodes are in T_0. This algorithm is formally stated as follows [110]. Consider a fully connected graph with M edges (i, j) of weights $P(A_i \cap A_j)$. Construct a set of edges T_0 according to the following steps:

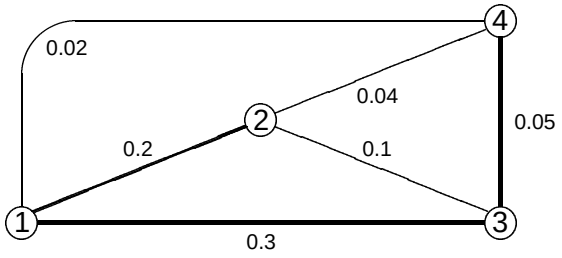

Figure 2.1: Forming the optimal spanning tree to evaluate a Bonferroni-type upper bound.

1. Set $T_0 = \emptyset$.

2. Add the edge with maximum weight to T_0.

3. From the remaining edges, add to T_0 the edge with maximum weight subject to the constraint that T_0 remains cycle-free.

4. Go back to step 3 until T_0 contains $M - 1$ edges (i.e., all nodes and a complete tree).

Figure 2.1 shows the result of applying the above algorithm to a set of events with $P(A_1 \cap A_2) = 0.2$, $P(A_1 \cap A_3) = 0.3$, $P(A_1 \cap A_4) = 0.02$, $P(A_2 \cap A_3) = 0.1$, $P(A_2 \cap A_4) = 0.04$, and $P(A_3 \cap A_4) = 0.05$. The first edge to add to the tree is the one between 1 and 3, because it is has the largest weight. The last edge is the one between 3 and 4. Note that although $P(A_2 \cap A_3)$ is larger than $P(A_3 \cap A_4)$, the edge corresponding to the former probability is not added to the tree, because it results in a loop.

2.2.2 The Kounias Lower Bound

A stepwise algorithm is proposed in [110] which finds an index set to maximize the right hand side of (2.2). The algorithm in [110] starts from two sets $\mathcal{I}_1 = \emptyset$ and $\mathcal{I}_2 = \mathcal{S}$,

and optimizes $\mathcal{I}_1$ and $\mathcal{I}_2$ in an iterative (stepwise) manner by adding an index to $\mathcal{I}_1$ and removing an index from $\mathcal{I}_2$ and vice versa, until they converge. The algorithm is detailed below [110]. In the following, $V(\mathcal{I})$ denotes the term to be maximized in (2.2) for a subset $\mathcal{I} \subseteq \mathcal{S}$. Also, $\mathcal{A}\backslash\mathcal{B}$ denotes the set which contains the elements in $\mathcal{A}$ but not in $\mathcal{B}$.

1. Begin from two sets $\mathcal{I}_1 = \emptyset$ and $\mathcal{I}_2 = \mathcal{S}$. Set $V(\mathcal{I}_1) = 0$ and compute $V(\mathcal{I}_2)$.

2. a. If possible, augment $\mathcal{I}_1$ by adding to it the best index $i \in \mathcal{S}\backslash\mathcal{I}_1$; that is, the index for which $V(\mathcal{I}_1 \cup \{i\})$ is maximized and $V(\mathcal{I}_1 \cup \{i\}) > V(\mathcal{I}_1)$.

   b. If possible, shrink $\mathcal{I}_2$ by removing from it the best index $i \in \mathcal{I}_2$; that is, the index for which $V(\mathcal{I}_2)$ is maximized and $V(\mathcal{I}_2\backslash\{i\}) > V(\mathcal{I}_2)$.

3. Repeat step 2 until the term on the right-hand side of (2.2) can no longer be improved.

4. a. If possible, shrink $\mathcal{I}_1$ by removing from it the best index $i \in \mathcal{I}_1$; that is, the index for which $V(\mathcal{I}_1)$ is maximized and $V(\mathcal{I}_1\backslash\{i\}) > V(\mathcal{I}_1)$.

   b. If possible, augment $\mathcal{I}_2$ by adding to it the best index $i \in \mathcal{S}\backslash\mathcal{I}_2$; that is, the index for which $V(\mathcal{I}_2 \cup \{i\})$ is maximized and $V(\mathcal{I}_2 \cup \{i\}) > V(\mathcal{I}_2)$.

5. Repeat step 4 until the term on the right-hand side of (2.2) can no longer be improved.

6. Go back to step 2 until the metric V can no longer be improved. In such a case, the output of the stepwise algorithm is

$$\max\{V(\mathcal{I}_1), V(\mathcal{I}_2)\}.$$

Note that this algorithm is sub-optimal and depends on the way it is initialized (in the above algorithm, the initial sets are the empty set and the global set $\mathcal{S}$). One can use different

initial sets (other than $\emptyset$ and $\mathcal{S}$) or use more than two initial sets to find a better (yet still sub-optimal) set of indices for $\mathcal{I}$.

2.3 Final Remarks

As is shown in the following chapters, the block error rate, the symbol error rate, and the bit error rate of single- and multi-antenna communication systems with arbitrary signaling schemes and symbol mappings can be expressed in terms of sums of probabilities of unions of error events. Therefore, the above bounds are powerful tools to establish upper and lower bounds for the error rates of the systems under study. When specialized to the analysis of the communication systems, the overall error rate of the system can be represented by a finite union of events, where $P(A_i)$ is the pairwise error probability, and $P(A_i \cap A_j)$ is the second order pairwise error probability.

Chapter 3

A Brief Review of Space-Time Orthogonal Block Codes

3.1 Introduction

Space-time orthogonal block codes are a sub-class of space-time codes whose codewords have orthogonal columns and hence they are full-rank. These codes are important because of their simple encoding and, specially, because their decoding complexity is polynomial (as opposed to exponential) in the size of the signaling scheme. Space-time orthogonal block codes were introduced by Alamouti in [9] for a system with two transmit antennas and any number of receive antennas. A theory to extend these codes for more than two transmit antennas was presented in [192].

In the following, we describe encoding and decoding for Alamouti's code, which is also known as the $\mathcal{G}^2$ code, in detail for a dual-transmit and single-receive antenna system. ML

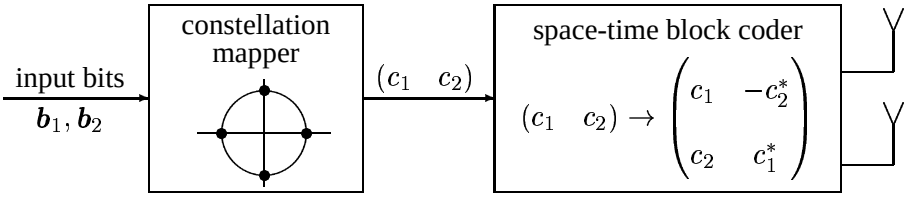

Figure 3.1: The transmitter of Alamouti's space-time orthogonal block coding scheme.

decoding and the symbol pairwise error probability (PEP) of general space-time orthogonal block codes are next explained. As a contribution, we present an alternative derivation of the codeword PEP of multi-antenna codes with arbitrary structure. This PEP expression is valid for both space-time codes and BLAST.

3.1.1 Encoding in Alamouti's System

Let us consider a dual-transmit single-receive antenna system. The encoding strategy of Alamouti's scheme is as follows (see Figure 3.1). First, every incoming p bits $\boldsymbol{b} = [b_1, ..., b_p]$ (where 2^p is the size of the signaling scheme) are mapped into a baseband signal using a scalar function. For example, if $\boldsymbol{b}_1$ and $\boldsymbol{b}_2$ are two consecutive blocks of p bits each, they are mapped to $c_1 = f(\boldsymbol{b}_1)$ and $c_2 = f(\boldsymbol{b}_2)$, respectively, where $f(\cdot)$ is the modulation function and c_1 and c_2 are baseband signals. At a given symbol period, two signals are simultaneously transmitted from the two transmit antennas. At symbol period one, we have $s_{1,1} = c_1$ and $s_{2,1} = c_2$. During the next symbol period, $s_{1,2} = -c_2^*$ is transmitted from antenna one and $s_{2,2} = c_1^*$ is transmitted from antenna two, where * denotes complex conjugate. Notice that no explicit channel coding is performed and because two consecutive

symbols are sent in two symbol intervals, the rate of this channel code is unity. We assume that the fading conditions remain the same during the two consecutive symbol periods used to transmit symbols c_1 and c_2. Denoting the channel fading coefficients by H_1 and H_2, at symbol period one, we receive

$$R_1 = H_1 c_1 + H_2 c_2 + N_1$$

and at symbol period two, we get

$$R_2 = -H_1 c_2^* + H_2 c_1^* + N_2.$$

3.1.2 Decoding in Alamouti's System

Defining

$$\bar{\boldsymbol{H}} \triangleq \begin{pmatrix} H_1 & H_2 \\ H_2^* & -H_1^* \end{pmatrix},$$

we note that $\bar{\boldsymbol{H}}$ is an orthogonal matrix; namely, $\bar{\boldsymbol{H}}^\dagger \bar{\boldsymbol{H}} = (|H_1|^2 + |H_2|^2)\mathbf{I}_2$.

For $\bar{\boldsymbol{r}} \triangleq (R_1 \quad R_2^*)^T$, $\boldsymbol{c} = (c_1 \quad c_2)^T$, and $\bar{\boldsymbol{n}} = (N_1 \quad N_2^*)^T$, we can write

$$\bar{\boldsymbol{r}} = \bar{\boldsymbol{H}}\boldsymbol{c} + \bar{\boldsymbol{n}}. \tag{3.1}$$

At this stage, ML decoding may be performed directly using (3.1); i.e., choosing $\hat{\boldsymbol{c}} = (\hat{c}_1 \quad \hat{c}_2)^T$ which satisfies

$$\hat{\boldsymbol{c}} = \arg\min_{\boldsymbol{c}} \|\bar{\boldsymbol{r}} - \bar{\boldsymbol{H}}\boldsymbol{c}\|^2, \tag{3.2}$$

where $\hat{x}$ denotes the estimate of x and minimization is done over all two-tuples whose elements are baseband signals. However, decoding may be further simplified by exploiting

the orthogonality of the path gains matrix $\bar{\boldsymbol{H}}$. Multiplying (3.1) from the left by $\bar{\boldsymbol{H}}^{\dagger}$, we have

$$\begin{aligned}\tilde{\boldsymbol{r}} &\triangleq \bar{\boldsymbol{H}}^{\dagger}\bar{\boldsymbol{r}} = \bar{\boldsymbol{H}}^{\dagger}\bar{\boldsymbol{H}}\boldsymbol{c} + \bar{\boldsymbol{H}}^{\dagger}\bar{\boldsymbol{n}} = (|H_1|^2 + |H_2|^2)\boldsymbol{c} + \bar{\boldsymbol{H}}^{\dagger}\bar{\boldsymbol{n}} \\ &= (|H_1|^2 + |H_2|^2)\boldsymbol{c} + \tilde{\boldsymbol{n}}. \end{aligned} \tag{3.3}$$

In other words, $\tilde{R}_1 = (|H_1|^2 + |H_2|^2)c_1 + \tilde{N}_1$ and $\tilde{R}_2 = (|H_1|^2 + |H_2|^2)c_2 + \tilde{N}_2$, where

$$\tilde{R}_1 \triangleq H_1^* R_1 + H_2 R_2, \tag{3.4}$$

$$\tilde{R}_2 \triangleq H_2^* R_1 - H_1 R_2, \tag{3.5}$$

$\tilde{N}_1 \triangleq H_1^* N_1 + H_2 N_2$, and $\tilde{N}_2 \triangleq H_2^* N_1 - H_1 N_2$. As the entries of $\tilde{\boldsymbol{n}}$ are i.i.d. and H_1 and H_2 are known to the receiver, ML decoding of the entries of $\boldsymbol{c}$ can be done independently via

$$\hat{c}_1 = \arg\min_{c} |\tilde{R}_1 - (|H_1|^2 + |H_2|^2)c|^2 \tag{3.6}$$

$$\hat{c}_2 = \arg\min_{c} |\tilde{R}_2 - (|H_1|^2 + |H_2|^2)c|^2, \tag{3.7}$$

where minimization is done over the signal alphabet. Since the modulation function $f(\cdot)$ is scalar, the estimated bits would simply be $\hat{\boldsymbol{b}}_1 = f^{-1}(\hat{c}_1)$ and $\hat{\boldsymbol{b}}_2 = f^{-1}(\hat{c}_2)$.

For a signaling scheme of size $M = 2^p$, while using the ML detection rule on the output vector $\bar{\boldsymbol{r}}$ as outlined in (3.2) will require M^2 ML cost function computations, the number of the computations will only be $2M$ if $\tilde{\boldsymbol{r}}$, defined in (3.4) and (3.5), is used for detection as outlined in (3.6) and (3.7). This will result in much shorter decoding times, specially for large signal alphabets. In a typical implementation of the system with 16-QAM signaling, decoding of 5 million bits with detection rule (3.2) took 62918 seconds, while employing the detection rules in (3.6) and (3.7) took about 100 seconds. The tests were run on a Sun Ultra 60 computer.

3.1.3 Extension to Three and Four Transmit Antennas

Alamouti's work was generalized to K transmit antennas, instead of only 2 antennas, in [192]. There, it was stated that it is not possible to construct space-time orthogonal block codes of rate one with complex signaling schemes when there are more than two transmit antennas. Also, two examples of space-time orthogonal block codes were introduced for three and four transmit antennas as

$$\mathcal{G}^3 = \begin{pmatrix} c_1 & -c_2 & -c_3 & -c_4 & c_1^* & -c_2^* & -c_3^* & -c_4^* \\ c_2 & c_1 & c_4 & -c_3 & c_2^* & c_1^* & c_4^* & -c_3^* \\ c_3 & -c_4 & c_1 & c_2 & c_3^* & -c_4^* & c_1^* & c_2^* \end{pmatrix} \tag{3.8}$$

and

$$\mathcal{G}^4 = \begin{pmatrix} c_1 & -c_2 & -c_3 & -c_4 & c_1^* & -c_2^* & -c_3^* & -c_4^* \\ c_2 & c_1 & c_4 & -c_3 & c_2^* & c_1^* & c_4^* & -c_3^* \\ c_3 & -c_4 & c_1 & c_2 & c_3^* & -c_4^* & c_1^* & c_2^* \\ c_4 & c_3 & -c_2 & c_1 & c_4^* & c_3^* & -c_2^* & c_1^* \end{pmatrix}. \tag{3.9}$$

Note that both of the above codewords transmit four symbols in eight symbol periods and hence they have a rate of $1/2$.

For encoding, four blocks of p bits each are mapped into a block of four signals $\boldsymbol{c} = (c_1, c_2, c_3, c_4)^T$. A codeword is then formed according to (3.8) or (3.9) and transmitted over the channel, with one column of the matrix transmitted at a time.

The decoding phase is similar to the dual input system. It is assumed that the channel is slow fading (quasi-static), with the path gains remaining constant during the transmission of a codeword (eight symbol intervals). Therefore, we can use the same approach as in

Subsection 3.1.2. In order to find the ML detection rules, we define the output and noise vectors as

$$\bar{\boldsymbol{r}} = (R_1, R_2, R_3, R_4, R_5^*, R_6^*, R_7^*, R_8^*)^T \quad \text{and} \quad \bar{\boldsymbol{n}} = (N_1, N_2, N_3, N_4, N_5^*, N_6^*, N_7^*, N_8^*)^T,$$

respectively, so that the input-output relationship becomes as in (3.1), with the path gains matrix $\bar{\boldsymbol{H}}$ given by

$$\bar{\boldsymbol{H}} = \begin{pmatrix} H_1 & H_2 & H_3 & 0 \\ H_2 & -H_1 & 0 & -H_3 \\ H_3 & 0 & -H_1 & H_2 \\ 0 & H_3 & -H_2 & -H_1 \\ H_1^* & H_2^* & H_3^* & 0 \\ H_2^* & -H_1^* & 0 & -H_3^* \\ H_3^* & 0 & -H_1^* & H_2^* \\ 0 & H_3^* & -H_2^* & -H_1^* \end{pmatrix}$$

for the three transmit antennas and by

$$\bar{\boldsymbol{H}} = \begin{pmatrix} H_1 & H_2 & H_3 & H_4 \\ H_2 & -H_1 & H_4 & -H_3 \\ H_3 & -H_4 & -H_1 & H_2 \\ H_4 & H_3 & -H_2 & -H_1 \\ H_1^* & H_2^* & H_3^* & H_4^* \\ H_2^* & -H_1^* & H_4^* & -H_3^* \\ H_3^* & -H_4^* & -H_1^* & H_2^* \\ H_4^* & H_3^* & -H_2^* & -H_1^* \end{pmatrix}$$

for systems with four transmit antennas. Note that the above matrices are orthogonal, and hence after multiplying (3.1) from the left by $\bar{\boldsymbol{H}}^{\dagger}$, we have

$$\tilde{\boldsymbol{r}} = 2Y\boldsymbol{c} + \tilde{\boldsymbol{n}} \tag{3.10}$$

where $Y = \sum_{i=1}^{K} |H_i|^2$. It can be shown that the elements of $\tilde{\boldsymbol{n}}$ are i.i.d. and hence ML detection can be performed separately on each entry of $\tilde{\boldsymbol{r}}$.

3.2 General Treatment of Space-Time Orthogonal Block Codes

Let us now consider a system with K transmit and L receive antennas. Let $\boldsymbol{c} = (c_1, ..., c_\tau)^T$ be a vector of τ consecutive symbols to encode and $\boldsymbol{S} = (\boldsymbol{s}_1, ..., \boldsymbol{s}_w)$ be the space-time codeword corresponding to it. In the case of STOB codes, we have $w = g\tau$, where $g = w/\tau$ is the coding gain and $\boldsymbol{S}\boldsymbol{S}^{\dagger} = g\|\boldsymbol{c}\|^2\mathbf{I}_K$. As an example, for the code $\mathcal{G}^3$ in (3.8), $w = 8$, $\tau = 4$, and $g = 2$, and for Alamouti's code, $g = 1$ and $w = \tau = 2$. It can be shown that (1.1) can be re-written as [140]

$$\bar{\boldsymbol{r}}^j = \sqrt{\frac{\gamma_s}{K}}\bar{\boldsymbol{H}}^j\boldsymbol{c} + \bar{\boldsymbol{n}}^j \qquad\qquad j = 1, \cdots, L, \tag{3.11}$$

where $\bar{\boldsymbol{r}}^j = [\bar{R}_1^j, ..., \bar{R}_w^j]^T$, $\bar{\boldsymbol{n}}^j = [\bar{N}_1^j, ..., \bar{N}_w^j]^T$, and we have $\bar{R}_t^j = R_t^j$ and $\bar{N}_t^j = N_t^j$ for $1 \le t \le \frac{w}{2}$, and $\bar{R}_t^j = R_t^{j*}$ and $\bar{N}_t^j = N_t^{j*}$ for $\frac{w}{2} < t \le w$ and $\bar{\boldsymbol{H}}^j$ is derived from the j^{th} row of $\boldsymbol{H}$ via negation and complex conjugation of some of its entries. It is clear that $\bar{N}_t^j$ are i.i.d. $\mathcal{CN}(0, 1)$.

We will hereafter consider the set[2] of orthogonal codes for which the corresponding matrix $\bar{\boldsymbol{H}}^j$ has orthogonal columns, i.e., $\bar{\boldsymbol{H}}^{j\dagger}\bar{\boldsymbol{H}}^j = gY_j\mathbf{I}_\tau$, where $Y_j = \sum_i |H_{ji}|^2, j = 1, ..., L$. Therefore, when (3.11) is multiplied from the left by $\bar{\boldsymbol{H}}^{j\dagger}$ we obtain

$$\tilde{\boldsymbol{r}}^j \triangleq \bar{\boldsymbol{H}}^{j\dagger}\bar{\boldsymbol{r}}^j = g\sqrt{\frac{\gamma_s}{K}}Y_j\mathbf{c} + \tilde{\boldsymbol{n}}^j, \tag{3.12}$$

where $\tilde{\boldsymbol{n}}^j \triangleq \bar{\boldsymbol{H}}^{j\dagger}\bar{\boldsymbol{n}}^j = [\tilde{N}_1^j, ..., \tilde{N}_\tau^j]^T$. Note that each entry of $\tilde{\boldsymbol{r}}^j = [\tilde{R}_1^j, ..., \tilde{R}_\tau^j]^T$ is associated with only one symbol. Since, given $\boldsymbol{H}$, $\tilde{\boldsymbol{R}} = [\tilde{\boldsymbol{r}}^1, ..., \tilde{\boldsymbol{r}}^L]$ is an invertible function of $\boldsymbol{R} = [\boldsymbol{r}_1, ..., \boldsymbol{r}_w]$, ML decoding can be based on $\tilde{\boldsymbol{R}}$ instead of $\boldsymbol{R}$ in the following way

$$c_i = \arg\max_c P(c|\{\tilde{R}_i^l\}_{l=1}^L, \boldsymbol{H}),$$

which can be shown to be equivalent to

$$c_i = \arg\min_c \sum_{l=1}^{L} \frac{|\tilde{R}_i^l - g'Y_l c|^2}{Y_l}, \tag{3.13}$$

where $g' = g\sqrt{\gamma_s/K}$.

3.3 The Symbol PEP for General Space-Time Orthogonal Block Codes

Based on (3.13), it can be verified that the PEP between a pair of symbols transmitted over the space-time orthogonal block coded channel conditioned on the path gains is given by

$$P(c_i \to c_j|\boldsymbol{H}) = Q\left(\delta_{ij}\sqrt{Y}\right), \tag{3.14}$$

[2]This class of orthogonal codes includes most of such codes published in the literature, including Alamouti's code and those in (3.8) and (3.9).

where $c_i \to c_j$ denotes the event that c_j has a smaller ML metric than c_i (in (3.13)) when c_i is sent (c_i and c_j are a pair of symbols input to the STOB encoder), $Q(\cdot)$ is the Gaussian tail function given by

$$Q(x) = \frac{1}{\sqrt{2\pi}} \int_x^\infty e^{-t^2/2} dt,$$

$\delta_{ij} = \sqrt{\frac{g\gamma_s}{2K}} |c_i - c_j|$, and

$$Y = \sum_{l=1}^{L} Y_l = \sum_{k=1}^{K} \sum_{l=1}^{L} |H_{l,k}|^2. \tag{3.15}$$

To find the PEP, one should average (3.14) with respect to the distribution of Y, which can be derived as follows. Let us define random variable Z_i as $Z_{(j-1)K+i} = \Re\{H_{j,i}\}$ and $Z_{KL+(j-1)K+i} = \Im\{H_{ji}\}$ for $i = 1, ..., K$ and $j = 1, ..., L$, where $\Re$ and $\Im$ are the real and imaginary parts, respectively. We note that $Z_k \sim$ i.i.d. $\mathcal{N}(0, \frac{1}{2})$, and we can write Y as

$$Y = \sum_{i,j} |H_{j,i}|^2 = \sum_{i,j} \Re\{H_{j,i}\}^2 + \Im\{H_{j,i}\} = \sum_{i=1}^{2n} Z_i^2,$$

where $n = KL$. Using the moment generating function of normal random variables yields the probability density function of Y as

$$f_Y(y) = \frac{1}{(n-1)!} y^{n-1} e^{-y}, \qquad y > 0, \tag{3.16}$$

Hence, Y has a scaled chi-squared distribution with $2n$ degrees of freedom. The expected value of (3.14) is therefore equal to

$$P(c_i \to c_j) = \frac{1}{(n-1)!} \int_0^\infty y^{n-1} e^{-y} Q\left(\delta_{ij}\sqrt{y}\right) dy. \tag{3.17}$$

As noticed in [19], the PEP of diversity reception systems with maximum ratio combining has a form similar to that of (3.17) with the exception that δ_{ij} is given by $\sqrt{\gamma_s/2}|c_i - c_j|$.

Therefore, the conditional PEP for those systems is the same as (3.14). MRC systems were previously analyzed, for example, in [150, 175], whose results can be used to obtain the expected value of (3.14) as

$$P(c_i \to c_j) = \frac{1}{2}\left(1 - \frac{\delta_{ij}}{\sqrt{\delta_{ij}^2+2}} \sum_{k=0}^{KL-1} \binom{2k}{k} \frac{1}{(2(\delta_{ij}^2+2))^k}\right). \tag{3.18}$$

3.4 The Codeword PEP of Arbitrary Space-Time Codes

Here we present a new simple derivation of the codeword PEP for arbitrary space-time codes. We show that the conditional PEP of any two space-time codewords is in the form of a double sum of an expression similar to (3.14), and hence its expectation can be evaluated with the same approach as that for the STOB codes.

For arbitrary space-time coding schemes the receiver computes the squared distance between any pair of faded transmitted coded sequences $\boldsymbol{S}$ and $\hat{\boldsymbol{S}}$

$$\Delta^2_{\boldsymbol{s},\hat{\boldsymbol{s}}} = \frac{\gamma_s}{K} \sum_{t=1}^{w} \sum_{j=1}^{L} \left| \sum_{i=1}^{K} H_{j,i} d_{i,t} \right|^2 = \frac{\gamma_s}{K} \sum_{j=1}^{L} \boldsymbol{h}_j^{\dagger} \mathbf{U}^T \boldsymbol{h}_j, \tag{3.19}$$

where $d_{i,t} = s_{i,t} - \hat{s}_{i,t}$, $\mathbf{D} = [d_{i,t}]$, $\mathbf{U} = \mathbf{D}\mathbf{D}^{\dagger}$, and $\boldsymbol{h}_j$ is the transpose of the j^{th} row of $\boldsymbol{H}$. Let $P(\boldsymbol{S} \to \hat{\boldsymbol{S}})$ denote the probability that $\hat{\boldsymbol{S}}$ has a larger metric than $\boldsymbol{S}$ when $\boldsymbol{S}$ is sent. It is easy to verify that [190]

$$P(\boldsymbol{S} \to \hat{\boldsymbol{S}}) = \mathrm{E}_{\Delta^2_{\boldsymbol{s},\hat{\boldsymbol{s}}}} \left\{ Q\left(\sqrt{\frac{1}{2}\Delta^2_{\boldsymbol{s},\hat{\boldsymbol{s}}}}\right) \right\}. \tag{3.20}$$

Let $\delta_k^2 = \frac{\gamma_s \lambda_k}{2K}$, where λ_k is the k^{th} non-zero eigenvalue of $\mathbf{U}$ with multiplicity n_k. To compute the expectation of (3.20), we determine the pdf of $\frac{1}{2}\Delta^2_{\boldsymbol{s},\hat{\boldsymbol{s}}}$ and write (3.20) as a weighted sum of expressions similar to (3.14).

Since $\mathbf{U}$ is Hermitian (i.e., $\mathbf{U}^\dagger = \mathbf{U}$) and non-negative definite, it can be decomposed as $\mathbf{U} = \mathbf{V}^\dagger \mathbf{D} \mathbf{V}$, where $\mathbf{V}$ is unitary (i.e., $\mathbf{V}^\dagger \mathbf{V} = \mathbf{I}_K$) and $\mathbf{D}$ is a non-negative definite diagonal matrix having the eigenvalues of $\mathbf{U}$ on its main diagonal. $\mathbf{V}$ is a unitary matrix (i.e., $\mathbf{V}^\dagger \mathbf{V} = \mathbf{I}_K$) and its columns are the unit-norm eigenvectors of $\mathbf{U}$. Substituting the decomposed $\mathbf{U}$ in (3.19), we have

$$\frac{1}{2}\Delta^2_{\boldsymbol{s},\hat{\boldsymbol{s}}} = \frac{\gamma_s}{2K}\sum_{j=1}^{L} \boldsymbol{h}_j^\dagger \mathbf{V}^\dagger \mathbf{D} \mathbf{V} \boldsymbol{h}_j = \frac{\gamma_s}{2K}\sum_{j=1}^{L} \boldsymbol{x}_j^\dagger \mathbf{D} \boldsymbol{x}_j = \sum_{j=1}^{L}\sum_{i=1}^{K} \frac{\gamma_s}{2K}\lambda_i |X_{j,i}|^2, \tag{3.21}$$

where $\boldsymbol{x}_j = \mathbf{V}\boldsymbol{h}_j$, $X_{j,i}$ is the i^{th} element of $\boldsymbol{x}_j$, and $\lambda_i = \mathbf{D}_{i,i}$. We note that the entries of $\boldsymbol{x}_j$ are i.i.d. $\mathcal{CN}(0,1)$. Therefore, the moment generating function of $\frac{1}{2}\Delta^2_{\boldsymbol{s},\hat{\boldsymbol{s}}}$ can be written as

$$\Phi_{\frac{1}{2}\Delta^2_{\boldsymbol{s},\hat{\boldsymbol{s}}}}(-s) = \prod_{k=1}^{K} \frac{1}{(1+\delta_k^2 s)^{Ln_k}}\,. \tag{3.22}$$

In order to find the pdf of $\frac{1}{2}\Delta^2_{\boldsymbol{s},\hat{\boldsymbol{s}}}$, which equals $\mathcal{L}^{-1}\left\{\Phi_{\frac{1}{2}\Delta^2_{\boldsymbol{s},\hat{\boldsymbol{s}}}}(-s)\right\}$ (where $\mathcal{L}$ is the Laplace transform), we convert (3.22) into a sum and use the linearity of the Laplace transform. Letting $p_k = \frac{2K}{\gamma_s \lambda_k}$ and using partial fraction expansion [112], we can write (3.22) as

$$\Phi_{\frac{1}{2}\Delta^2_{\boldsymbol{s},\hat{\boldsymbol{s}}}}(-s) = \sum_{k=1}^{K}\sum_{i=0}^{Ln_k-1} \frac{\alpha_{i+1,k}}{(s+\delta_k^{-2})^{i+1}}, \tag{3.23}$$

where

$$\alpha_{Ln_k-i,k} = \frac{1}{i!}\left\{\frac{d^i}{ds^i}\left[(s+p_k)^{Ln_k}\Phi_{\frac{1}{2}\Delta^2_{\boldsymbol{s},\hat{\boldsymbol{s}}}}(-s)\right]\right\}\Bigg|_{s=p_k}, i = 0, ..., Ln_k - 1. \tag{3.24}$$

Taking the inverse Laplace transform of (3.23), we have

$$f_{\frac{1}{2}\Delta^2_{\boldsymbol{s},\hat{\boldsymbol{s}}}}(x) = \sum_{k=1}^{K}\sum_{i=0}^{Ln_k-1} \frac{\alpha_{i+1,k}}{i!} x^i e^{-\frac{2K}{\gamma_s\lambda_k}x}, \qquad x \geq 0. \tag{3.25}$$

The next step is simply using (3.25) to evaluate (3.20). This yields

$$P(\boldsymbol{S} \to \hat{\boldsymbol{S}}) = \sum_{k=1}^{K} \sum_{i=1}^{Ln_k} \frac{\alpha_{i,k}}{(i-1)!} \int_0^{\infty} x^{i-1} e^{-\frac{2K}{\gamma_s \lambda_k} x} Q\left(\sqrt{x}\right) dx. \tag{3.26}$$

The integral in (3.26) is the same as the one in (3.17) which was solved in (3.18). Using (3.17) and (3.18) in (3.26) and setting $\delta_k^2 = \frac{\gamma_s \lambda_k}{2K}$, we obtain the expression for the codeword pairwise error probability of arbitrary space-time codes as

$$P(\boldsymbol{S} \to \hat{\boldsymbol{S}}) = \sum_{k=1}^{K} \sum_{i=1}^{Ln_k} \frac{\beta_{i,k}}{2} \left(1 - \frac{\delta_k}{\sqrt{\delta_k^2 + 2}} \sum_{j=0}^{i-1} \binom{2j}{j} \frac{1}{(2\delta_k^2 + 4)^j}\right), \tag{3.27}$$

where $\beta_{i,k} = \delta_k^{2i} \alpha_{i,k}$. The above result agrees with the result in [131].

Chapter 4

Bounds on the Block and Bit Error Rates of Coded AWGN and Block Rayleigh Fading Channels

4.1 Introduction

Let us consider the communication system of Figure 1.4. This system can use any type of channel coding and any complex signaling scheme. In this chapter, we assume the input to the system to be uniform i.i.d. and hence we consider ML decoding at the receiver. Our goal is to establish upper and lower bounds on the block error rate (BlER) and bit error rate (BER) of the system. To this end, we first write the BlER and BER in terms of a sum of the probabilities of a union of error events. We will then use the Kounias and KAT lower bounds as well as Hunter upper bound, whose general forms were described in Chapter 2,

to derive bounds on the block and bit error rates of SISO AWGN and block Rayleigh fading channels under ML decoding. Theoretically, these approaches can be applied to any signaling schemes and channel codes of any type or rate. For large m, where m/n is the channel code rate, computation of most of the bounds in the literature, including those considered here, becomes infeasible. One of the contributions of this chapter is to use a subset of the codebook to evaluate the bounds. In fact, it is shown that the performance of the lower bounds can be improved in that the bounds become tightened by considering a subset of the codebook. Another contribution of this chapter is deriving a closed-form formula for the probability of the intersection of two pairwise error events for the block Rayleigh fading channel.

4.2 The Error Rates in Terms of Probabilities of a Union

As explained is Subsection 1.4.1, we consider a communication system which maps blocks of input bits $\{\boldsymbol{b}_u\}, u = 0, ..., M-1$ into blocks of baseband signals $\{\boldsymbol{s}_u\}, u = 0, ..., M-1$ which are transmitted over the channel. The block error rate of the system is given by

$$\text{BlER} = \sum_{u=0}^{M-1} P(\epsilon|\boldsymbol{s}_u)p(\boldsymbol{s}_u) = \sum_{u=0}^{M-1} p(\boldsymbol{s}_u)P_u\left(\bigcup_{i\neq u}\epsilon_{ui}\right), \tag{4.1}$$

where $p(\boldsymbol{s}_u) = p(\boldsymbol{b}_u)$ is the probability that $\boldsymbol{b}_u$ is emitted from the source, $P_u(\cdot) \triangleq P(\cdot|\boldsymbol{s}_u)$ is the conditional probability given that $\boldsymbol{s}_u$ was sent, and ϵ_{ui} indicates the pairwise error event between $\boldsymbol{s}_u$ and $\boldsymbol{s}_i$; i.e., the event that when $\boldsymbol{s}_u$ is sent and between $\boldsymbol{s}_u$ and $\boldsymbol{s}_i$, $\boldsymbol{s}_i$ is detected at the decoder. Similarly, the BER can be computed from

$$\text{BER} = \sum_{u=0}^{M-1} p(\boldsymbol{s}_u)P_u(\epsilon^{(b)}), \tag{4.2}$$

where

$$\begin{aligned} P_u(\epsilon^{(b)}) &= \frac{1}{m}\sum_{j=0}^{M-1} D_H(j,u)P(\hat{\boldsymbol{s}}=\boldsymbol{s}_j|\boldsymbol{s}=\boldsymbol{s}_u) \\ &= \frac{1}{m}\sum_{j=0}^{M-1} D_H(j,u)\left(1-P_u\left(\bigcup_{i\neq j}\epsilon_{ji}\right)\right), \end{aligned} \tag{4.3}$$

where $\hat{\boldsymbol{s}}$ is the decoded signal sequence and $D_H(j,u)$ is the Hamming distance between the data bits corresponding to $\boldsymbol{s}_j$ and $\boldsymbol{s}_u$. Note in the above equations that because we assume the input bit-stream to be uniform i.i.d., all symbols are equally likely and $p(\boldsymbol{s}_u) = 1/M$.

Equations (4.1) and (4.3) express both the BlER and BER in terms of the probability of a union, which can be bounded using the KAT, Kounias, and Cohen and Merhav's lower bounds as well as the Hunter upper bound which are presented in Chapter 2.

In the computation of the above bounds, we need to compute the first and the second order PEPs (see (2.1)-(2.5)). Clearly, the PEP expressions depend on the channel model. In the following, we will consider two channel models: the AWGN and the block Rayleigh fading channel.

4.3 The AWGN Channel

For the AWGN channel, we have

$$R_t = s_t + N_t,$$

where R_t is the received signal at symbol interval t and $N_t \sim \mathcal{CN}(0, N_0)$ is the additive white Gaussian noise at the receiver. Let $\boldsymbol{s}_u = [s_1^u, \cdots, s_w^u]$ be the u^{th} possible sequence of

signals in a block, and let $d_t^{i,u} = s_t^i - s_t^u$. The ML decoding rule in this case is given by

$$\hat{\boldsymbol{s}} = \arg\min_{\boldsymbol{s}} \|\boldsymbol{r} - \boldsymbol{s}\|^2,$$

where $\boldsymbol{r} = [R_1, ..., R_w]$.

The pairwise error probability between $\boldsymbol{s}_u$ and $\boldsymbol{s}_i$ is given by

$$\begin{aligned} P_u(\epsilon_{iu}) &= P(\boldsymbol{s}_u \to \boldsymbol{s}_i) = P(\|\boldsymbol{r} - \boldsymbol{s}_u\|^2 \geq \|\boldsymbol{r} - \boldsymbol{s}_i\|^2 \,|\, \boldsymbol{s} = \boldsymbol{s}_u) \\ &= P\left(\frac{\sqrt{2}\langle \boldsymbol{s}_u - \boldsymbol{s}_i, \boldsymbol{n}\rangle}{\|\boldsymbol{s}_u - \boldsymbol{s}_i\| N_0} \geq \frac{1}{\sqrt{2}}\|\boldsymbol{s}_u - \boldsymbol{s}_i\|\right) \qquad (4.4) \\ &= Q\left(\Delta_{i,u}\right), \qquad (4.5) \end{aligned}$$

where $\boldsymbol{n} = [N_1, ..., N_w]$, $\langle x, y\rangle$ is the standard inner product of x and y, $\Delta_{i,u}^2 = \gamma_s \sum_t |d_t^{i,u}|^2$, and $Q(\cdot)$ is the Gaussian tail function. We also have $\gamma_s = E_s/N_0$ for BPSK signaling and $\gamma_s = E_s/2N_0$ for two dimensional signaling. Note that the argument of the expression on the left-hand side of (4.4) is a unit-variance real Gaussian random variable and hence (4.5) easily follows.

The probability of the intersection of two pairwise error events is equal to

$$P_u(\epsilon_{iu} \cap \epsilon_{ju}) = P(\boldsymbol{s}_u \to \boldsymbol{s}_i, \boldsymbol{s}_u \to \boldsymbol{s}_j) = \Psi\left(\rho_{uij}, \Delta_{i,u}, \Delta_{j,u}\right), \qquad (4.6)$$

where

$$\Psi(\rho, x, y) = \frac{1}{2\pi\sqrt{1-\rho^2}} \int_x^\infty \int_y^\infty e^{-\frac{\tau^2 - 2\rho\tau\lambda + \lambda^2}{2(1-\rho^2)}} d\tau d\lambda \qquad (4.7)$$

is the bivariate Gaussian function and

$$\rho_{uij} = \frac{\sum_{t=1}^w \langle d_t^{i,u}, d_t^{j,u}\rangle}{\left(\sum_{t=1}^w |d_t^{i,u}|^2\right)^{\frac{1}{2}} \left(\sum_{t=1}^w |d_t^{j,u}|^2\right)^{\frac{1}{2}}}.$$

From (4.3), we need to evaluate $P_u(\epsilon_{ji})$ and $P_u(\epsilon_{ji} \cap \epsilon_{jk})$ for the BER bounds. These quantities are given by

$$\begin{aligned} P_u(\epsilon_{ji}) &= P(\|\boldsymbol{r} - \boldsymbol{s}_j\|^2 \geq \|\boldsymbol{r} - \boldsymbol{s}_i\|^2 \big| \boldsymbol{s} = \boldsymbol{s}_u) \\ &= Q\left(\frac{\Delta_{i,u}^2 - \Delta_{j,u}^2}{\Delta_{i,j}}\right) \end{aligned}$$

and

$$P_u(\epsilon_{ji} \cap \epsilon_{jk}) = \Psi\left(\rho_{jik}, \frac{\Delta_{i,u}^2 - \Delta_{j,u}^2}{\Delta_{i,j}}, \frac{\Delta_{k,u}^2 - \Delta_{j,u}^2}{\Delta_{k,j}}\right).$$

4.4 The Block Rayleigh Fading Channel

For the block Rayleigh fading channel, we have

$$R_t = H s_t + N_t,$$

where H, which is the only parameter added to the channel model, is a zero-mean unit-variance complex Gaussian random variable: $H \sim \mathcal{CN}(0, 1)$. We assume that H remains unchanged during the transmission of a codeword and changes in an i.i.d. manner to a new value afterwards.

Similar to the AWGN channel case, we first need to evaluate the first and second order PEPs to calculate the BlER and BER upper and lower bounds. The pairwise error probabilities conditioned on the path gain H are similar to the AWGN case. More specifically, we have

$$P_u(\epsilon_{iu}) = E_H\left\{Q\left(\Delta_{i,u}|H|\right)\right\}, \tag{4.8}$$

and

$$P_u(\epsilon_{iu} \cap \epsilon_{ju}) = E_H \left\{ \Psi \left(\rho_{uij}, \Delta_{i,u}|H|, \Delta_{j,u}|H| \right) \right\}. \tag{4.9}$$

We note that equation (4.8) is the same as (3.14) with $Y = |H|^2$. Hence, it equals (3.18) with $K = L = 1$. Therefore, the PEP is given by

$$P_u(\epsilon_{iu}) = \frac{1}{2} \left(1 - \frac{\Delta_{i,u}}{\sqrt{2 + \Delta_{i,u}^2}} \right).$$

As for the expectation in (4.9), we can use the result of [174] to write the $\Psi(\cdot,\cdot,\cdot)$ function as

$$\begin{aligned} \Psi \left(\rho_{uij}, \Delta_{i,u}|H|, \Delta_{j,u}|H| \right) &= \frac{1}{2\pi} \int_0^{\varphi\left(\frac{\Delta_{iu}}{\Delta_{ju}}, \rho_{uij}\right)} \exp\left\{ \frac{-\Delta_{iu}^2}{2\sin^2\theta} |H|^2 \right\} d\theta \\ &\quad + \frac{1}{2\pi} \int_0^{\varphi\left(\frac{\Delta_{ju}}{\Delta_{iu}}, \rho_{uij}\right)} \exp\left\{ \frac{-\Delta_{ju}^2}{2\sin^2\theta} |H|^2 \right\} d\theta, \end{aligned} \tag{4.10}$$

where $\varphi(x,\rho) = \tan^{-1}\left(x\sqrt{1-\rho^2}/(1-\rho x) \right)$, and $\tan^{-1}(x)$ is re-defined here as $\pi - \tan^{-1}(-x)$ for negative x. We then use [175, Eq. 5A.35] (with $n = 1$) to finally derive the expression for the second order PEP in the block Rayleigh fading case as

$$P_u\left(\epsilon_{iu} \cap \epsilon_{ju}\right) \stackrel{\triangle}{=} \Omega(\rho_{uij}, \Delta_{i,u}, \Delta_{j,u}) = I(\Delta_{iu}, \Delta_{ju}, \rho_{uij}) + I(\Delta_{ju}, \Delta_{iu}, \rho_{uij}), \tag{4.11}$$

where

$$I(x,y,\rho) = \frac{1}{\pi} \left(\phi - T \frac{x}{\sqrt{1+x^2}} \right),$$

with

$$\begin{aligned} \phi &= \tan^{-1}\left(\frac{x\sqrt{1-\rho^2}}{y - \rho x} \right), \\ T &= \frac{1}{2} \left\{ \tan^{-1}\frac{N}{D} + \pi \left[1 - \left(\frac{1+\mathrm{sgn}(D)}{2} \right) \mathrm{sgn}(N) \right] \right\}, \end{aligned}$$

$N = 2x\sqrt{1+x^2}\sin 2\phi$, and $D = (1+2x^2)\cos 2\phi - 1$ (with the definition of $\tan^{-1}(x)$ being the same as that in (4.10)).

For the BER bounds, one can similarly obtain the first and second order error probabilities as follows

$$P_u(\epsilon_{ij}) = \frac{1}{2}\left(1 - \frac{\Delta_{i,u}^2 - \Delta_{j,u}^2}{\sqrt{2\Delta_{i,j}^2 + (\Delta_{i,u}^2 - \Delta_{j,u}^2)^2}}\right)$$

and

$$P_u(\epsilon_{ij} \cap \epsilon_{kj}) = \Omega\left(\rho_{jik}, \frac{\Delta_{i,u}^2 - \Delta_{j,u}^2}{\Delta_{i,j}}, \frac{\Delta_{k,u}^2 - \Delta_{j,u}^2}{\Delta_{k,j}}\right),$$

where $\Omega(\cdot,\cdot,\cdot)$ is defined in (4.11) and when the second and the third arguments of $\Psi(\cdot,\cdot,\cdot)$ are non-negative. If at least one of the two arguments are negative, the $\Psi(\cdot,\cdot,\cdot)$ function can be written as sum of a number of $\Psi(\cdot,\cdot,\cdot)$ functions with non-negative arguments as follows

$$\Psi(\rho,\alpha,\beta) = \begin{cases} \Psi(\rho,\alpha,0) + \Psi(-\rho,\alpha,0) - \Psi(-\rho,\alpha,-\beta) & \alpha \geq 0, \beta < 0, \\ \Psi(\rho,0,\beta) + \Psi(-\rho,0,\beta) - \Psi(-\rho,-\alpha,\beta) & \alpha < 0, \beta \geq 0, \\ 1 - \Psi(\rho,0,-\beta) - \Psi(-\rho,0,-\beta) & \\ \quad -\Psi(\rho,-\alpha,0) - \Psi(-\rho,-\alpha,0) + \Psi(\rho,-\alpha,-\beta) & \alpha < 0, \beta < 0. \end{cases} \tag{4.12}$$

Therefore, the closed-form expression for the probability of the intersection of two pairwise error events can always be computed from (4.11).

4.5 Linear Block Codes and BPSK Signaling

4.5.1 Preliminaries

Since the number of the block PEPs grows exponentially in m, the computational complexity of the above bounds becomes prohibitive for large data blocks. In important special cases, such as when linear block codes and BPSK modulation are used or for geometrically uniform codes [55] with matched signaling [128], it is possible to consider only one codeword instead of the sums in (4.1) and (4.2). In other words, one can use

$$\text{BlER} = P_u\left(\bigcup_{i\neq u}\epsilon_{ui}\right), \quad \text{and} \quad \text{BER} = \frac{1}{m}\sum_{j=0}^{M-1} D_H(j,u)\left(1 - P_u\left(\bigcup_{i\neq j}\epsilon_{ji}\right)\right), \quad (4.13)$$

where $\boldsymbol{c}_u$ is *an arbitrary* codeword. Further simplification can be made by considering the all-zero codeword ($u = 0$) when binary modulation is used, because this will allow to benefit from information such as the weight distribution of codes to simplify or speed up analysis. We illustrate this in the following via reviewing Séguin's lower bound on the BlER of a coded BPSK modulated system with AWGN channel based on de Caen's lower bound on the probability of a union which is given in (2.3).

de Caen's lower bound can be used to derive a lower bound for the block error rate from

$$\text{BlER} = P_0\left(\bigcup_{i\neq 0}\epsilon_{0i}\right) \geq \sum_{i=1}^{M-1}\frac{P^2(\epsilon_{0i})}{\sum_{j=1}^{M-1}P(\epsilon_{0i}\cap\epsilon_{0j})}, \quad (4.14)$$

where, from [156],

$$P(\epsilon_{0i}) = Q\left(\sqrt{\frac{2E_b r_c}{N_0}W(\boldsymbol{c}_i)}\right),$$

and

$$P(\epsilon_{0i}\cap\epsilon_{0j}) = \Psi\left(\rho_{ij}, \sqrt{\frac{2E_b r_c}{N_0}W(\boldsymbol{c}_i)}, \sqrt{\frac{2E_b r_c}{N_0}W(\boldsymbol{c}_j)}\right),$$

where $W(\boldsymbol{c}_i)$ is the weight (i.e., the number of ones) of codeword $\boldsymbol{c}_j$ and

$$\rho_{ij} = \frac{W(\boldsymbol{c}_i) + W(\boldsymbol{c}_j) - W(\boldsymbol{c}_i + \boldsymbol{c}_j)}{2\sqrt{W(\boldsymbol{c}_i)W(\boldsymbol{c}_j)}}.$$

It is shown in [156] that $\Psi(\rho, x, y)$ is strictly increasing in the correlation coefficient ρ. This allows to compute an upper bound on ρ_{ij} and hence on $P(\epsilon_{0i} \cap \epsilon_{0j})$ on the denominator of (4.14) which depends only on the codeword weights and is therefore very fast to compute. The upper bound on ρ_{ij} is as follows

$$\rho_{ij} \leq \frac{W(\boldsymbol{c}_i) + W(\boldsymbol{c}_j) - D_{min}}{2\sqrt{W(\boldsymbol{c}_i)W(\boldsymbol{c}_j)}},$$

where D_{min} is the minimum weight of the code.

Finally, we present Cohen and Merhav's dot-product lower bound [30]. Assuming that $\boldsymbol{c}_0$ is sent, this bound reduces to

$$\text{BlER} \geq e^{(\beta' - 2\beta)E_b m} \sum_{i=1}^{M-1} \frac{Q^2(\kappa(\alpha, \boldsymbol{c}_i, N_0))}{\sum_{j=1}^{M-1} \Psi(\rho_{ij}, \kappa(\alpha', \boldsymbol{c}_i, N_0), \kappa(\alpha', \boldsymbol{c}_j, N_0))}, \tag{4.15}$$

where $\alpha = 1 + aN_0/2$, $\alpha' = 1 + aN_0$, $\beta = (1 - \alpha^2)/N_0$, $\beta' = (1 - (1 + aN_0)^2)/N_0$, and

$$\kappa(\alpha, \boldsymbol{c}_i, N_0) = 2\alpha\sqrt{\frac{E_b r_c W(\boldsymbol{c}_i)}{N_0}}.$$

Parameter a can be chosen to tighten the bound. The best value of a is found in [30] through an exhaustive search.

4.5.2 Evaluation of the Algorithmic Bounds for Large Blocks

It follows from (2.4) that evaluating the KAT bound on a subset of the codebook will result in a lower bound to the original KAT lower bound. This follows from

$$P\left(\bigcup_{i=1}^{M} A_i\right) \geq P\left(\bigcup_{i \in \mathcal{I}} A_i\right) \geq \text{KAT}\left(P(A_i), i \in \mathcal{I}\right),$$

where $\mathcal{I} \subseteq \{1, ..., M\}$. The above can be further tightened by

$$P\left(\bigcup_{i=1}^{M} A_i\right) \geq \max_{\mathcal{I}} \text{KAT}(P(A_i) : i \in \mathcal{I}).$$

The evaluation of the algorithmic Hunter and Kounias bounds may still be tedious for large m. It would be desirable to use only a subset of the codebook to compute these bounds. An examination of the lower bound in (2.2) directly indicates that computing this bound on a subset of the codebook will result in a lower bound for (2.2). We shall refer to this bound as the "Kounias lower bound, subset". It is exponentially expensive to find the optimal subset for the Kounias lower bound. To find a sub-optimal solution with a low complexity, one option is to employ the step-wise algorithm used in Subsection 2.1.3 to find a good (yet still sub-optimal) subset. A typical behavior of the application of the stepwise algorithm to the KAT bound is described in the following for a code with a small codebook size for clarification purposes. We have observed the same behavior for many other codes, such as Golay and BCH codes. Hamming (7, 4) code has 15 non-zero codewords and its generator matrix is given by

$$g = \begin{pmatrix} 1000101 \\ 0100111 \\ 0010110 \\ 0001011 \end{pmatrix}.$$

Table 4.1 shows the indices of the codewords for various codeword weights. Each index is the decimal equivalent of the data bits which correspond to a codeword (e.g., data bits 0001 are encoded into codeword 0001011, which has a weight of 3). Table 4.2 reports which codewords are chosen by the stepwise algorithm to compute the KAT lower bound. The

initial index sets are $\mathcal{I}_1 = \emptyset$ and $\mathcal{I}_2 = \mathcal{S} = \{1, ..., 15\}$. We notice that at low E_b/N_0 (e.g., -5 dB), only the closest codewords to codeword 0 are used. As the signal-to-noise ratio increases (e.g., at 4 dB), more codewords are added to the index set. Eventually, at hight E_b/N_0 (e.g., at 10 dB), the entire codebook is used to calculate the KAT lower bound. For the Golay (23, 12) code, using the codewords with weight 7 allows us to compute the KAT bound using 253 codewords instead of using 2047 codewords. For the BCH (63, 24) code, we only consider codewords of weight 15. There are only 651 codewords with this weight and computation of the KAT bound takes a very small amount of time and memory, while using the entire codebook of size 16777216 codewords is computationally not feasible.

If one evaluates the expression on the right hand side of (2.1) for a subset of the codebook, one will obtain neither an upper nor a lower bound. We will refer to this quantity as the "Hunter-based estimate". Restricting the maximization of the second sum (e.g., via Kruskal's algorithm) on the right hand side of (2.1) will lead to a loose upper bound. To tighten this bound, more nodes need to be added to the "sub-tree" which contains the nodes corresponding to the subset. Figure 4.1 demonstrates an idea to derive an upper bound based on Kruskal's algorithm. First, we consider a subset that contains the codewords with minimum weight and apply Kruskal's algorithm. This will maximize the sum of the second order PEPs for those codewords. We next consider the remaining codewords (whose weights are larger than D_{min}). Let $\boldsymbol{c}_i, i = 1, ..., I$ be the subset of the codewords with minimum weight and let $\boldsymbol{c}_j$ be a codeword not in this subset. For each j, we compute $P_{ij} \stackrel{\triangle}{=} P_0(\epsilon_{0i} \cap \epsilon_{0j})$ for $i = 1, ..., I$. To include every node j in the spanning tree, we add the edge with maximum P_{ij}.

4.6 Numerical Results

We consider a system with a uniform i.i.d. binary source, various channel codes, and 2- and 1-dimensional signaling. A typical plot for a two dimensional signaling scheme is shown in Figure 4.2, where the incoming bits are BCH (15, 5) coded, 8-PSK modulated, and sent over the AWGN channel. The entire codebook is used to calculate the bounds for this figure. We consider the Hunter upper bound and the Kounias, KAT and de Caen lower bounds and observe that the Kounias lower bound is the tightest among the lower bounds. A similar behavior is observed for other codes and code rates, such as that in Figure 4.3, which shows the bounds for a system with BCH (15, 7) code, AWGN channel, and BPSK modulation.

Figure 4.4 compares the result of computing the KAT lower bound using the entire codebook with that of using only the codewords with the minimum Hamming weight for the Golay (23, 12) code. For the subset, we only use the closest codewords to codeword $\boldsymbol{c}_0$ in the Hamming distance sense being motivated by the result of Table 4.2, which suggests that at low E_b/N_0, it is enough to consider the codewords with the minimum weight. Interestingly, we notice that the KAT bound computed on the subset, gives a *tighter* lower bound at low to moderate E_b/N_0 as compared with the KAT bound computed on the codebook and also the best lower bound in [30]. As predicted by Table 4.2, at high E_b/N_0, the KAT bound used on the entire codebook is slightly tighter; but this tightness is achieved at the price of having a much higher complexity and the improvement is almost negligible.

Figures 4.5, 4.6, and 4.7 compare the tightness of the BlER bounds for the case where only a subset of the codebook is used to compute the bounds for the Golay (23, 12), BCH

(31, 16), and BCH (63, 24) codes, respectively. BPSK modulation is used, hence the lower bound of [156] can also be computed. The Kounias and KAT lower bounds (using a subset of the closest codewords) are still tight, but the Hunter upper bound is loose at low E_b/N_0. Poltyrev's upper bound [149] is superior to the Hunter upper bound optimized on the subset, although they are both the same as the union bound at BlER values of interest (BlER $< 10^{-3}$). Note first that the Hunter upper bound is easier to compute than Poltyrev's; therefore, it is the choice at BlER values of interest. Second, the KAT and Kounias lower bounds are tighter than Séguin's bound; hence they are also tighter than Shannon's lower bound [164] at least at medium to high E_b/N_0. Also notice that the KAT bound is always tighter than the Cohen and Merhav (dot-product) lower bound of [30].

Figures 4.8 and 4.9 demonstrate the performance of the union, Hunter, Kounias, KAT, and Séguin bounds for the Rayleigh fading channel for Hamming (7, 4) and BCH (15, 5) codes. The Kounias lower bound is still tight, but the Hunter upper bound is not as tight for the Rayleigh fading channel, suggesting that the higher order probabilities are significant in the block fading case. As for the BER, we observe in our calculations that the upper bound (resulting from the Kounias lower bound) is tight, but the lower bound (derived from the Hunter upper bound) is too loose to be useful.

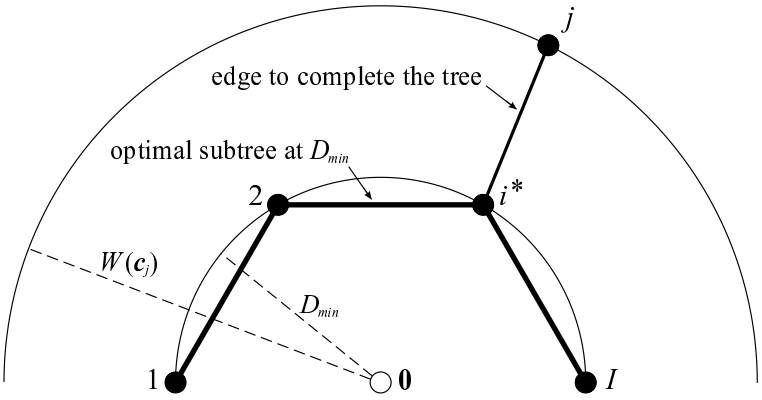

Figure 4.1: The idea to form a spanning tree and compute an upper bound for the BlER. i^* is the index of codeword $\boldsymbol{c}_{i^*}$ for which $P_{i^*j} \geq P_{ij}, i = 1, ..., I$.

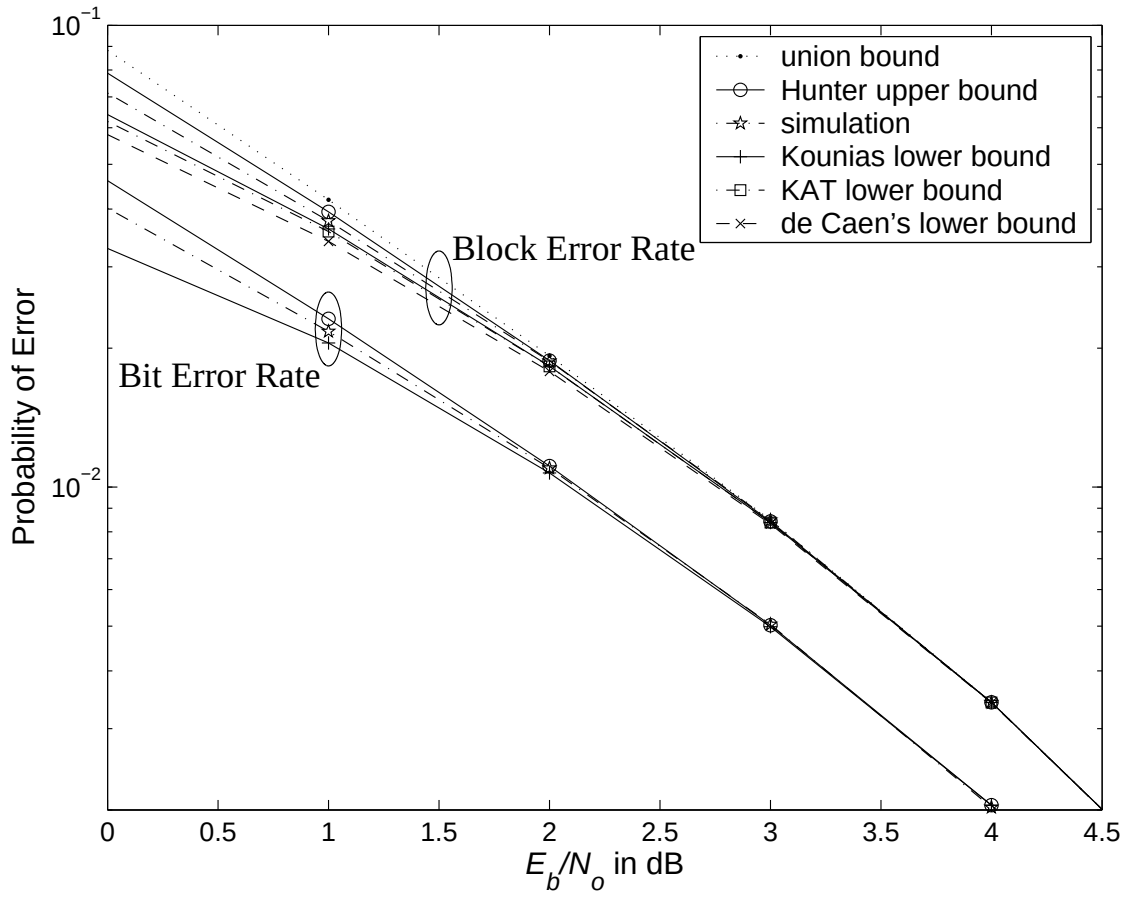

Figure 4.2: Block and bit error rate curves for BCH (15, 5) code, 8-PSK modulation, and AWGN channel.

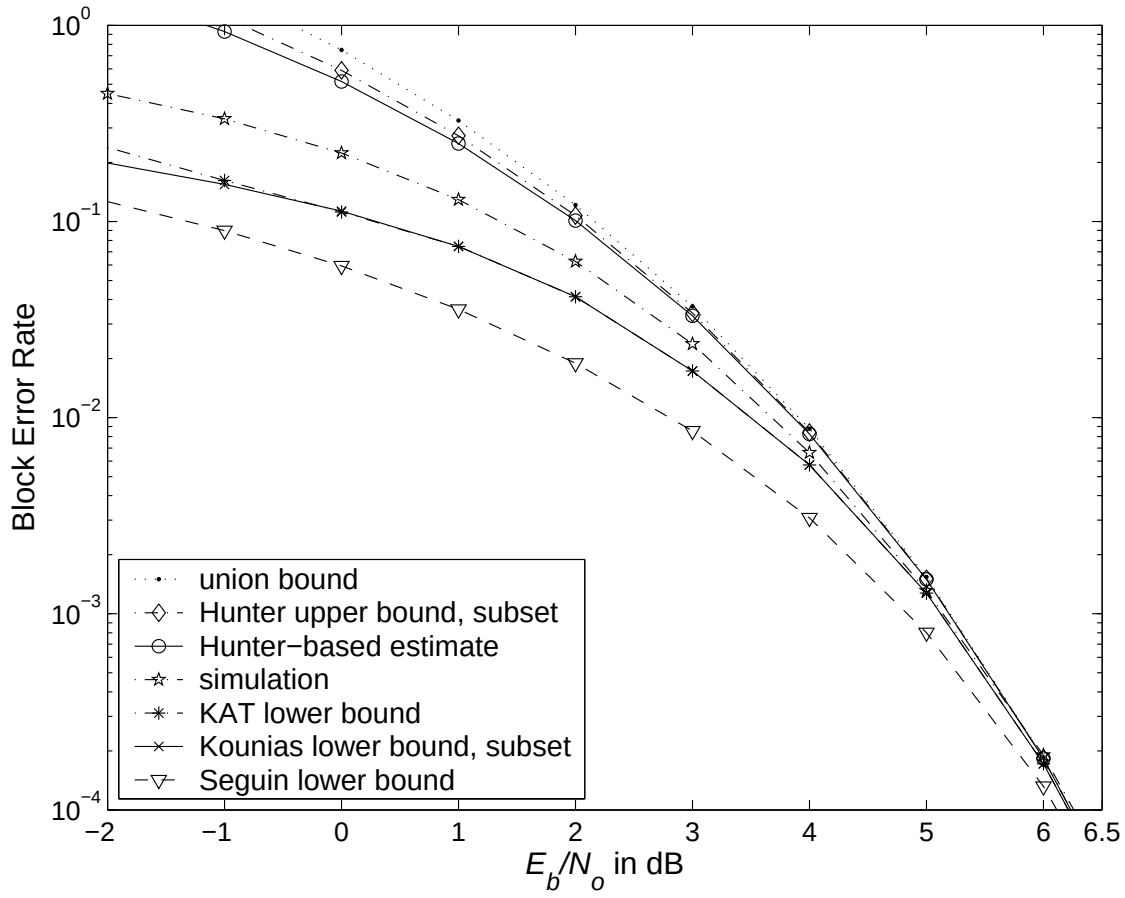

Figure 4.3: Block error rate curves for BCH (15, 7) code, BPSK modulation, and AWGN channel.

codeword weight	data bits (in decimal)
3	1, 2, 5, 6, 8, 11, 12
4	3, 4, 7, 9, 10, 13, 14
7	15

Table 4.1: The data bits (in decimal) corresponding to various codeword weights for Hamming (7, 4) code.

E_b/N_0	codeword indices
-5 dB	1, 2, 5, 6, 8, 11, 12
4 dB	1, 2, 5, 6, 8, 9, 10, 11, 12, 14
10 dB	1, 2, 3, 4, 5, 6, 7, 8, 9, 10, 11, 12, 13, 14, 15

Table 4.2: Codewords used in the optimization of the KAT bound via the stepwise algorithm. Only the closest codewords are selected at low E_b/N_0, while the whole codebook is used at high E_b/N_0.

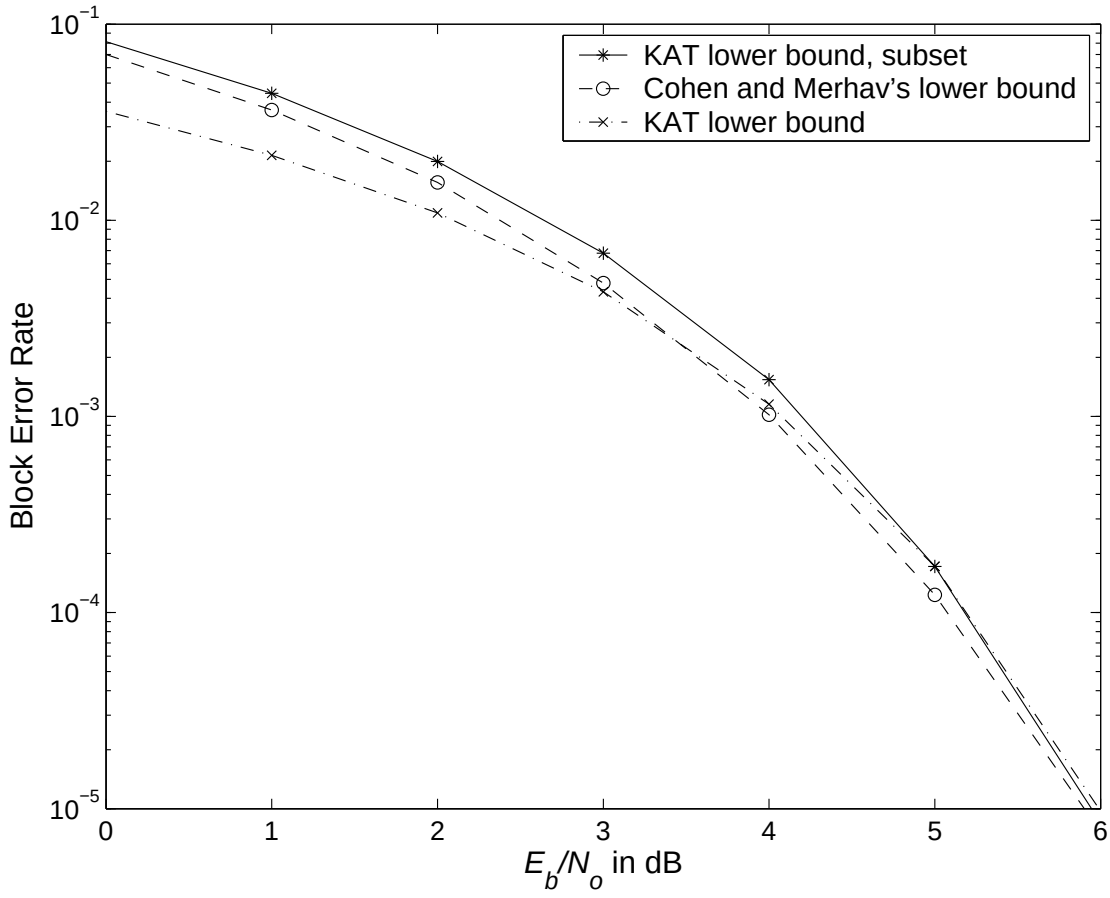

Figure 4.4: Comparison among three lower bounds on the BlER. Golay (23, 12) code, BPSK signaling, and AWGN channel.

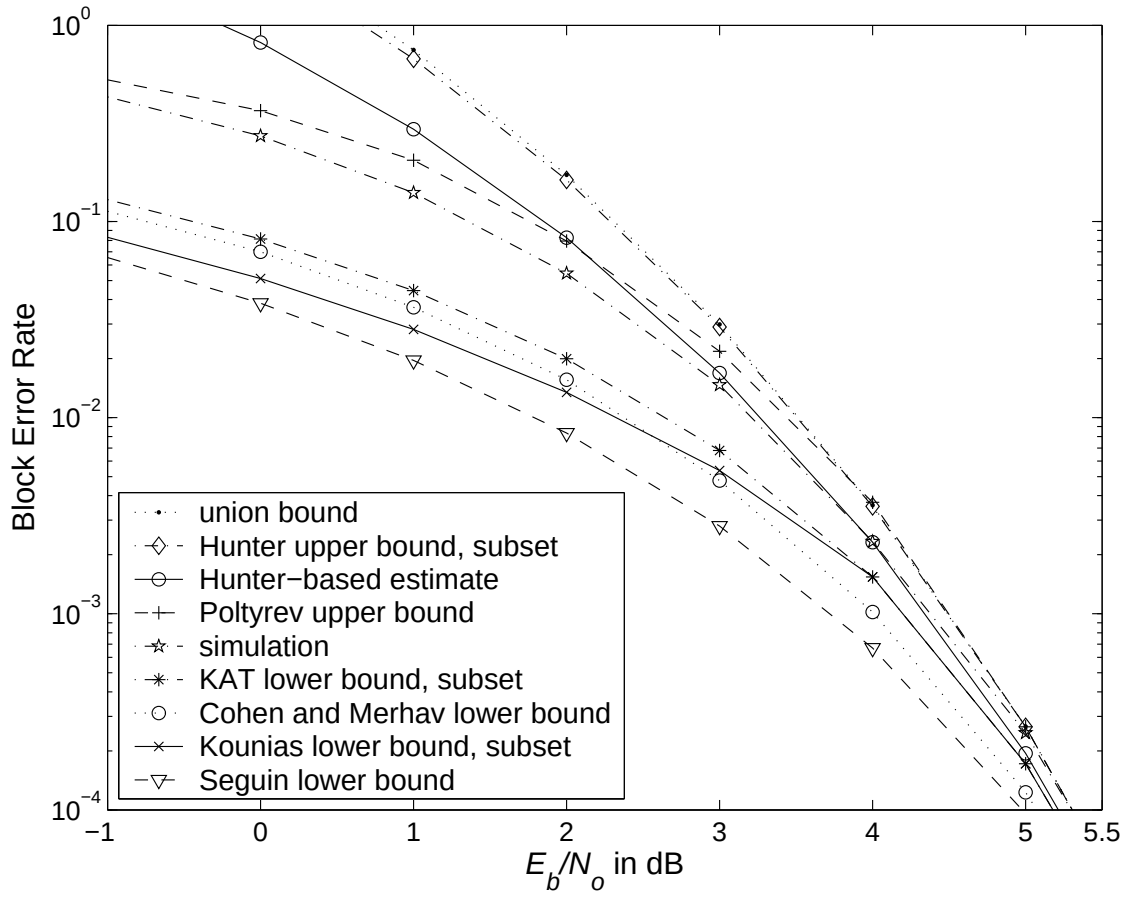

Figure 4.5: Block error rate bounds for Golay (23, 12) code, BPSK signaling, and AWGN channel.

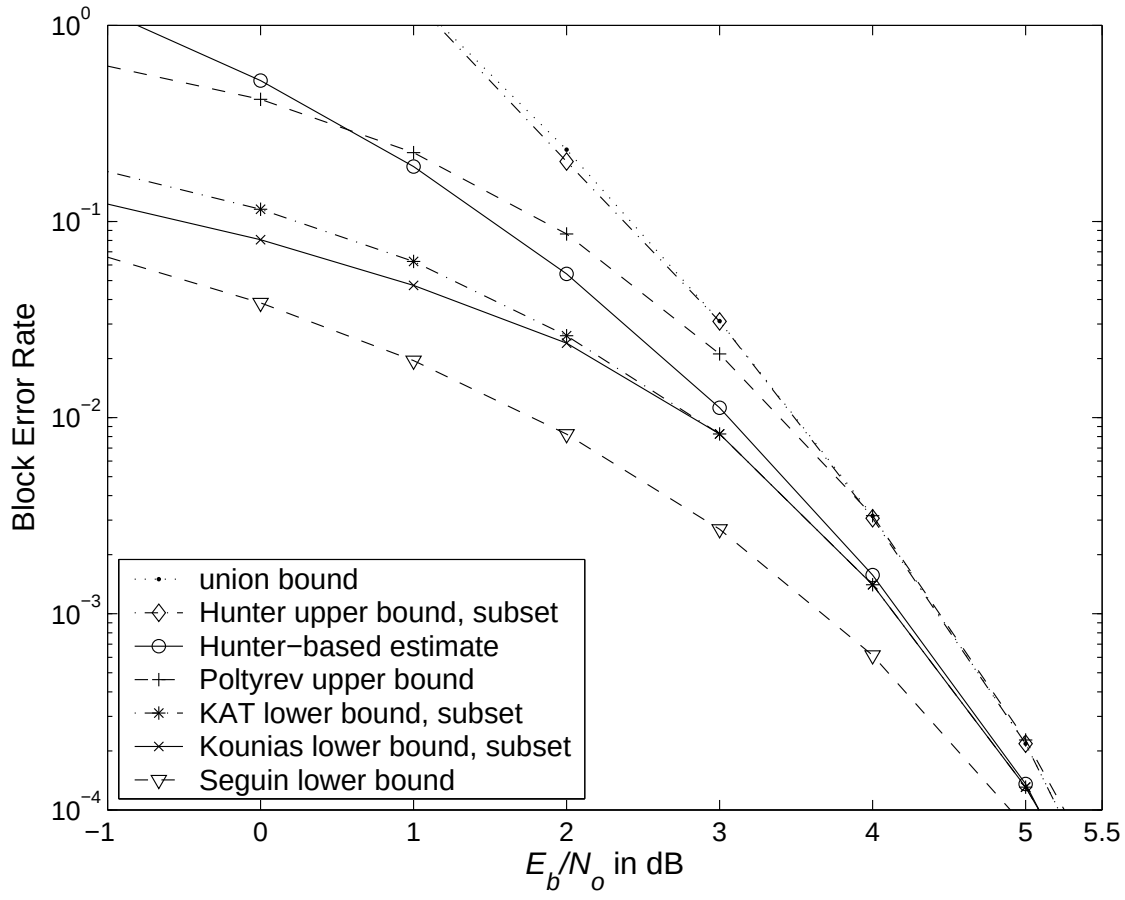

Figure 4.6: Block error rate bounds for BCH (31, 16) code, BPSK signaling, and AWGN channel.

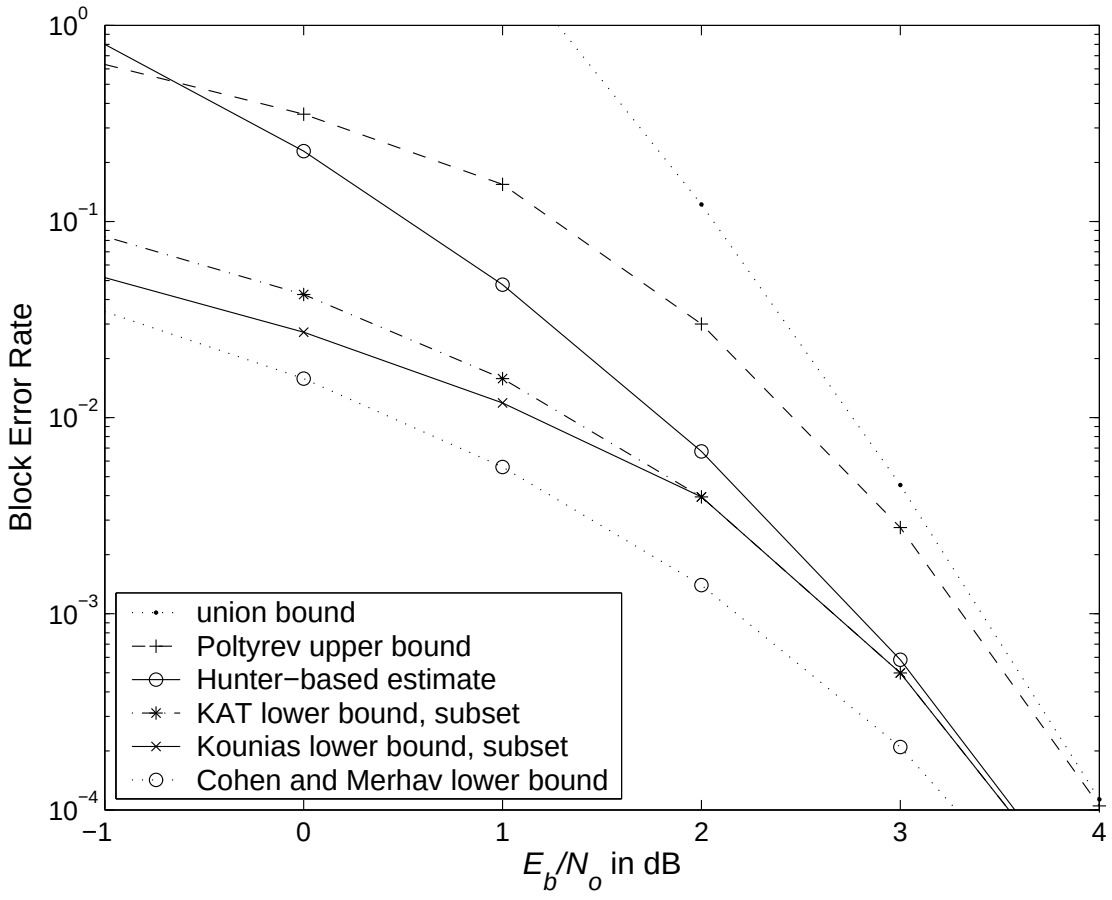

Figure 4.7: Block error rate bounds for BCH (63, 24) code, BPSK signaling, and AWGN channel.

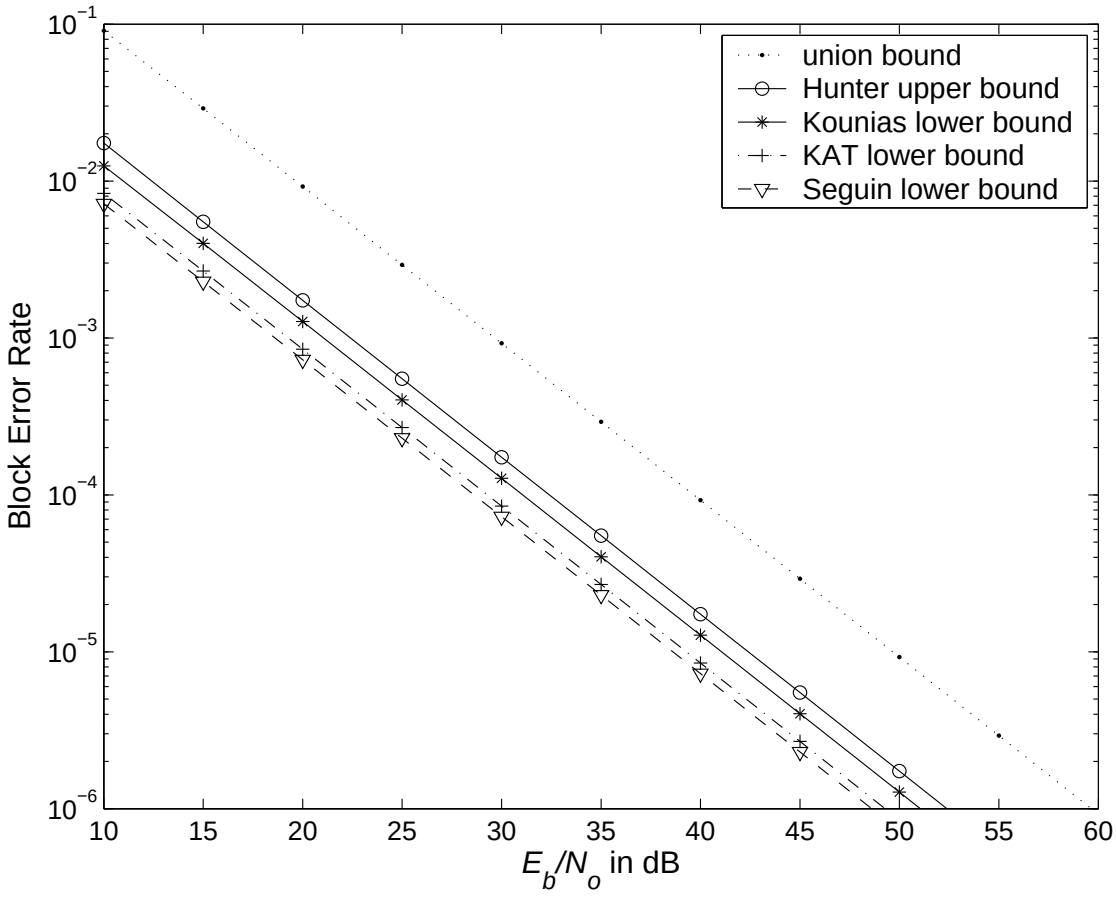

Figure 4.8: Block error rate bounds for Hamming (7, 4) code, BPSK signaling, and Rayleigh fading channel.

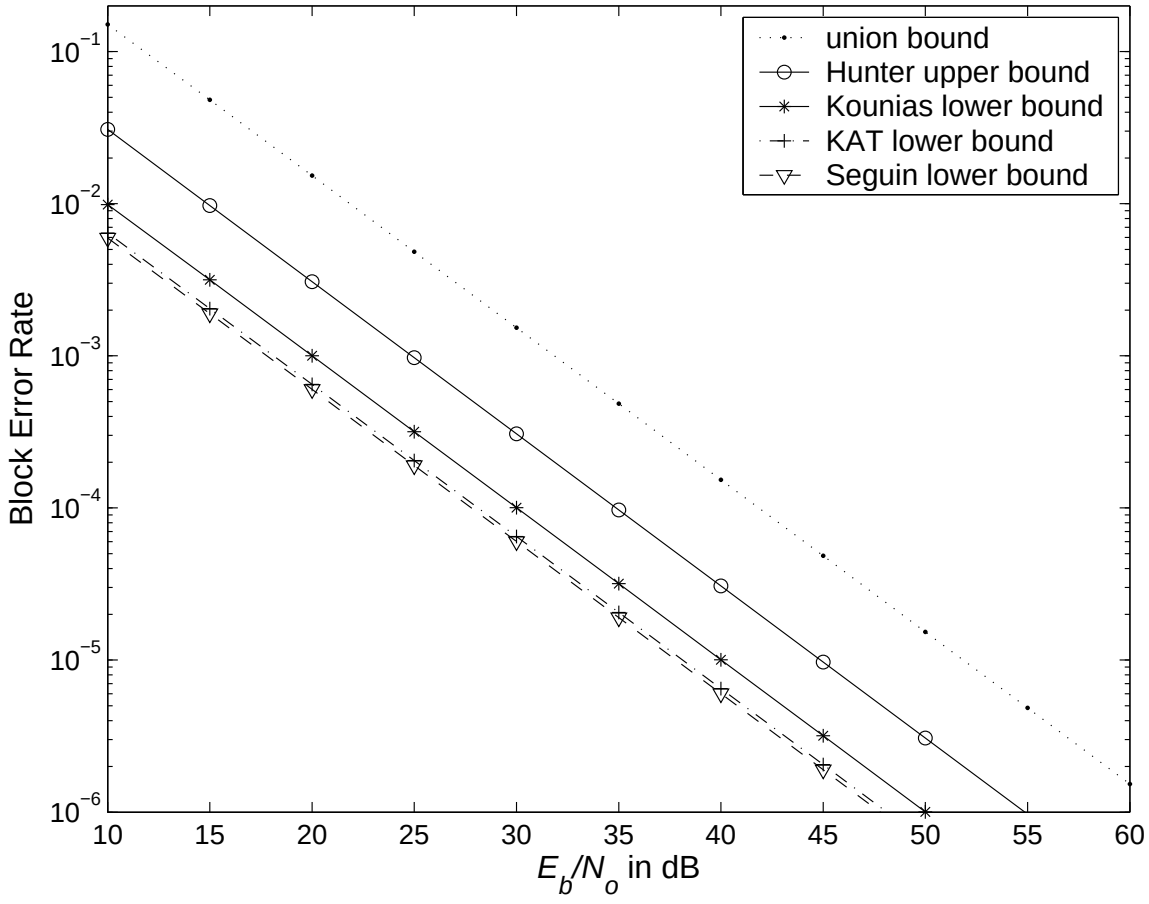

Figure 4.9: Block error rate bounds for BCH (15, 5) code, BPSK signaling, and Rayleigh fading channel.

Chapter 5

Bounds for the Symbol and Bit Error Rates of Space-Time Orthogonal Block Codes

5.1 Introduction

The original papers on space-time trellis codes [194] and space-time orthogonal block codes [192] adopt the Chernoff upper bound to estimate the pairwise error probability of codewords and to establish code design criteria. Although the Chernoff bound yields successful code constructions, it is quite loose even at high values of the channel signal-to-noise ratio. Furthermore, it is common practice to use the union bound to approximate the symbol error rate or bit error rate. However, the union bound is loose, particularly at low CSNRs. Therefore, using the Chernoff bound together with the union bound may result in

poor approximations to system performance (see, e.g., Section 5.4).

With respect to the SER/BER analysis of space-time orthogonal block codes, one can use the closed-form conditional SER formulas in [175] (see (1.2) and (1.3)) and average them over the fading coefficients distribution to derive exact SER formulas for standard PSK and square 2^{2m}-ary QAM, where m is a positive integer; this approach is taken in [167]. However, the resulting SER formulas do not hold for arbitrary constellations such as star-QAM and it is not clear how to extend this approach to evaluate the BER, specially if Gray mapping is not used. The symbol PEPs can be used to derive an upper bound on the BER; however, as will be shown in the sequel, the resulting BER upper bound is very loose even at medium CSNRs.

In this chapter, we show how to use the symbol PEP results to derive bounds for the SER and BER of STOB codes via establishing the Hunter and Kounias bounds. One important feature of the bounds is that they hold for arbitrary constellations and signal mappings since they do not depend on the geometry of the system at hand. Numerical results indicate that the bounds for STOB codes often *coincide* with the true error probabilities obtained via simulations even at low CSNRs. Furthermore, the computational complexity of these algorithmic bounds is very modest even for large constellations and larger number of antennas.

The approach presented in the previous chapter can also be applied to study the error rate of space-time orthogonal block coded MIMO channels used in conjunction with error-control block codes; we however do not consider this for the sake of simplicity.

5.2 Bounds on the Codeword Pairwise Error Probability of Space-Time Orthogonal Block Codes

Let us denote two STOB codewords by $\boldsymbol{S}$ and $\hat{\boldsymbol{S}}$, and define matrix $\mathbf{D} = [d_{i,t}]$ with $d_{i,t} = s_{i,t} - \hat{s}_{i,t}$ and matrix $\mathbf{U} = \mathbf{D}\mathbf{D}^{\dagger}$. For STOB codes, $\mathbf{U}$ has only one eigenvalue λ with multiplicity K. To verify this point, we note that a STOB codeword has the property that $\boldsymbol{S}\boldsymbol{S}^{\dagger} = \|\boldsymbol{S}\|^2\mathbf{I}_K$, hence we have

$$\mathbf{U} = \mathbf{D}\mathbf{D}^{\dagger} = (\boldsymbol{S} - \hat{\boldsymbol{S}})(\boldsymbol{S} - \hat{\boldsymbol{S}})^{\dagger} = (\|\boldsymbol{S}\|^2 + \|\hat{\boldsymbol{S}}\|^2)\mathbf{I}_K,$$

which indicates that

$$\lambda_1 = \cdots = \lambda_K \stackrel{\triangle}{=} \lambda = \|\boldsymbol{S}\|^2 + \|\hat{\boldsymbol{S}}\|^2.$$

It is shown in [131] that the PEP between $\boldsymbol{S}$ and $\hat{\boldsymbol{S}}$ is given by

$$P(\boldsymbol{S} \to \hat{\boldsymbol{S}}) = \frac{1}{\pi}\int_0^{\frac{\pi}{2}} \left(\frac{\sin^2\theta}{\frac{1}{4}\gamma_s\lambda + \sin^2\theta}\right)^n d\theta. \tag{5.1}$$

A lower bound is given in [131] which is derived by replacing $\sin^2\theta$ at the denominator of (5.1) by 1, resulting in

$$P(\boldsymbol{S} \to \hat{\boldsymbol{S}}) > \frac{\kappa}{2}\left(1 + \frac{1}{4}\gamma_s\lambda\right)^{-n},$$

where $\kappa = 4^{-n}\binom{2n}{n}$. A simple upper bound can be derived by minimizing the denominator of (5.1), i.e., by replacing $\sin^2\theta$ by zero, to get

$$P(\boldsymbol{S} \to \hat{\boldsymbol{S}}) < \frac{\kappa}{2}\left(\frac{1}{4}\gamma_s\lambda\right)^{-n}. \tag{5.2}$$

Note that as the CSNR grows, the above upper and lower bounds converge. Figure 5.1 shows a typical behavior of the above bounds for the codewords $\boldsymbol{S} = \left(\begin{smallmatrix} 1 & -1 \\ 1 & 1 \end{smallmatrix}\right)$ and $\hat{\boldsymbol{S}} =$

$\begin{pmatrix} -i & -i \\ -i & i \end{pmatrix}$ for Alamouti's scheme with one receive antenna and quadrature phase-shift keying (Q-PSK) signaling. The tightness of the new upper bound and the lower bound in [131] is obvious. Our upper bound is closer to the actual PEP at medium to high CSNR and can be used for space-time code design as in [131].

5.3 Bounds on the Error Rates of Space-Time Orthogonal Block Codes

In this section, we show how the approach of the previous chapter for the Hunter upper and Kounias lower bounds can be used for space-time orthogonal block codes.

5.3.1 The Symbol Error Rate

Following the approach in (4.1), for a constellation $\{c_i, i = 1, ..., M\}$, where $m = \log_2(M)$ is a positive integer, and a uniform i.i.d. bit-stream, the SER is given by

$$\text{SER} = \frac{1}{M} \sum_{u=1}^{M} P_u \left(\bigcup_{i \neq u} \epsilon_{ui} \right). \tag{5.3}$$

$P_u(\epsilon_{ui})$ is the PEP and is given in (3.18). In order to find lower and upper bounds on the probability of each union in (5.3) via (2.2) and (2.1), respectively, we also need to find the probability of the intersection of ϵ_{ui} and ϵ_{uj}, the second order PEP of symbols c_i and c_j with c_u. This probability can be derived from

$$P_u(\epsilon_{iu} \cap \epsilon_{ju}) = \mathrm{E}_Y \left\{ \Psi \left(\rho_{iju}, \delta_{iu}\sqrt{Y}, \delta_{ju}\sqrt{Y} \right) \right\}, \tag{5.4}$$

where

$$\rho_{iju} = \frac{\langle c_i - c_u, c_j - c_u \rangle}{|c_i - c_u||c_j - c_u|},$$

$\langle x, y \rangle = \Re\{x\}\Re\{y\} + \Im\{x\}\Im\{y\}$ ($\Re\{\cdot\}$ and $\Im\{\cdot\}$ are the real and imaginary parts, respectively), Y is defined in (3.15), and $\Psi(\rho, \phi_i(y), \phi_j(y))$ is the bivariate Gaussian function (given in (4.7)) with $\phi_i(y) = \delta_{iu}\sqrt{y}$. As $\phi_i(y)$ and $\phi_j(y)$ are non-negative, we can use the result of [174] to write $\Psi(\rho, \phi_i(y), \phi_j(y))$ as

$$\begin{aligned} \Psi\left(\rho, \delta_{iu}\sqrt{y}, \delta_{ju}\sqrt{y}\right) &= \frac{1}{2\pi}\int_0^{\varphi\left(\frac{d_{iu}}{d_{ju}}, \rho\right)} \exp\left(\frac{-\delta_{iu}^2}{2\sin^2\theta} y\right) d\theta \\ &\quad + \frac{1}{2\pi}\int_0^{\varphi\left(\frac{d_{ju}}{d_{iu}}, \rho\right)} \exp\left(\frac{-\delta_{ju}^2}{2\sin^2\theta} y\right) d\theta, \end{aligned} \tag{5.5}$$

where $d_{iu} = |c_i - c_u|$, $\varphi(x, \rho) = \tan^{-1}\left(x\sqrt{1-\rho^2}/(1-\rho x)\right)$, and $\tan^{-1}(x)$ is as redefined below (4.10). Using the pdf of Y in (3.16), we find the expected value of each of the integrals in (5.5) as follows.

$$\begin{aligned} E_Y\left[\int_0^{\varphi} e^{-a(\theta)Y} d\theta\right] &= \frac{1}{(n-1)!}\int_0^{\infty} y^{n-1}e^{-y}\int_0^{\varphi} e^{-a(\theta)y} d\theta dy \\ &= \frac{1}{(n-1)!}\int_0^{\varphi}\int_0^{\infty} y^{n-1}e^{-(1+a(\theta))y} dy d\theta \qquad (5.6) \\ &= \int_0^{\varphi}\left(\frac{1}{1+a(\theta)}\right)^n d\theta, \qquad (5.7) \end{aligned}$$

where $a(\theta)$ is a given non-negative function of θ. The step from (5.6) to (5.7) follows by writing the inner integral in (5.6) in terms of the $(n-1)^{\text{st}}$ derivative of the Laplace transform of the unit step function. Using (5.7) with $a(\theta) = \delta^2/2\sin^2\theta$ and [175, Eq. 5A.35], we

have

$$\begin{aligned} I(\varphi,\delta) &\triangleq \frac{1}{2\pi}\int_0^{\varphi}\left(\frac{2\sin^2\theta}{\delta^2+2\sin^2\theta}\right)^n d\theta \\ &= \frac{\varphi}{2\pi}-\frac{\beta}{2\pi}\frac{\delta}{\sqrt{2+\delta^2}}\sum_{k=0}^{n-1}\binom{2k}{k}\frac{1}{(2(2+\delta^2))^k} \\ &\quad -\frac{\delta}{\pi\sqrt{2+\delta^2}}\sum_{k=0}^{n-1}\sum_{m=0}^{k-1}\binom{2k}{m}\frac{(-1)^{m+k}}{(2(2+\delta^2))^k}\frac{\sin[2\beta(k-m)]}{2(k-m)}, \end{aligned} \tag{5.8}$$

where

$$\beta=\frac{1}{2}\tan^{-1}\frac{A}{B}+\frac{\pi}{2}\left[1-\left(\frac{1+\mathrm{sgn}(B)}{2}\right)\mathrm{sgn}(A)\right],$$

with $A=\delta\sqrt{2+\delta^2}\sin 2\varphi$, $B=(1+\delta^2)\cos 2\varphi-1$, and $\mathrm{sgn}(x)\triangleq |x|/x$ if $x\neq 0$ and 0 otherwise. From (5.4) and (5.5), we obtain the following expression for the second order PEP

$$P_u(\epsilon_{iu}\cap\epsilon_{ju})=I\left(\varphi\left(\frac{\delta_{iu}}{\delta_{ju}},\rho_{iju}\right),\delta_{iu}\right)+I\left(\varphi\left(\frac{\delta_{ju}}{\delta_{iu}},\rho_{iju}\right),\delta_{ju}\right), \tag{5.9}$$

where $I(\cdot,\cdot)$ is defined in (5.8).

5.3.2 The Bit Error Rate

The same algorithm can be used as outlined in the previous chapter to estimate the BER. We have

$$\mathrm{BER}=\frac{1}{M}\sum_{u=1}^{M}P_u(\epsilon^{(b)}),$$

where $P_u(\epsilon^{(b)})$ is the bit error probability when c_u is sent and is given by

$$P_u(\epsilon^{(b)})=\frac{1}{m}\sum_{j=1}^{M}D_H(j,u)P(\hat{c}=c_j|c=c_u)=\frac{1}{m}\sum_{j=1}^{M}D_H(j,u)\left(1-P_u\left(\bigcup_{i\neq j}\epsilon_{ij}\right)\right), \tag{5.10}$$

where $D_H(j,u)$ is the Hamming distance between the bit assignments of c_j and c_u. From the above, it is clear that finding upper and lower bounds on the BER requires evaluating lower and upper bounds on the probability of the union in (5.10), respectively. These bounds, in turn, require the computation of

$$\begin{aligned} P_u(\epsilon_{ij}) &= E_Y\left\{Q\left(\frac{\delta_{iu}^2-\delta_{ju}^2}{\delta_{ij}}\sqrt{Y}\right)\right\} \\ &= \frac{1}{2}\left(1-\sqrt{\frac{\delta_{iu}^2-\delta_{ju}^2}{(\delta_{iu}^2-\delta_{ju}^2)^2-2\delta_{ij}^2}}\right)\sum_{k=0}^{KL-1}\binom{2k}{k}\left(\frac{\delta_{ij}^2}{2((\delta_{iu}^2-\delta_{ju}^2)^2+2\delta_{ij}^2)}\right)^k, \end{aligned}$$

as well as

$$\begin{aligned} P_u(\epsilon_{ij}\cap\epsilon_{kj}) &= E_Y\left\{\Psi\left(\rho_{ikj},\frac{\delta_{iu}^2-\delta_{ju}^2}{\delta_{ij}}\sqrt{Y},\frac{\delta_{ku}^2-\delta_{ju}^2}{\delta_{kj}}\sqrt{Y}\right)\right\} \\ &= I\left(\varphi\left(\frac{\delta_{kj}(\delta_{iu}^2-\delta_{ju}^2)}{\delta_{ij}(\delta_{ku}^2-\delta_{ju}^2)},\rho_{ikj}\right),\frac{\delta_{iu}^2-\delta_{ju}^2}{\delta_{ij}}\right) \\ &\quad +I\left(\varphi\left(\frac{\delta_{ij}(\delta_{ku}^2-\delta_{ju}^2)}{\delta_{kj}(\delta_{iu}^2-\delta_{ju}^2)},\rho_{ikj}\right),\frac{\delta_{ku}^2-\delta_{ju}^2}{\delta_{kj}}\right), \end{aligned} \tag{5.11}$$

where $I(\cdot,\cdot)$ is defined in (5.8). Equation (5.11) holds when the second and the third arguments of $\Psi(\cdot,\cdot,\cdot)$ are non-negative. Negative arguments should be dealt with as explained below (4.12), showing that, in any case, an expression exists for the second order PEP.

5.4 Numerical Results

For this part, the length of the input bit-sequence is max(100000, 100 $\times$ BER^{-1}). The computation time of the algorithmic Bonferroni bounds is negligible for our code that is written in C and runs on a SUN Ultra 60 machine. The Chernoff and the union bounds are also given for the SER.

The SER and BER versus CSNR curves are presented in Figures 5.5 through 5.9 for various K, L, space-time codes, and M-ary PSK and QAM constellations with Gray mapping. Figures 5.5 and 5.6 show the performance of Alamouti's $\mathcal{G}^2$ code [9], while the performance of the codes $\mathcal{G}^3$ and $\mathcal{G}^4$ of [192] are presented in Figures 5.7 and 5.9, respectively. The Hunter and Kounias bounds for both SER and BER curves are very tight and can hardly be distinguished from each other and from the performance curve obtained via simulation. It can be seen that as the constellation size grows, the union bound becomes less reliable and the Chernoff bound gets farther from the other curves, while the lower and upper bounds remain very tight. Figure 5.7 shows the BER upper and lower bounds as well as simulation results for a system with three transmit and $L = 1, 2,$ and 4 receive antennas for a wide range of CSNRs. The bounds are tight even at negative CSNR values and high diversity orders. Notice that the Star 8-QAM constellation of Figure 5.9 (with signal points and mappings as depicted in Figure 5.8) is not a regular square QAM nor 8-PSK, but the bounds are still very tight.

An upper bound on the BER can be computed by upper bounding $P(\hat{c} = c_j | c = c_u)$ in (5.10) by the PEP to get

$$\text{BER} \leq \frac{1}{Mm} \sum_{u} \sum_{j} D_H(u, j) P(c_u \to c_j).$$

This bound is also plotted in all figures. It is clearly observed that our upper bound is much tighter, particularly for larger constellations.

As Gray mapping is used in the above systems, it is expected that at high enough CSNRs the BER of PSK-modulated systems converges to [150] BER $\approx \frac{1}{m}$ SER, where 2^m is the constellation size. The curves labeled with "SER/m" in Figure 5.5 show this approxima-

tion. We also observe that as the constellation size shrinks or the number of the receive antennas grows, this estimate becomes tighter. Therefore, at high enough CSNR values, it would be enough to find only one of the SER bounds to obtain a good estimate of system SER and BER. For example, for 16-PSK signaling and at a CSNR of 15 dB, the coinciding SER lower and upper bounds are equal to 0.195682. The above approximation yields BER $\approx$ 0.048921, while the lower and upper bounds on the BER coincide and equal 0.051838. It is also important to note that although we have presented the BER results for the Gray signal mapping (except for Figure 5.9), our bounds also apply to any other mapping and show the same behavior.

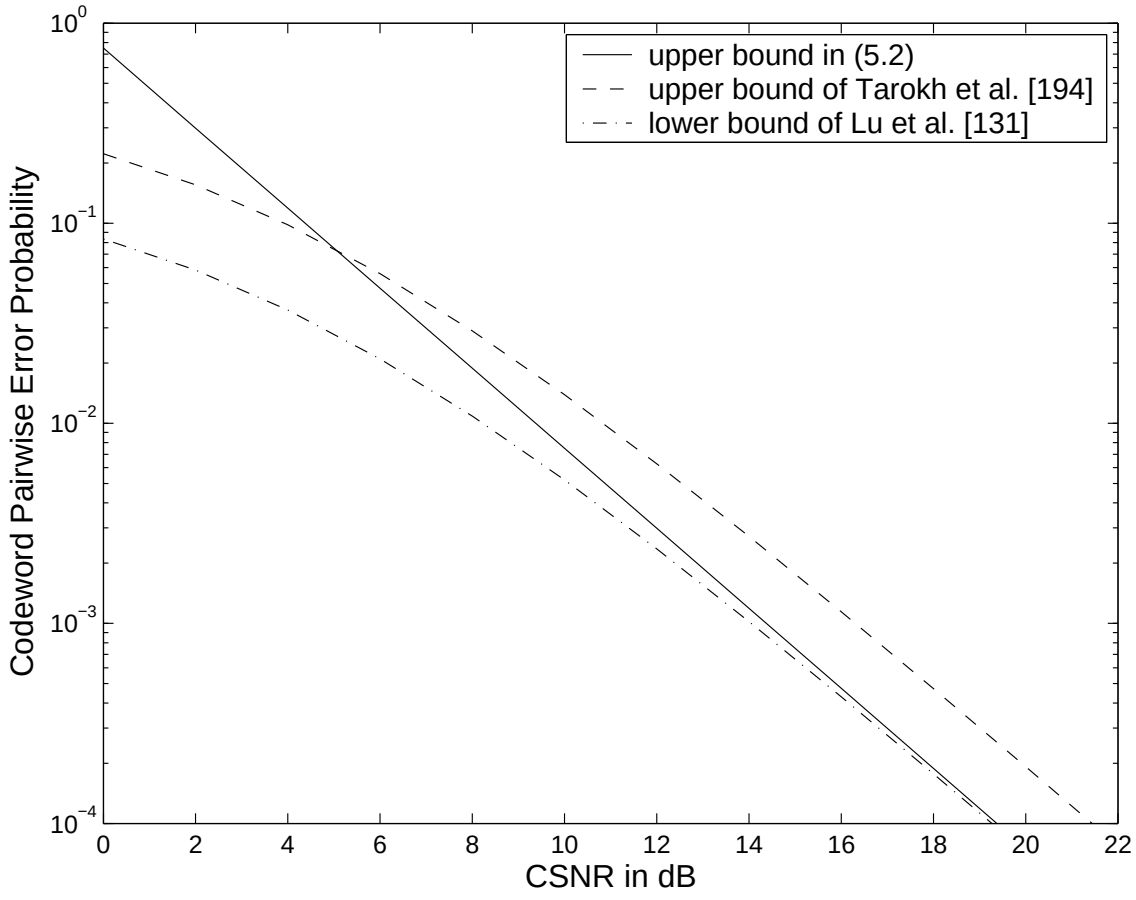

Figure 5.1: Our upper bound and the lower bounds on $P\left(\left(\begin{smallmatrix}1 & -1\\ 1 & 1\end{smallmatrix}\right) \rightarrow \left(\begin{smallmatrix}-i & -i\\ -i & i\end{smallmatrix}\right)\right)$, Alamouti's code with Q-PSK modulation, $K = 2$, and $L = 1$.

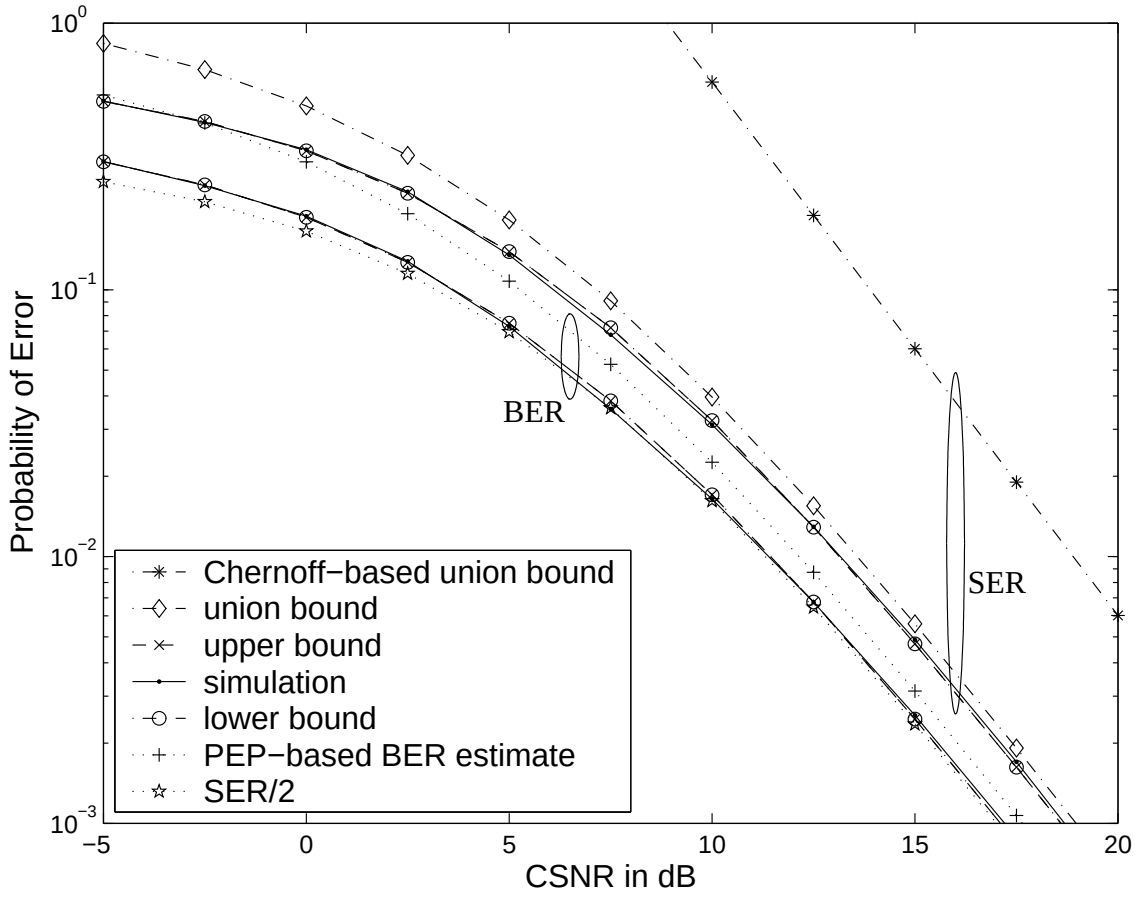

Figure 5.2: Results for Q-PSK signaling with $K = 2$ and $L = 1$ (2 bits/s/Hz).

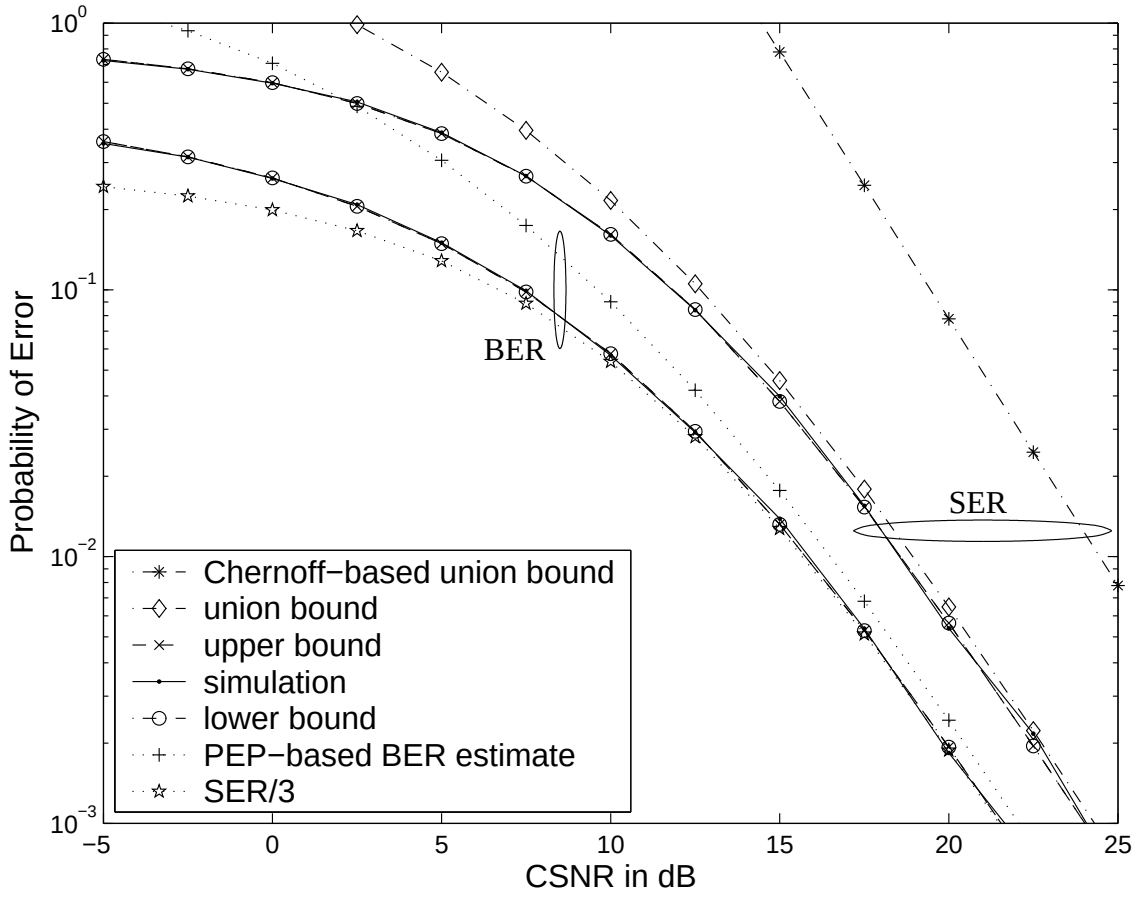

Figure 5.3: Results for 8-PSK signaling with $K = 2$ and $L = 1$ (3 bits/s/Hz).

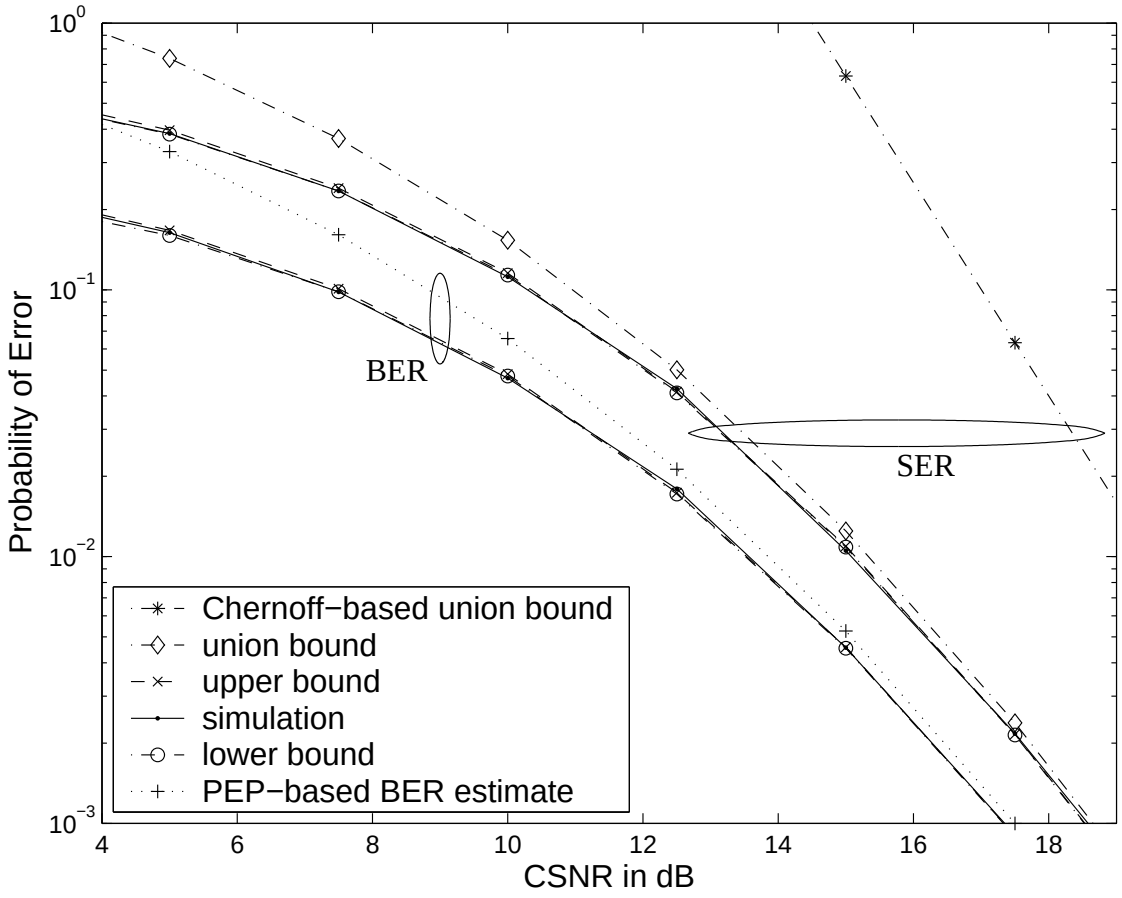

Figure 5.4: Results for 16-QAM signaling with $K = 2$ and $L = 2$ (4 bits/s/Hz).

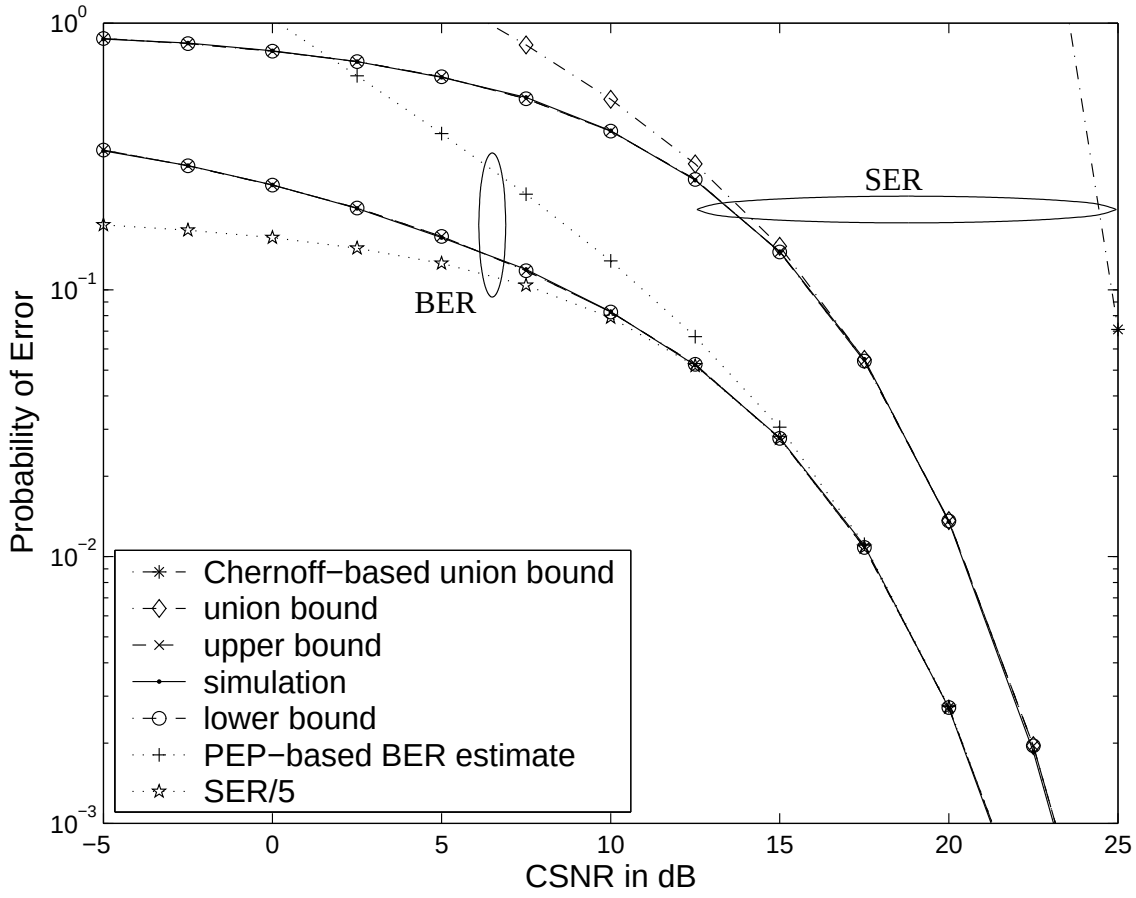

Figure 5.5: Results for 32-PSK signaling with $K = 2$ and $L = 4$ (5 bits/s/Hz).

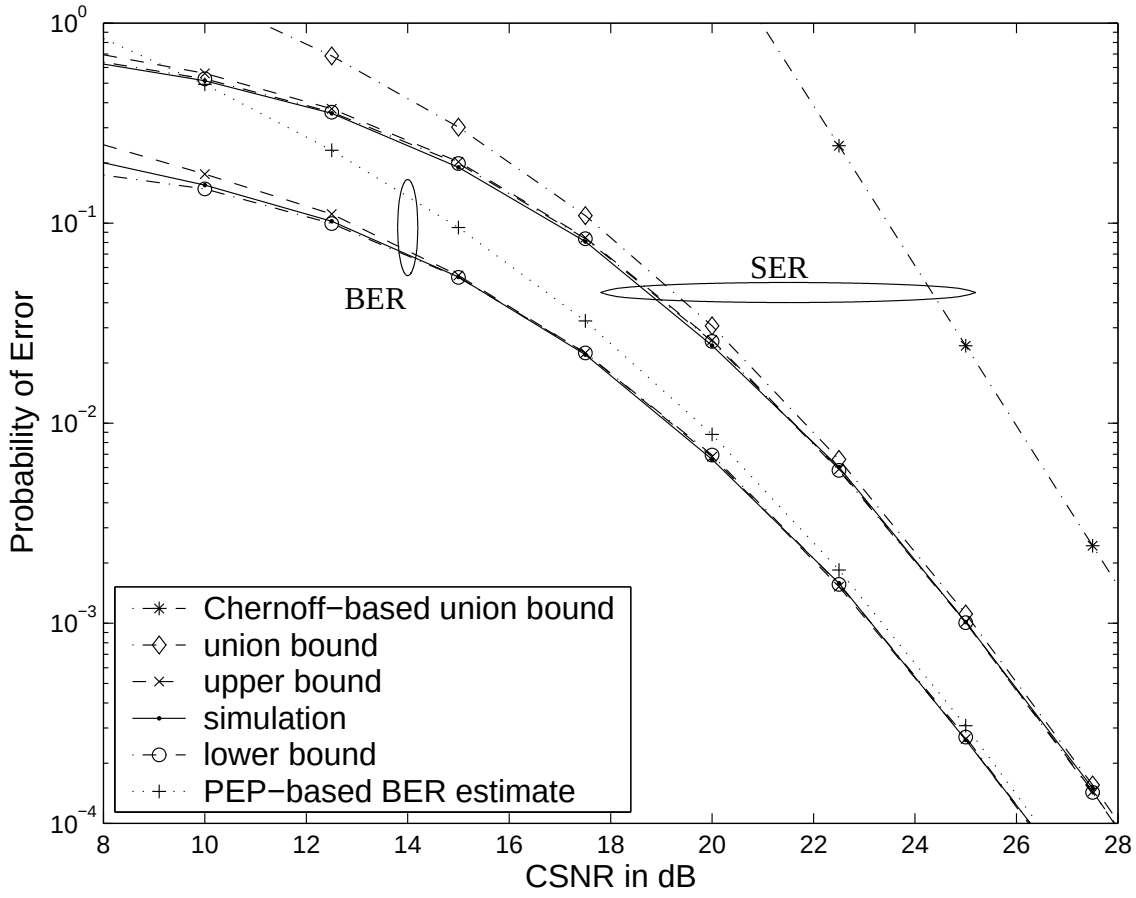

Figure 5.6: Results for 64-QAM signaling with $K = 2$ and $L = 2$ (6 bits/s/Hz).

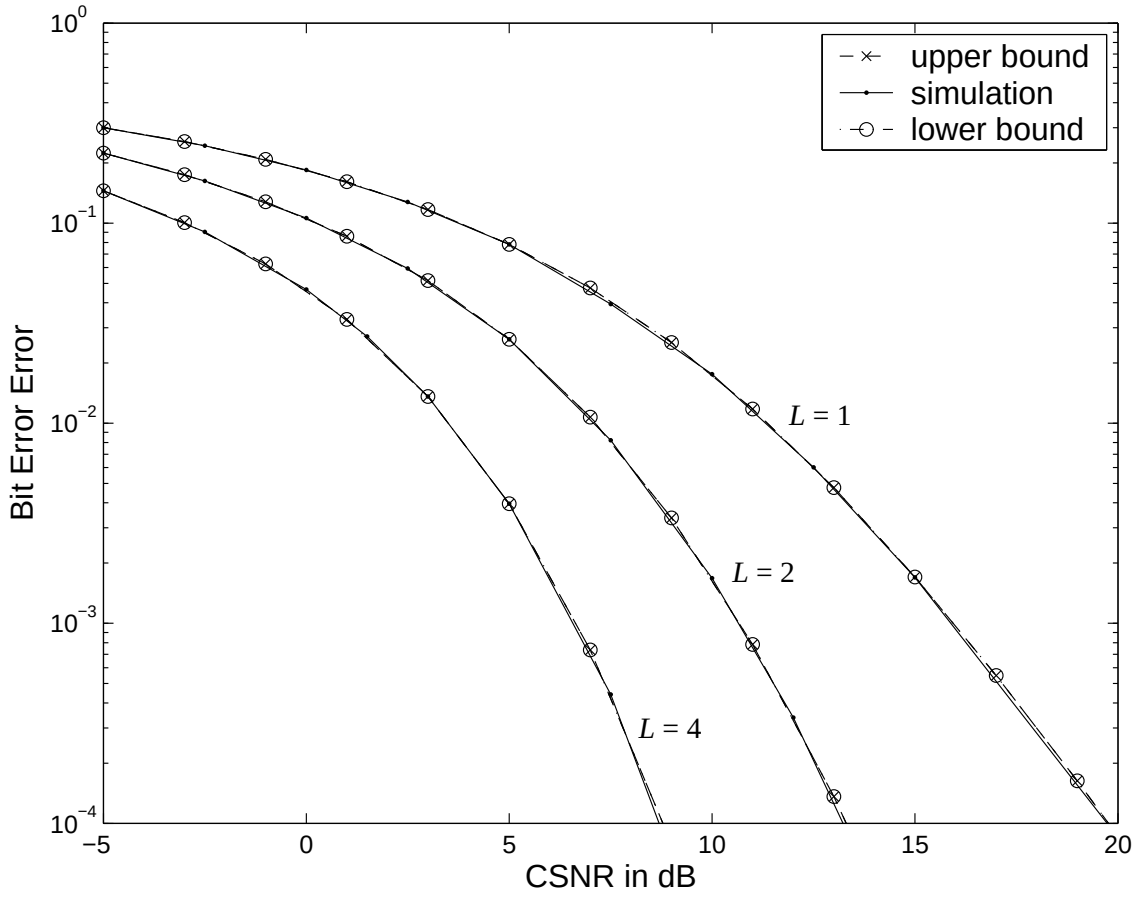

Figure 5.7: Results for 8-PSK signaling with $K = 3$ and $L = 1, 2,$ and 4 (1.5 bits/s/Hz).

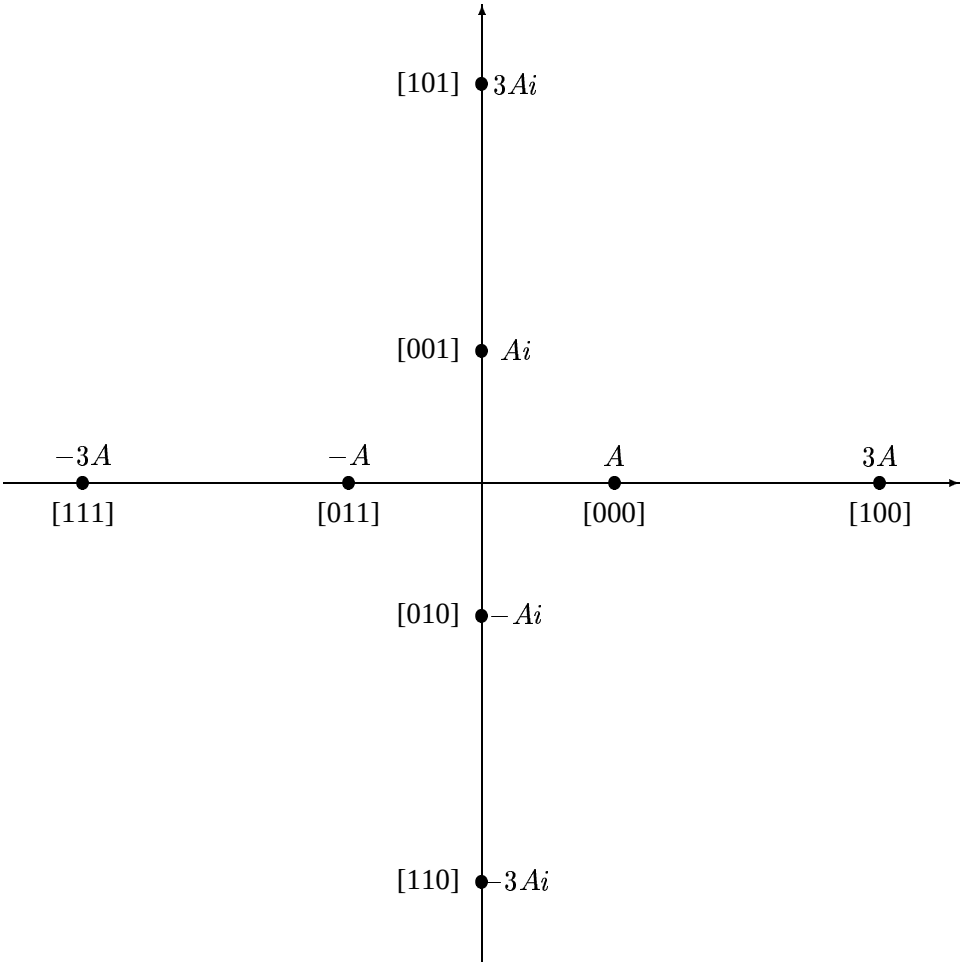

Figure 5.8: The star-QAM signaling scheme with quasi-Gray mapping. A is a normalizing factor and equals $1/2\sqrt{10}$ and $i = \sqrt{-1}$.

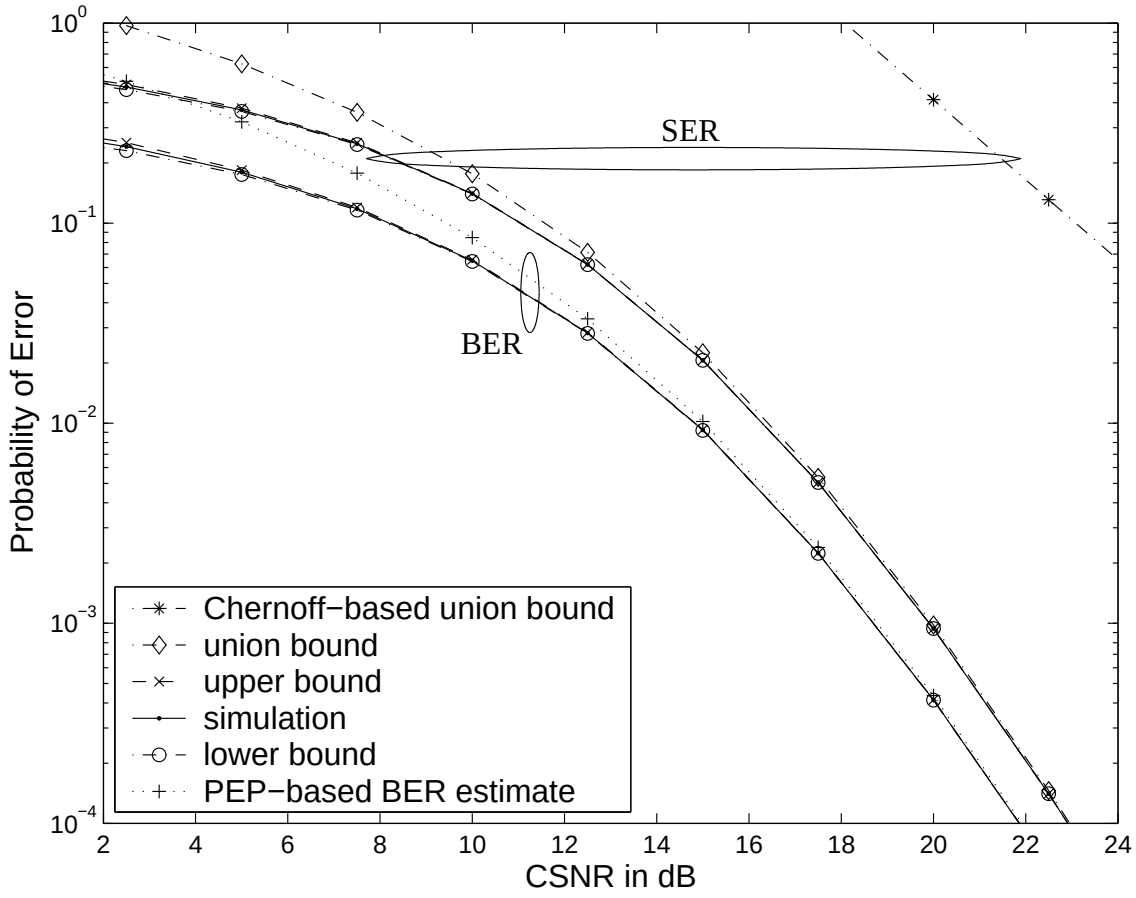

Figure 5.9: Results for Star 8-QAM signaling with $K = 4$ and $L = 1$ (1.5 bits/s/Hz).

Chapter 6

Error Rates of STOB Coded Systems under MAP Decoding

6.1 Introduction

When the input to the communication system is uniform i.i.d., the optimal decoding rule in the minimum codeword error rate sense, is the ML decoding rule. This case was considered in the previous chapter, where we derived tight upper and lower bounds on the symbol and bit error rates of space-time orthogonal block coded channels with arbitrary signal geometry and signal mappings.

In this chapter, we study how exploiting the non-uniform source distribution at the transmitter and/or the receiver can improve the performance of MIMO systems. In particular, the effects of symbol MAP decoding as well as signal design and mapping are addressed for systems which use space-time orthogonal block coding. As will be seen in

the sequel, obtaining the symbol pairwise error probability of the MAP decoded symbols requires finding the expected value of $Q(X + \frac{\lambda}{X})$, where λ is a real number. This is more involved than the related derivation in the ML decoding case, where the problem is computing the expected value of $Q(X)$. The MAP decoding rule, which we also derive here, and the pairwise error probability expression under MAP decoding show that there can be a large gain in performing MAP decoding as compared with ML decoding.

MAP decoding for sources with redundancy (due to non-uniform distribution and/or memory) is a form of joint source-channel coding. It would then be interesting to compare the performance of MAP-detected schemes with that of separate, independent source and channel coded (tandem) systems. For BPSK signaling, it is observed that at low CSNR values, MAP decoding is superior to tandem coding. As the size of the signaling scheme grows, this result holds for all practical error rates of interest.

Another contribution of this chapter is the establishment of tight Hunter (upper) and Kounias (lower) bounds on the SER and BER of STOB coded channels under MAP decoding. Similar to the previous chapter, we determine the probability of the intersection of two pairwise error events and use it together with our closed-form PEP formula to derive Hunter and Kounias bounds. We demonstrate that the bounds provide an excellent estimate of the error rates even at low (negative) CSNR values. For moderate values of the CSNR, the upper and lower bounds are often the same up to four significant digits. The SER bounds are much tighter than the union bound, and the BER bounds are significantly better than two computationally less expensive estimates.

6.2 The MAP Decoding Rule

6.2.1 Decoupled Symbol Detection

As outlined in Chapter 3, the input-output relation for a MIMO channel which uses space-time orthogonal block coding can be converted to the form given by (3.12), which we repeat here for simplicity

$$\tilde{\boldsymbol{r}}^j \triangleq \bar{\boldsymbol{H}}^{j\dagger}\bar{\boldsymbol{r}}^j = g\sqrt{\frac{\gamma_s}{K}}Y_j\mathbf{c} + \tilde{\boldsymbol{n}}^j.$$

We recall in the above equation that each entry of $\tilde{\boldsymbol{r}}^j$ is associated with only one symbol. Therefore, in the new case (i.e., under MAP decoding), if we show that the noise vector $\tilde{\boldsymbol{n}}^j$ is composed of i.i.d. random variables, then we can detect symbol i by only considering the i^{th} entry of the vectors $\tilde{\boldsymbol{r}}^j$, $1 \leq j \leq L$, which means that detection of symbols is decoupled under MAP decoding.

In order to find the distribution of the noise vector $\tilde{\boldsymbol{n}}^j$, we consider two noise samples $\tilde{N}^k_{\tau_1}$ and $\tilde{N}^q_{\tau_2}$ at two arbitrary symbol intervals τ_1 and τ_2, and for two arbitrary receive antennas k and q. Since $\tilde{N}^k_{\tau_1}$ and $\tilde{N}^q_{\tau_2}$ are weighted sums of independent normal random variables, they have Gaussian distribution. Also, it is straightforward to verify that $E\{\tilde{N}^k_{\tau_1}\} = E\{\tilde{N}^q_{\tau_2}\} = 0$. Hence, the correlation of these noise samples is

$$\begin{aligned}
\mathrm{E}\left\{\tilde{N}^k_{\tau_1}\tilde{N}^{q*}_{\tau_2}\right\} &= E\left\{\left(\sum_{i=1}^{w}\bar{H}^{k*}_{i,\tau_1}\bar{N}^k_i\right)\left(\sum_{j=1}^{w}\bar{H}^{q*}_{j,\tau_2}\bar{N}^q_j\right)^*\right\} \\
&= \sum_i\sum_j \bar{H}^{k*}_{i,\tau_1}\bar{H}^q_{j,\tau_2}E\left\{\bar{N}^k_i\bar{N}^{q*}_j\right\}
\end{aligned}$$

Since $\bar{N}^j_i, 1 \leq j \leq L$, are zero-mean i.i.d., the above sum is zero unless $k = q$ and $i = j$,

in which case it equals

$$\sum_{i=1}^{w} \bar{H}_{i,\tau_1}^{k*} \bar{H}_{i,\tau_2}^{k} E\left\{|\bar{N}_i^k|^2\right\} = \sum_{i} \bar{H}_{i,\tau_1}^{k*} \bar{H}_{i,\tau_2}^{k} \tag{6.1}$$

$$= \begin{cases} \sum_i |\bar{H}_{i,\tau_1}^k|^2 = gY_k & \text{if } \tau_1 = \tau_2 \\ 0 & \text{otherwise,} \end{cases} \tag{6.2}$$

where (6.1) follows from the fact that $\bar{N}_i^j$ is unit-variance and (6.2) follows from the orthogonality of $\bar{\boldsymbol{H}}$. Thus, we obtain that

$$\tilde{N}_i^k \sim \text{i.i.d. } \mathcal{CN}(0, gY_k). \tag{6.3}$$

As we mentioned in the first paragraph of this section, the above result, i.e., the fact that the entries of the noise vector $\tilde{\boldsymbol{n}}^k = [\tilde{N}_1^k, ..., \tilde{N}_\tau^k]^T$ are i.i.d., proves that symbol detection is decoupled, similar to the ML decoding case.

6.2.2 The MAP Decoding Rule

For MAP decoding, $\tilde{\boldsymbol{R}} = [\tilde{\boldsymbol{r}}^1, ..., \tilde{\boldsymbol{r}}^L]$ can be used instead of $\boldsymbol{R} = [\boldsymbol{r}_1, ..., \boldsymbol{r}_w]$ because $\tilde{\boldsymbol{R}}$ is generated from $\boldsymbol{R}$ through invertible operations. The detection rule is given by

$$\begin{aligned} c_i &= \arg\max_c P(c|\{\tilde{R}_i^l\}_{l=1}^L, \boldsymbol{H}) \\ &= \arg\max_c f(\{\tilde{R}_i^l\}_{l=1}^L|c, \boldsymbol{H}) \cdot p(c) \\ &= \arg\max_c \prod_{l=1}^{L} f_{\tilde{N}_i^l}(\{\tilde{R}_i^l - g'Y_l c\}_{l=1}^L) \cdot p(c) \qquad (6.4) \\ &= \arg\max_c \left\{ \ln\{p(c)\} - \sum_{l=1}^{L} \frac{|\tilde{R}_i^l - g'Y_l c|^2}{gY_l} \right\}, \qquad (6.5) \end{aligned}$$

where $g' = g\sqrt{\frac{\gamma_s}{K}}$, and (6.4) and (6.5) hold because $\tilde{N}_i^k$ are i.i.d. and Gaussian, respectively, as indicated in (6.3).

6.3 Exact Symbol Pairwise Error Probability with MAP Detection

6.3.1 The Conditional PEP

Without loss of generality, we consider MAP decoding for the k^{th} symbol period. The error probabilities may be determined using the MAP detection metric given in (6.5). The receiver should evaluate this metric for symbols c_i and c_j given that c_i is transmitted (hence $\tilde{R}_k^l = g' Y_l c_i + \tilde{N}_k^l$) and decide in favor of the one which yields a larger metric.

From (6.5), the probability that c_j is preferred over c_i when c_i is sent, $\Pr(c_i \to c_j)$, is the probability of the event

$$\ln\{p(c_i)\} - \frac{1}{2g}\sum_{l=1}^{L}\frac{|\tilde{R}_k^l - g' Y_l c_i|^2}{Y_l} \leq \ln\{p(c_j)\} - \frac{1}{2g}\sum_{l=1}^{L}\frac{|\tilde{R}_k^l - g' Y_l c_j|^2}{Y_l},$$

which is equivalent to

$$\sum_{l=1}^{L}\frac{\sqrt{2}\langle c_j - c_i, \tilde{N}_k^l\rangle}{|c_j - c_i|} \geq \frac{1}{|c_j - c_i|}\sqrt{\frac{K}{2\gamma_s}}\ln\frac{p(c_i)}{p(c_j)} + g|c_j - c_i|\sqrt{\frac{\gamma_s}{2K}}\sum_{l=1}^{L} Y_l. \tag{6.6}$$

From (6.3), it follows that $\frac{\sqrt{2}\langle c_j - c_i, \tilde{N}_k^l\rangle}{|c_j - c_i|}$ are i.i.d. $\mathcal{CN}(0, gY_l)$. Hence the sum on the left hand side of (6.6) is $\mathcal{CN}(0, g\sum_{l=1}^{L} Y_l)$. Therefore, the probability of the event in (6.6), which is the pairwise error probability conditioned on the path gains, is given by

$$P(c_i \to c_j | \boldsymbol{H}) = Q\left(\sqrt{\frac{g\gamma_s}{2K}}|c_i - c_j|\sqrt{Y} + \sqrt{\frac{K}{2g\gamma_s}}\frac{1}{|c_i - c_j|}\ln\frac{p(c_i)}{p(c_j)}\frac{1}{\sqrt{Y}}\right), \tag{6.7}$$

where, as mentioned in the Chapter 3,

$$Y = \sum_{l=1}^{L} Y_l = \sum_{k=1}^{K}\sum_{l=1}^{L}|H_{lk}|^2.$$

6.3.2 Interpretation of the PEP as a Laplace Transform

Based on the probability density function of Y, which was derived in (3.16), and using a change of variables, the average of (6.7) can be written as

$$P(c_i \to c_j) = \frac{1}{(n-1)!\delta_{ij}^{2n}} \int_0^\infty y^{n-1} e^{-y/\delta_{ij}^2} Q\left(\sqrt{y} + \frac{\lambda_{ij}}{\sqrt{y}}\right) dy, \tag{6.8}$$

where $\delta_{ij} = \sqrt{\frac{q\gamma_s}{2K}}|c_i - c_j|$ and $\lambda_{ij} = \frac{1}{2}\ln\frac{p(c_i)}{p(c_j)}$. We note that the integral in (6.8) is the Laplace transform of $y^{n-1}Q\left(\sqrt{y} + \frac{\lambda_{ij}}{\sqrt{y}}\right)$ evaluated at $s = \delta_{ij}^{-2}$. We know that if $f(t)$ and $F(s)$ are Laplace transform pairs ($F(s) = \mathcal{L}\{f(t)\}$), so are $t^n f(t)$ and $(-1)^n \frac{d^n}{ds^n}F(s)$. Therefore, we need to find the $n-1^{\text{st}}$ derivative of $\mathcal{L}\left\{Q\left(\sqrt{y} + \frac{\lambda_{ij}}{\sqrt{y}}\right)\right\}$. Using integration by parts, we have derived the Laplace transform of $Q\left(\sqrt{y} + \frac{\lambda_{ij}}{\sqrt{y}}\right)$ as

$$\begin{aligned} F_{\text{MAP}}(s) &= \mathcal{L}\left\{Q\left(\sqrt{y} + \frac{\lambda_{ij}}{\sqrt{y}}\right)\right\} \\ &= \frac{1 - \text{sgn}(\lambda_{ij})}{2s} - \frac{1}{2}\left(\frac{1}{s\sqrt{2s+1}} + \frac{\text{sgn}(\lambda_{ij})}{s}\right) e^{-(\lambda_{ij} + |\lambda_{ij}|\sqrt{2s+1})}. \end{aligned} \tag{6.9}$$

We now need to evaluate the n^{th} derivative of (6.9) which is calculated in the next subsection.

6.3.3 The PEP in Closed Form

Here we derive the n^{th} derivative of (6.9) with respect to s. First, we present a lemma which can be proved easily via induction.

Lemma– The following hold

a) $\frac{d^n}{ds^n}\left(\frac{1}{s}\right) = \frac{(-1)^n n!}{s^{n+1}}$

b) $\frac{d^n}{ds^n}(2s+1)^{\frac{p}{2}} = (2s+1)^{\frac{p}{2}-n}\prod_{i=0}^{n-1}(p-2i)$

c) $\frac{d^n}{dy^n}e^{-(a+by)} = (-1)^n b^n e^{-(a+by)}$.

The derivative of the first term in (6.9) may be found via (a). As for the product term, we use the Leibniz's formula [1] to treat the two terms separately. The formula is

$$\frac{d^n}{dx^n}uv = \sum_{i=0}^{n} \binom{n}{i} \frac{d^i u}{dx^i} \frac{d^{n-i} v}{dx^{n-i}} \,. \tag{6.10}$$

We apply (6.10) with $u = \frac{a}{s} + \frac{1}{s\sqrt{2s+1}}$ and $v = e^{-\left(a+b\sqrt{2s+1}\right)}$. Using (6.10) again to find the i^{th} derivative of the second term in u with $u_1 = \frac{1}{s}$ and $v_1 = \frac{1}{\sqrt{2s+1}}$, and applying (a) and (b) with $p = -1$ results in

$$\begin{aligned} \frac{d^i}{ds^i}\left(\frac{a}{s} + \frac{1}{s\sqrt{2s+1}}\right) &= \frac{(-1)^i i! a}{s^{i+1}} + \sum_{j=0}^{i} \frac{(-1)^i i!}{(i-j)!} \frac{\prod_{l=1}^{i-j}(2l-1)}{s^{j+1}(2s+1)^{i-j+\frac{1}{2}}} \\ &= \frac{(-1)^i i! a}{s^{i+1}} + \frac{(-1)^i i!}{s^{i+1}} \sum_{k=0}^{i} \binom{2k}{k} \frac{s^k}{2^k (2s+1)^{k+\frac{1}{2}}}. \end{aligned} \tag{6.11}$$

As for the exponential term, we use a formula for the n^{th} derivative of a composite function from [71] which states that for $f(x) = F(y)$, $y = \phi(x)$, we have

$$\frac{d^n}{dx^n} f(x) = \sum_{i=1}^{n} \frac{U_i}{i!} F^{(i)}(y), \quad \text{where} \quad U_i = \sum_{k=0}^{i-1} \binom{i}{k} (-1)^k y^k \frac{d^n}{dx^n} y^{i-k}. \tag{6.12}$$

Letting $F(y) = e^{-(a+by)}$ and $y = \sqrt{2s+1}$, we use (6.12), (b), and (c) to get

$$\frac{d^{n-i}}{ds^{n-i}} e^{-\left(a+b\sqrt{2s+1}\right)} = e^{-\left(a+b\sqrt{2s+1}\right)} \sum_{j=1}^{n-i} \frac{(2s+1)^{\frac{j}{2}-n+i} b^j}{j!} \sum_{k=0}^{j-1} \binom{j}{k} (-1)^{j+k} \prod_{l=0}^{n-i-1} (j-k-2l). \tag{6.13}$$

Using (6.11) and (6.13) in (6.10) with $a = \lambda_{ij}$ and $b = |\lambda_{ij}|$ yields the n^{th} derivative of

(6.9) as

$$\begin{aligned}\frac{d^n}{ds^n}F_{\text{MAP}}(s) &= \frac{(1-\text{sgn}(\lambda_{ij}))(-1)^n n!}{2s^{n+1}} - \frac{1}{2}e^{-\left(\lambda_{ij}+|\lambda_{ij}|\sqrt{2s+1}\right)} \\ &\quad \times \sum_{k=0}^{n}\binom{n}{k}\frac{(-1)^k k!}{s^{k+1}}\left(\text{sgn}(\lambda_{ij}) + \sum_{m=0}^{k}\binom{2m}{m}\frac{s^m}{2^m(2s+1)^{m+\frac{1}{2}}}\right) \\ &\quad \times \sum_{l=1}^{n-k}\frac{|\lambda_{ij}|^l}{l!(2s+1)^{n-k-\frac{l}{2}}}\sum_{p=0}^{l-1}\binom{l}{p}(-1)^{l+p}\prod_{q=0}^{n-k-1}(l-p-2q). \quad (6.14)\end{aligned}$$

Using (6.14) with (6.8) results in the following expression for the exact PEP of MAP decoded space-time orthogonal block codes

$$\begin{aligned}P(c_i \to c_j) &= \frac{1-\text{sgn}(\lambda_{ij})}{2} - \frac{1}{2}e^{-\left(\lambda_{ij}+|\lambda_{ij}|\sqrt{2\delta_{ij}^{-2}+1}\right)} \\ &\quad \times \sum_{k=0}^{n-1}\frac{(-1)^{n+k-1}}{(2+\delta_{ij}^2)^{n-k-1}}\left(\text{sgn}(\lambda_{ij}) + \frac{\delta_{ij}}{\sqrt{2+\delta_{ij}^2}}\sum_{m=0}^{k}\binom{2m}{m}\frac{1}{(2\delta_{ij}^2+4)^m}\right) \\ &\quad \times \sum_{l=1}^{n-k-1}\frac{|\lambda_{ij}|^l(\delta_{ij}^2+2)^{l/2}}{l!\delta_{ij}^l}\sum_{p=0}^{l-1}\binom{l}{p}(-1)^{l+p}\prod_{q=0}^{n-k-2}(l-p-2q), \quad (6.15)\end{aligned}$$

where we have set $\sum_{i=L}^{U} w_i = 1$ for $L > U$.

A special case is ML decoding for which $\lambda_{ij} = \frac{1}{2}\ln\frac{p(c_i)}{p(c_j)} = 0$. Hence, the first sum in (6.15) is non-zero only for $k = n-1$ and we have

$$P(c_i \to c_j) = \frac{1}{2}\left(1 - \frac{\delta_{ij}}{\sqrt{2+\delta_{ij}^2}}\sum_{k=0}^{n-1}\binom{2k}{k}\frac{1}{(2\delta_{ij}^2+4)^k}\right),$$

which agrees with the result in (3.18).

6.4 The Optimal Binary Antipodal Signaling

In this subsection we consider binary antipodal signaling and optimize it in the sense of minimizing the BER given by

$$\text{BER} = P(\hat{c} = c_2 | c = c_1) \cdot p(c_1) + P(\hat{c} = c_1 | c = c_2) \cdot p(c_2). \tag{6.16}$$

Normally, one should use the averaged PEP in (6.16) with $c_1 = a$ and $c_2 = -b$, differentiate the result, and find the optimal a and b. However, this can be a tedious job considering the PEP given in (6.15). Therefore, we use the PEPs at the *receiver* side, i.e., given $\boldsymbol{H}$, to find the solution in an easier way. The optimal constellation derived in this way will not depend on $\boldsymbol{H}$, thus justifying our approach.

Let us assume that $p(c_1) = p$, and the bits 0 and 1 are mapped to $c_2 = -b$ and $c_1 = a$, respectively. Letting $\beta = \sqrt{\frac{2g\gamma_s}{K}}$, $\sqrt{A} = \beta\frac{(a+b)}{2}\sqrt{y}$, and $B = \frac{1}{2}\ln\frac{1-p}{p}$, we can write the BER conditioned on Y as

$$\text{BER}_Y = pQ\left(\sqrt{A} - \frac{B}{\sqrt{A}}\right) + (1-p)Q\left(\sqrt{A} + \frac{B}{\sqrt{A}}\right). \tag{6.17}$$

It is easy to verify that the BER is a strictly decreasing function of A (regardless of B). Hence, given γ_s and p, in order to minimize the BER, one has to maximize A. Note that A is a scaled distance between the signal points, therefore, signaling schemes with the same distance between their signals have identical performance. It is clear that the constellation with constant average signal energy $\frac{\gamma_s}{K}$ which maximizes A is the zero-mean constellation, because a constellation with a non-zero mean can simply be shifted to reduce its energy without performance loss.

From the zero-mean condition, we have

$$b = \frac{p}{1-p}a,$$

and the average energy condition requires that

$$pa^2 + (1-p)b^2 = \frac{\gamma_s}{K}.$$

The above two equalities result in

$$(-b, a) = \sqrt{\frac{\gamma_s}{K}} \left(-\sqrt{\frac{p}{1-p}}, \sqrt{\frac{1-p}{p}} \right),$$

which is therefore the optimal binary antipodal constellation. The above constellation is identical to the antipodal signaling result in [107] for the case of the AWGN channel.

6.5 Bounds on the SER and BER of STOB Coded Channels under MAP Decoding

In this section, we show how the approach of the previous chapter in deriving Bonferroni-type upper and lower bounds can be applied to space-time orthogonal block codes under MAP decoding. Two less expensive upper and a lower bounds on the BER are also presented in Section 6.6 and compared with the Bonferroni bounds.

6.5.1 The Symbol Error Rate

As seen in the previous chapter, for a constellation of size $M = 2^m$, where m is a positive integer, and an i.i.d. bit-stream, the SER is given by

$$\text{SER} = \sum_{u=0}^{M-1} P(\epsilon|c_u)p(c_u) = \sum_{u=0}^{M-1} p(c_u) P_u\left(\bigcup_{i\neq u} \epsilon_{iu}\right). \tag{6.18}$$

Note that $P_u(\epsilon_{ui})$ is the PEP and is given in (6.15). We now need to find the probability of the intersection of ϵ_{ui} and ϵ_{uj} which is given by

$$P_u(\epsilon_{ui} \cap \epsilon_{uj}) = \mathrm{E}_Y\left\{\Psi\left(\rho_{iju}, \delta_{ui}\sqrt{Y} + \frac{\lambda_{ui}}{\delta_{ui}\sqrt{Y}}, \delta_{uj}\sqrt{Y} + \frac{\lambda_{uj}}{\delta_{uj}\sqrt{Y}}\right)\right\}, \tag{6.19}$$

where $\rho_{iju} = \frac{\langle c_i - c_u, c_j - c_u\rangle}{d_{iu}d_{ju}}$, $d_{iu} = |c_i - c_u|$, Y is defined in (3.15), and $\Psi(\rho, a, b)$ is the bivariate Gaussian function defined in (4.7). After trying a few numerical methods, we chose to compute (6.19) using a combination of 96-point Gaussian integration [1] together with Donnelly's algorithm [42] for each $Y = y$. This selection led to the fastest and the most accurate results.

6.5.2 The Bit Error Rate

Similar to the previous chapter, we write the BER as

$$\text{BER} = \sum_{u=0}^{M-1} p(c_u) P_u(\epsilon^{(b)}), \tag{6.20}$$

where $P_u(\epsilon^{(b)})$ is given in (5.10). Now, we need to compute the pairwise error probability between c_i and c_j given that c_u is sent. i.e.,

$$P_u(\epsilon_{ij}) = E_Y\left\{Q\left(\frac{\delta_{ui}^2 - \delta_{uj}^2}{\delta_{ij}}\sqrt{Y} + \frac{\lambda_{ij}}{\delta_{ij}\sqrt{Y}}\right)\right\},$$

whose closed-form solution is given in (6.15). We also need to find the probability of the intersection of ϵ_{ji} and ϵ_{jk} given that c_u is sent, which is given by

$$P_u(\epsilon_{ij} \cap \epsilon_{kj}) = E_Y \left\{ \Psi \left(\rho_{ikj}, \frac{\delta_{iu}^2 - \delta_{ju}^2}{\delta_{ij}} \sqrt{Y} + \frac{\lambda_{ij}}{\delta_{ij}\sqrt{Y}}, \frac{\delta_{ku}^2 - \delta_{ju}^2}{\delta_{kj}} \sqrt{Y} + \frac{\lambda_{kj}}{\delta_{kj}\sqrt{Y}} \right) \right\}.$$

Therefore, the results of Section 6.5.1 can be used here to compute lower and upper bounds on the BER.

6.6 Numerical Results

6.6.1 Binary Antipodal Signaling

We first study the BER of binary antipodal signaling to show the exactness of our PEP formulas. We simulate the transmission of an i.i.d. bit sequence over the MIMO channel. The length of the bit-sequence is max $(10^5, 100\times \text{ BER}^{-1})$ bits. We also let $P(X = 0) = p$.

We consider a system with two transmit and one receive antennas using the $\mathcal{G}^2$ (Alamouti) space-time code in Figure 6.1. It is seen that the analysis and simulation curves coincide everywhere. This simulation also indicates how MAP decoding can improve the BER performance. The MAP decoding gain over ML decoding is 0.63, 1.57, and 5.98 dB for $p = 0.8, 0.9$, and 0.99, respectively, at BER = 10^{-3}. Figure 6.2 presents the results of Section 6.4. It shows that a large gain can be obtained through modifying the constellation according to the prior probabilities. At a BER of 10^{-3}, the gain of using the optimal binary signaling and MAP detection is respectively 2.7, 6.1, and 20.1 dB for $p = 0.8, 0.9$, and 0.99 over an ML decoded system with BPSK modulation.

In Figure 6.3, we compare four systems, i.e., two systems with BPSK signaling and ML or MAP decoding, and two systems with optimal signaling and ML or MAP decoding. These systems are indicated by ML symmetric, MAP symmetric, ML optimum, and MAP optimum, respectively. We see that if the CSNR is high enough, optimum signaling and ML detection outperforms BPSK and MAP detection. In other words, using adaptive signaling is superior to MAP detection. When receiver noise is strong (i.e., at low γ_s), the second term in the argument of the $Q(\cdot)$ function in (6.7) has the dominant effect; hence MAP decoding with BPSK signals is more effective than ML decoding with optimum signals. In less noisy channel conditions (high γ_s), the first term in the argument of the $Q(\cdot)$ function becomes dominant and hence ML decoding with optimum signaling outperforms MAP decoding with symmetric signals. As previously mentioned, MAP decoding with optimum signaling is always better than other systems.

6.6.2 Tandem versus Joint Source-Channel Coding

Figures 6.4 and 6.5 compare a MAP decoded system with two tandem systems for a dual transmit-single receive channel with BPSK and 16-QAM signaling, respectively. The input bit-stream is i.i.d. with $P(X = 0) = 0.89$ so that the source entropy is $H(X) = 0.5$. The tandem systems are composed of 4$^{\text{th}}$ order Huffman coding followed by either a 16-state or a 64-state rate-1/2 convolutional coding block. The convolutional codes are non-systematic and chosen from [101]. The length of the input bit-stream is 10000 bits. The test is repeated 1000 times and the average BER is reported. It is observed that the tandem system breaks down (due to error propagation in Huffman decoding) for $E_b/N_0 < 13$ dB

for the system with BPSK signaling and a much higher E_b/N_0 of 30 dB for the system with 16-QAM modulation. For the system with 16-QAM signaling, the MAP-decoded system outperforms the 16-state (64-state) tandem coded system for BER $> 4\times10^{-7}$ ($> 2\times10^{-7}$), which is the range of the error rates of interest in most practical applications. This is a very interesting result which shows that MAP decoding, which is far less complex than tandem coding, should be the choice for applications in which the input bit-stream is not uniformly distributed (such as FAX). Notice that as the constellation size (which translates to the system bit rate) grows, the MAP decoded system becomes more superior.

6.6.3 SER and BER Bounds for M-ary Signaling

Figures 6.8 to 6.14 show the SER and BER bounds and the simulation results for various PSK and QAM signaling schemes for a dual transmit-single receive system. They compare the curves for two systems: one with an equiprobable i.i.d. bit-stream and ML decoding and another with an i.i.d. bit-stream with $P(X = 0) = 0.9$ and MAP decoding. The length of the bit-sequence is 2000000 bits. For the SER, the union bound given by

$$\text{Union bound} = \sum_u p(c_u) \sum_i P(c_u \to c_i)$$

is also plotted. For the BER, we also plot SER$/p$, where 2^p is the constellation size. This approximation is good only at high CSNR values and when Gray mapping is used for signal mapping. The other curve as a BER estimate is based on the symbol PEPs. The exact BER is given in (6.20). At high CSNR, one can replace $P(\hat{c} = c_j|c = c_i)$ with $P(c_i \to c_j)$. This will result in an upper bound on the BER, because clearly $P(c_i \to c_j) > P(\hat{c} = c_j|c = c_i)$.

Figure 6.8 demonstrates the SER bounds for 16-QAM signaling and Gray mapping (the mapping is shown in [186, Figure 8]). The upper and lower bounds provide an excellent approximation to the SER for all (even negative) CSNR values. It is interesting to note that as the source becomes more biased, the bounds become tighter. The curves also show that the union bound becomes looser as the CSNR decreases. Finally, we observe that the MAP-decoded system is considerably superior to the ML-decoded system. The MAP decoding gain at BER $= 10^{-3}$ is 5.5 dB.

The SER and BER curves of 32-PSK signaling are shown in Figure 6.9 and Figure 6.10, respectively. We observe from Figure 6.10 that the BER upper and lower bounds are also very tight for the entire CSNR range. This figure also shows that the PEP-based BER estimate is often very loose as compared with the other bounds. The MAP decoding gain for BER (SER) = 10^{-3} is 1.85 dB (1.68 dB). Figure 6.11 presents the SER curves for 64-QAM and Gray mapping. The MAP decoding gain at SER = 10^{-3} is as large as 6.7 dB. The upper bound for the ML-decoded system is up to 10% larger than the lower bound at low CSNR values, but it becomes tight as the CSNR grows. Both bounds are tight for the MAP-decoded case. The bounds for smaller constellations are tighter and other values of $P(X = 0)$ are at least as tight as those reported above.

6.6.4 The Effect of Constellation Mapping

We next demonstrate that a large gain can be achieved via signal mappings designed according to the source non-uniform distribution over Gray and quasi-Gray mappings. The M1 mapping was introduced in [186] and was designed for the transmission of non-uniform

binary sources over single antenna additive white Gaussian noise channels. It minimizes the SER union bound for single antenna Rayleigh fading channels with M-ary PSK and square QAM signaling [217].

Based on the design criteria proposed in [186], we construct an M1-type signal mapping for the star-QAM signaling scheme as shown in Figure 6.12. The SER performance of the M1 and quasi-Gray mappings are compared in Figure 6.13. It is observed that even for this small signaling scheme, the CSNR gain of M1 mapping over quasi-Gray mapping is nearly 2 dB with MAP decoding at SER = 10^{-3}. The gain due to source redundancy when the source distribution varies between 0.5 to 0.9 is 7 dB with M1 mapping. Figure 6.14 compares the SER curves for the Gray and M1 mappings for 64-QAM signaling. This figure shows that the M1 map performs very well for MIMO channels. The gain of the M1 mapping over Gray mapping is 3.7 dB at SER = 10^{-3}. The gain due to source redundancy is 10.4 dB.

Note that the specific M1 mappings used in the above scenarios are not designed to minimize the BER at all p; they outperform the Gray mapping for $p = 0.9$. This is demonstrated for 64-QAM signaling in Figure 6.15, where the M1 mapping is shown to have superior performance to the Gray mapping for $p = 0.9$, but it is outperformed by Gray mapping for $p = 0.5$.

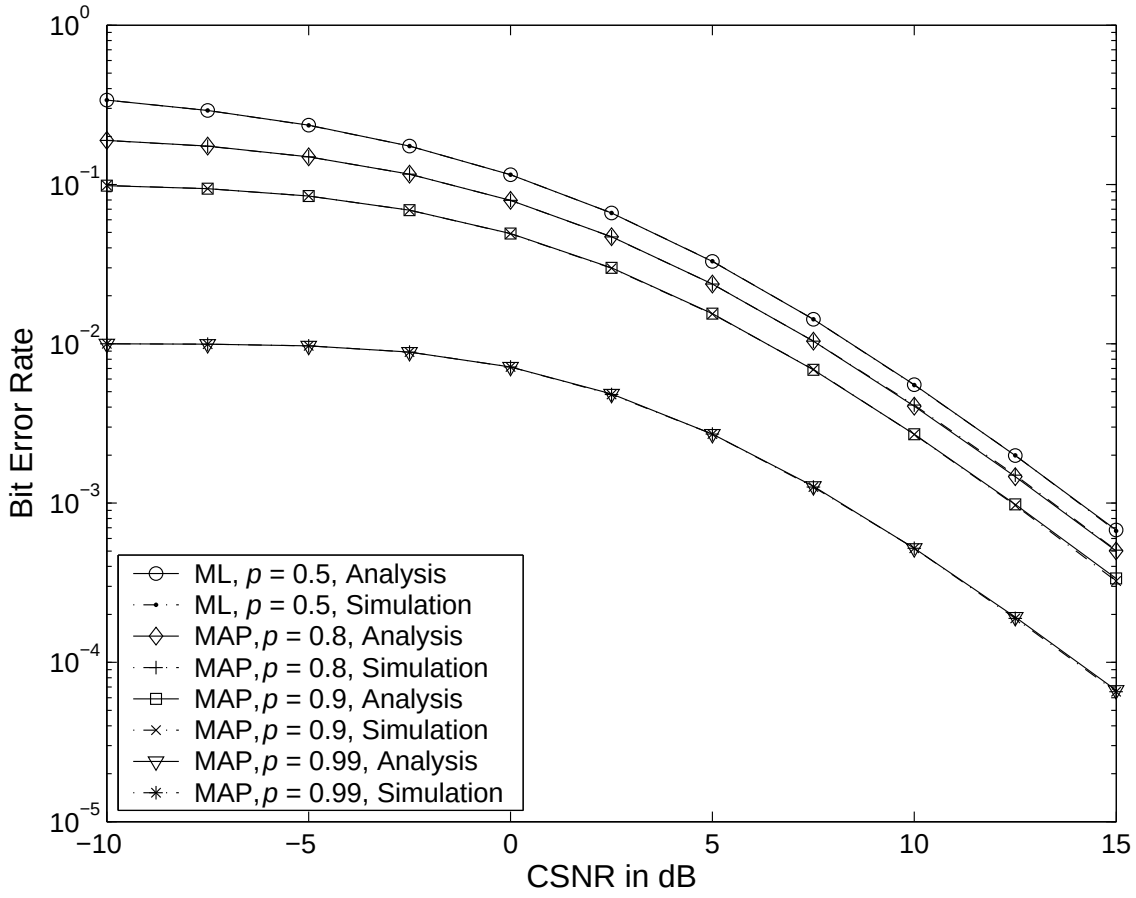

Figure 6.1: Results for BPSK signaling, $K = 2$, and $L = 1$.

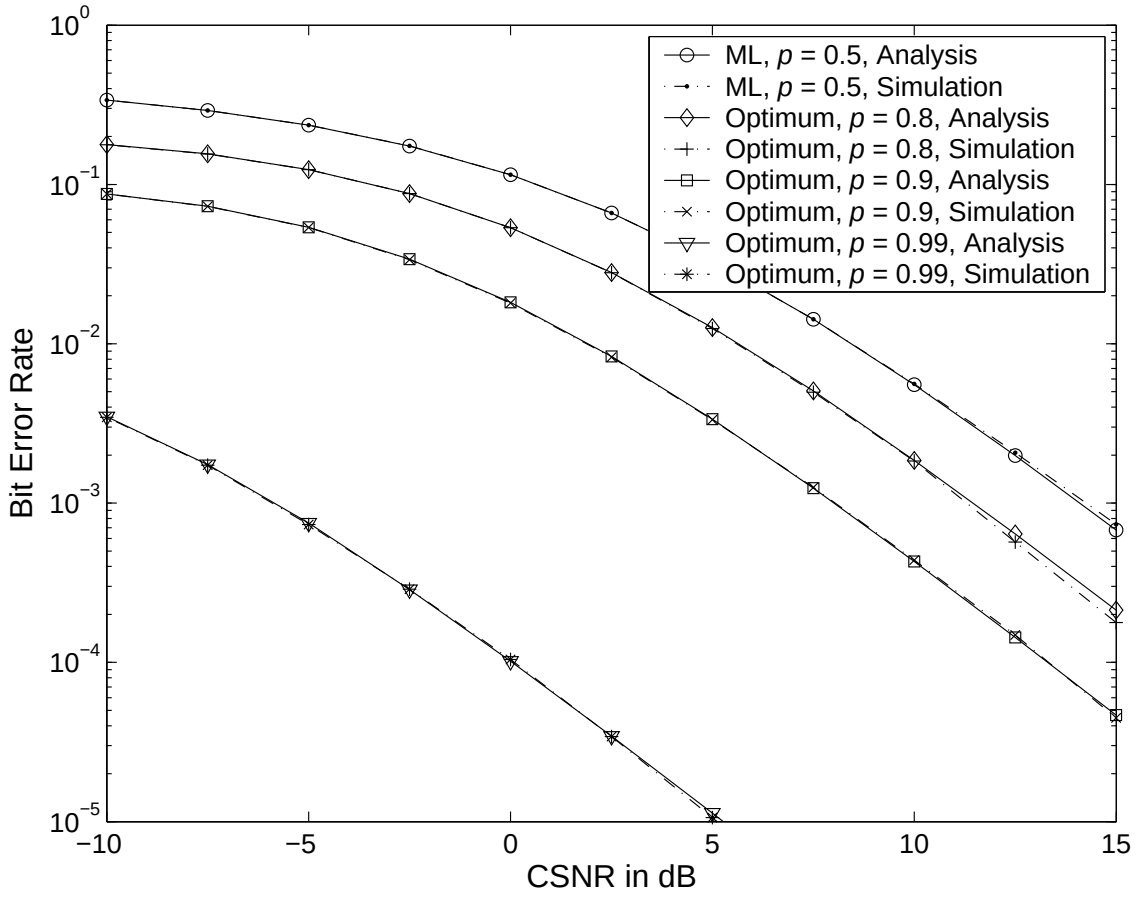

Figure 6.2: Results for the optimum binary antipodal signaling, $K = 2$, and $L = 1$.

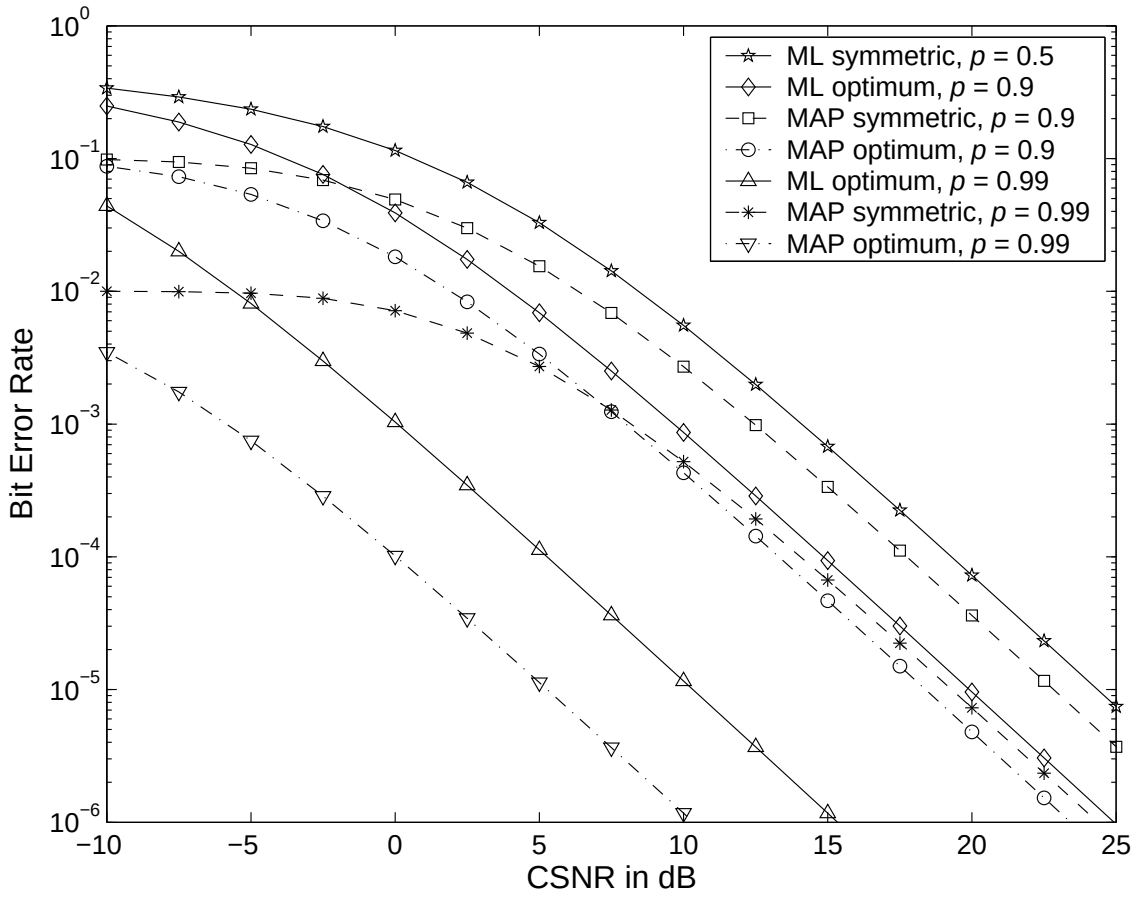

Figure 6.3: Comparison between BPSK and optimum signaling schemes, $K = 2$, and $L = 1$.

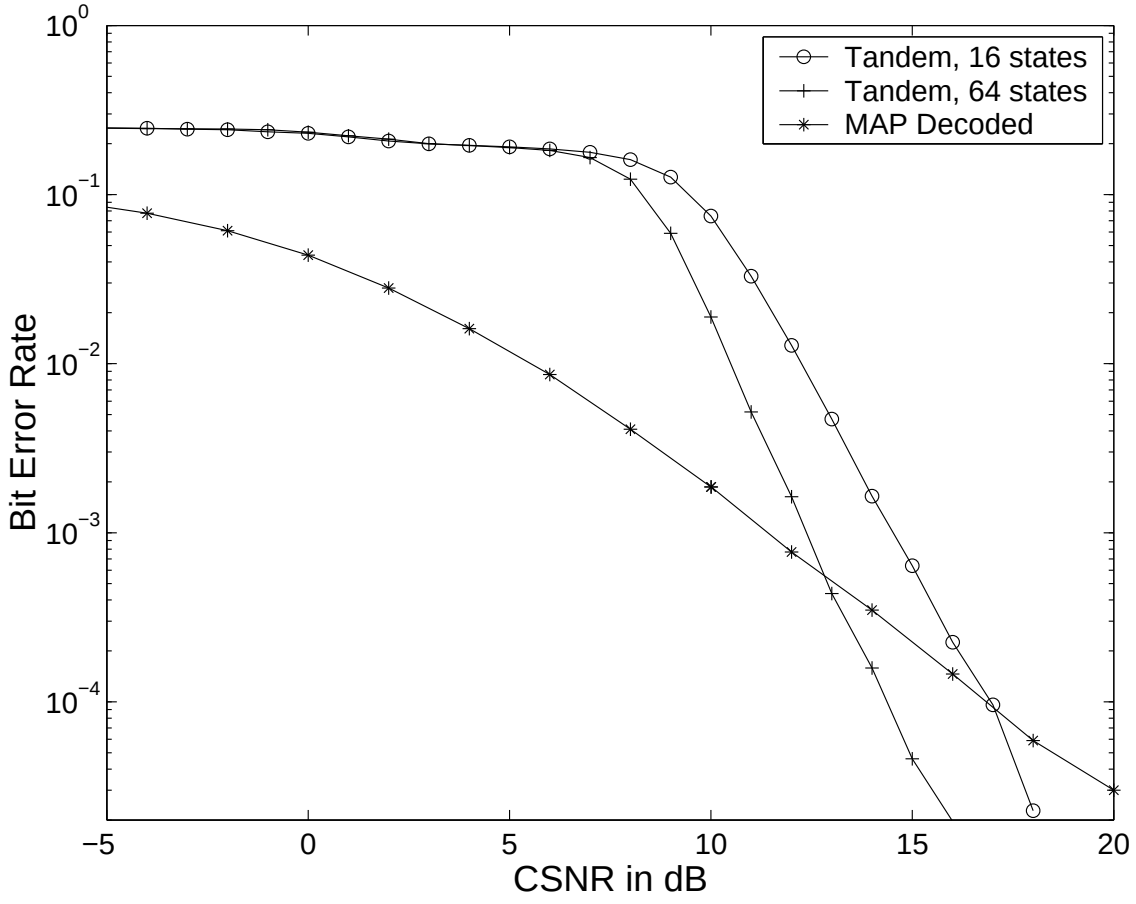

Figure 6.4: Comparison between tandem and MAP-decoded schemes for BPSK signaling, $K = 2$, and $L = 1$.

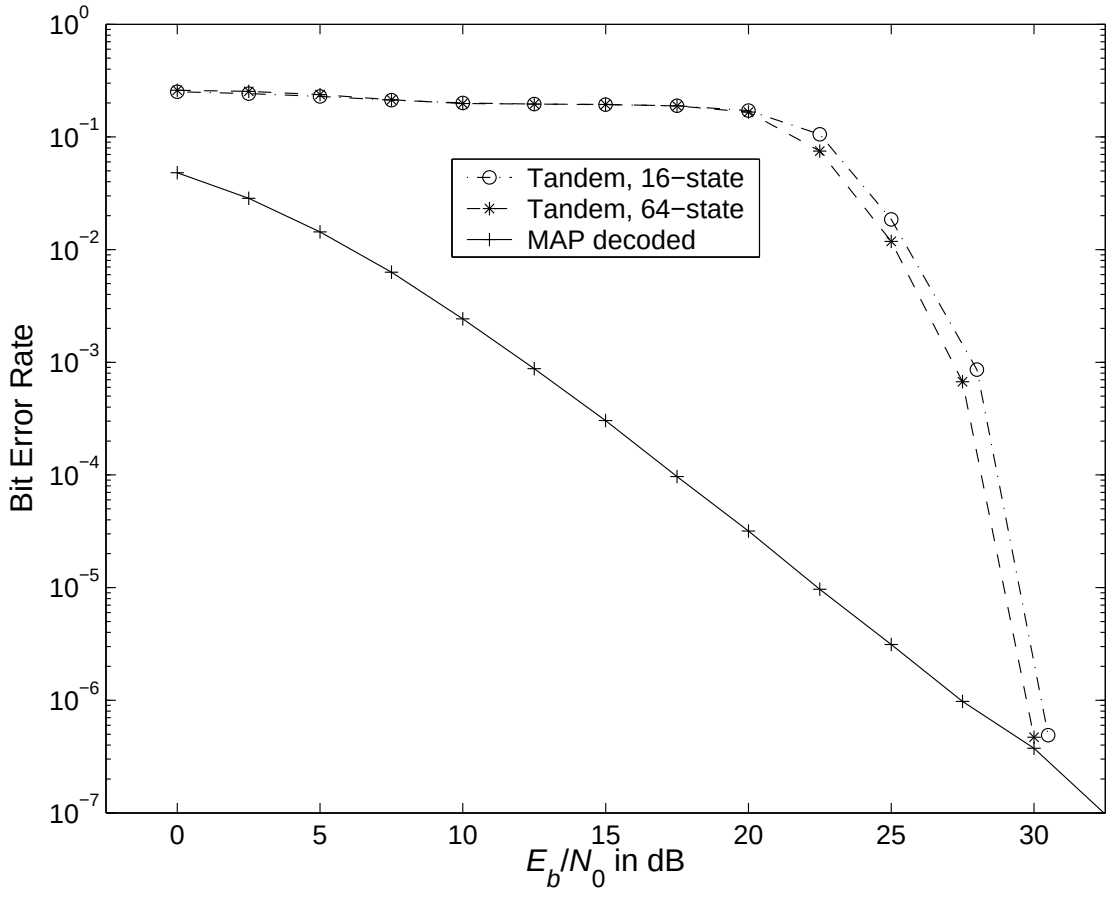

Figure 6.5: Comparison between tandem and MAP-decoded schemes for 16-QAM signaling, $K = 2$, and $L = 1$.

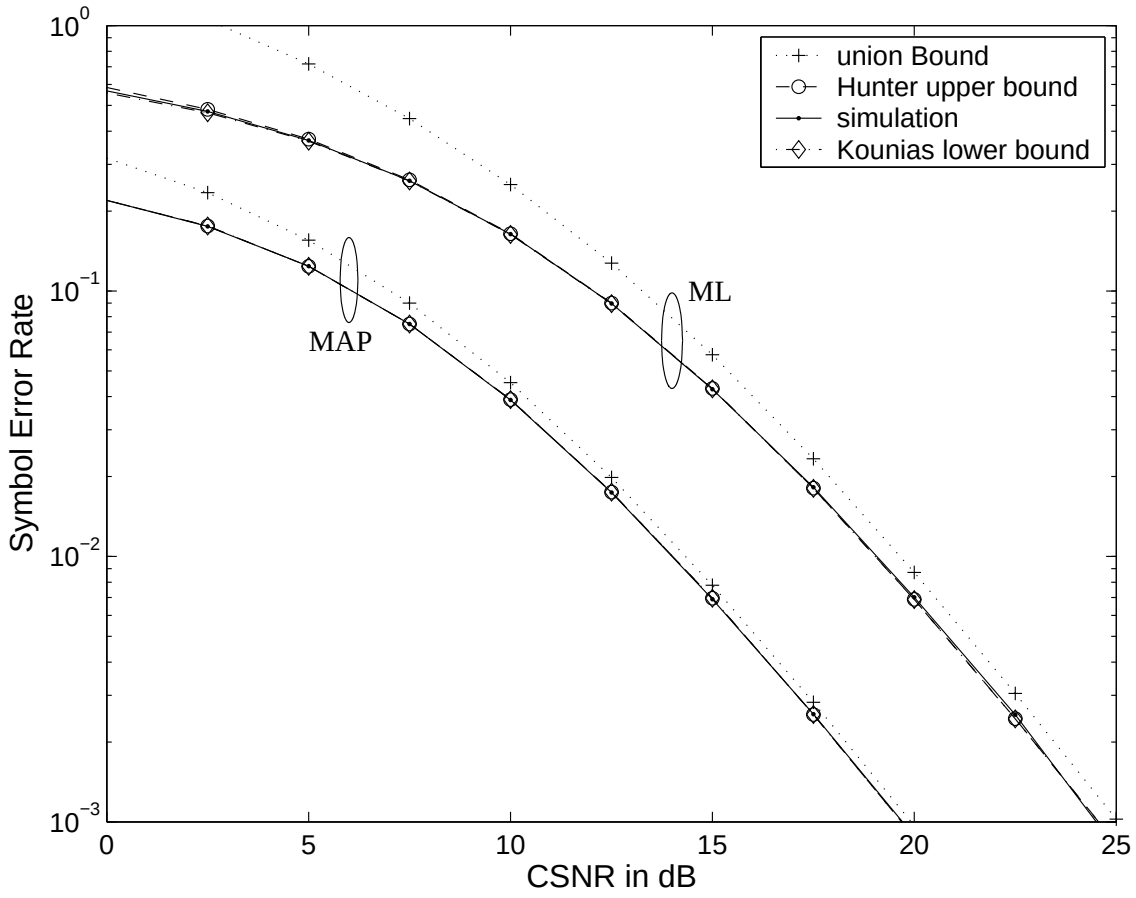

Figure 6.6: SER curves for 8-Point Star QAM modulation with quasi-Gray mapping, $K = 2$, and $L = 1$.

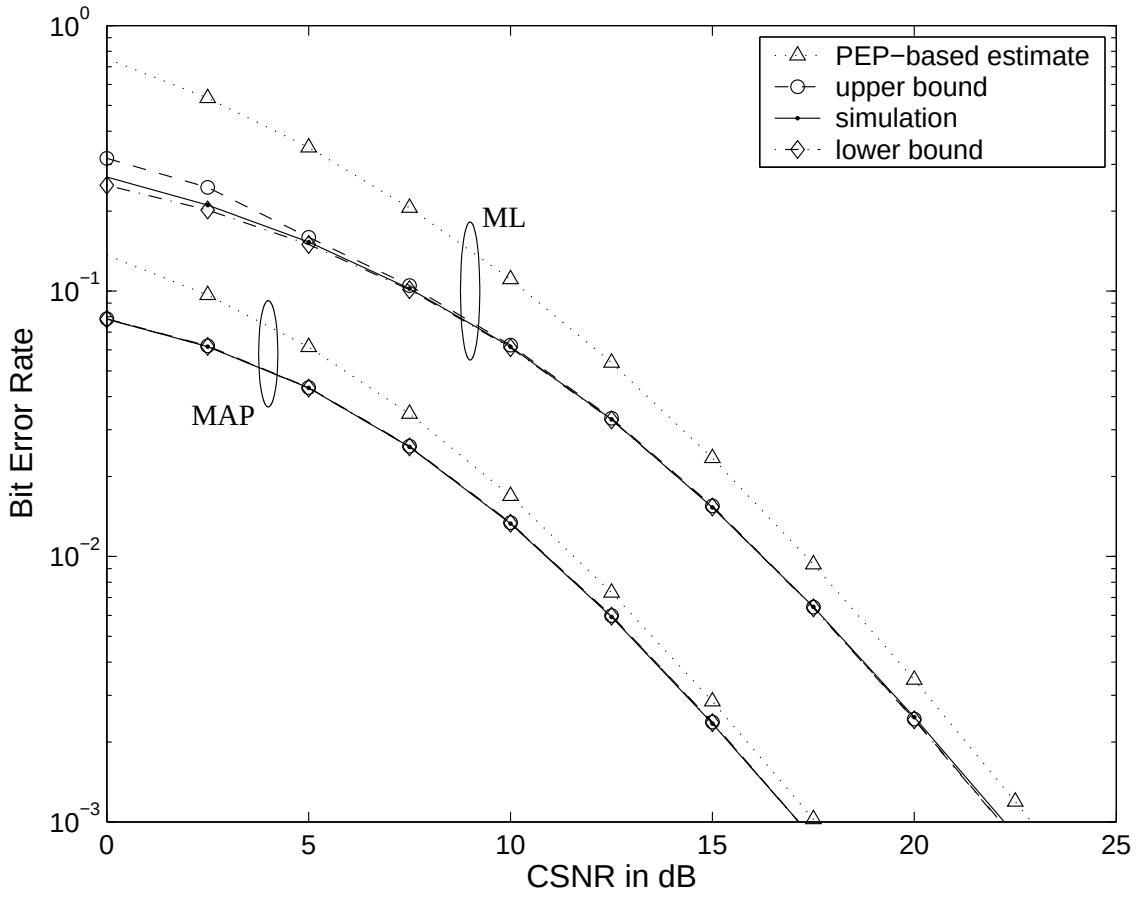

Figure 6.7: BER curves for 8-Point Star QAM modulation with quasi-Gray mapping, $K = 2$, and $L = 1$.

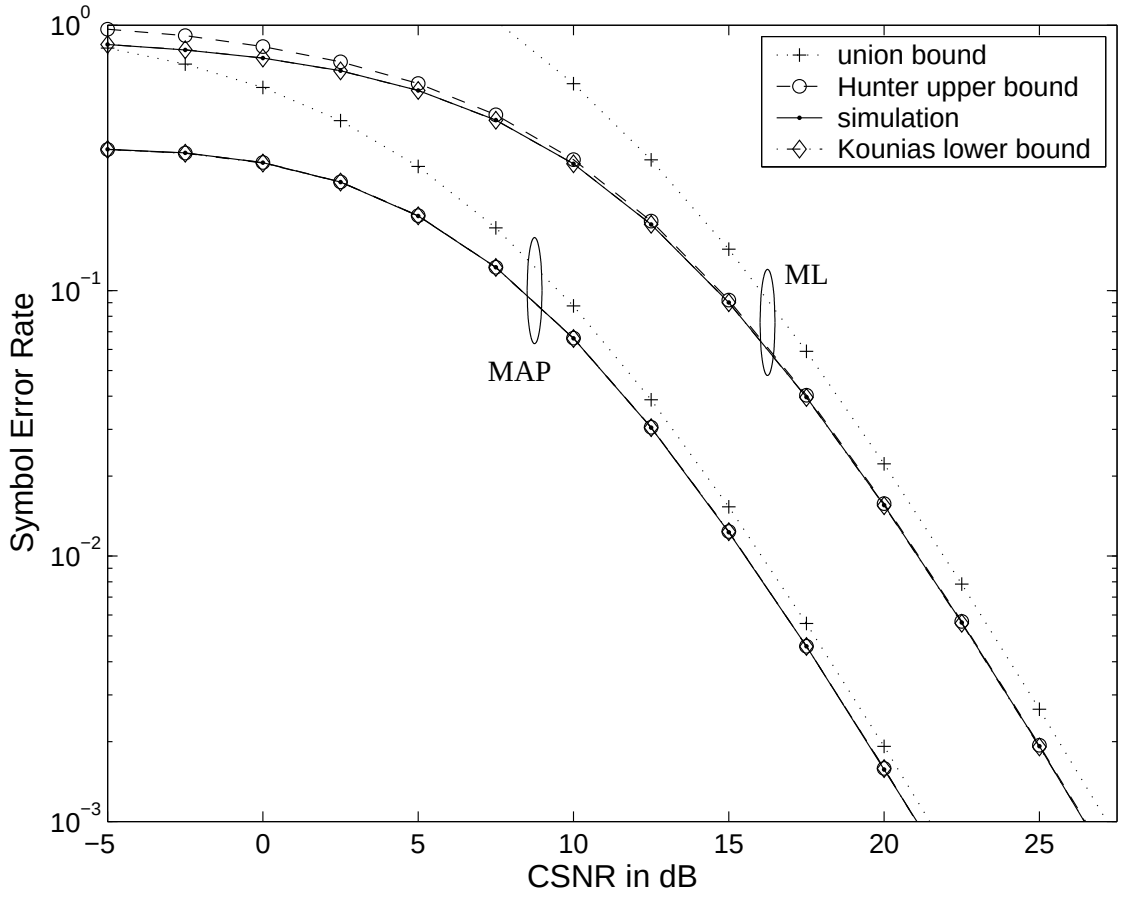

Figure 6.8: SER curves for 16-QAM signaling, $K = 2$, and $L = 1$.

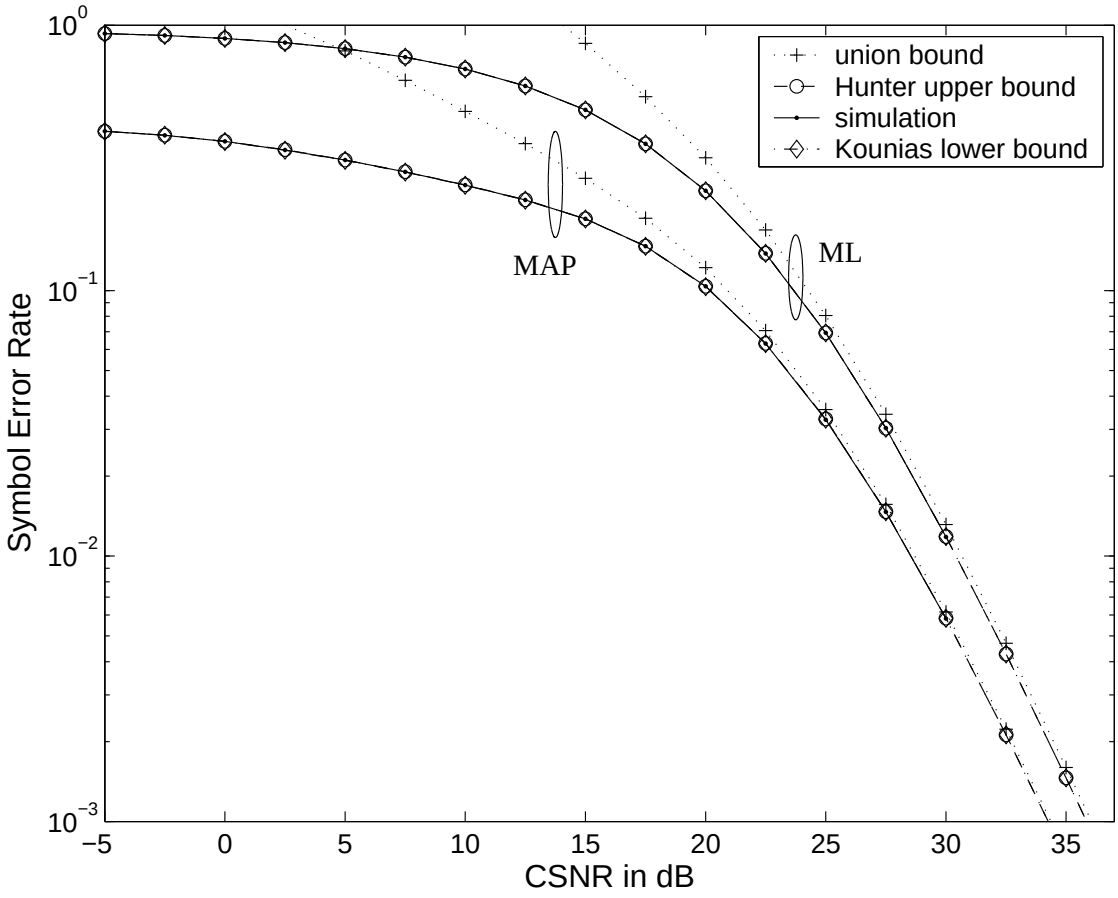

Figure 6.9: SER curves for 32-PSK signaling, $K = 2$, and $L = 1$.

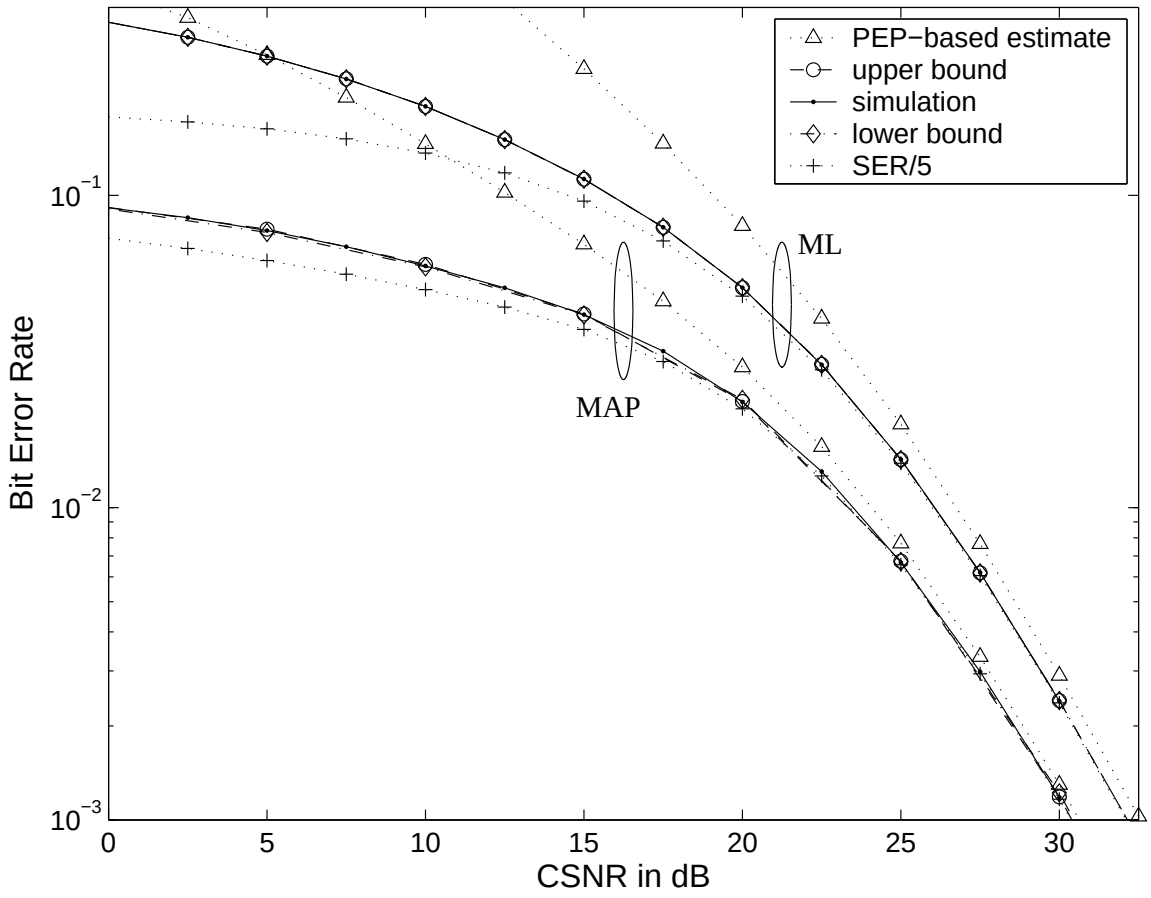

Figure 6.10: BER curves for 32-PSK signaling, $K = 2$, and $L = 1$.

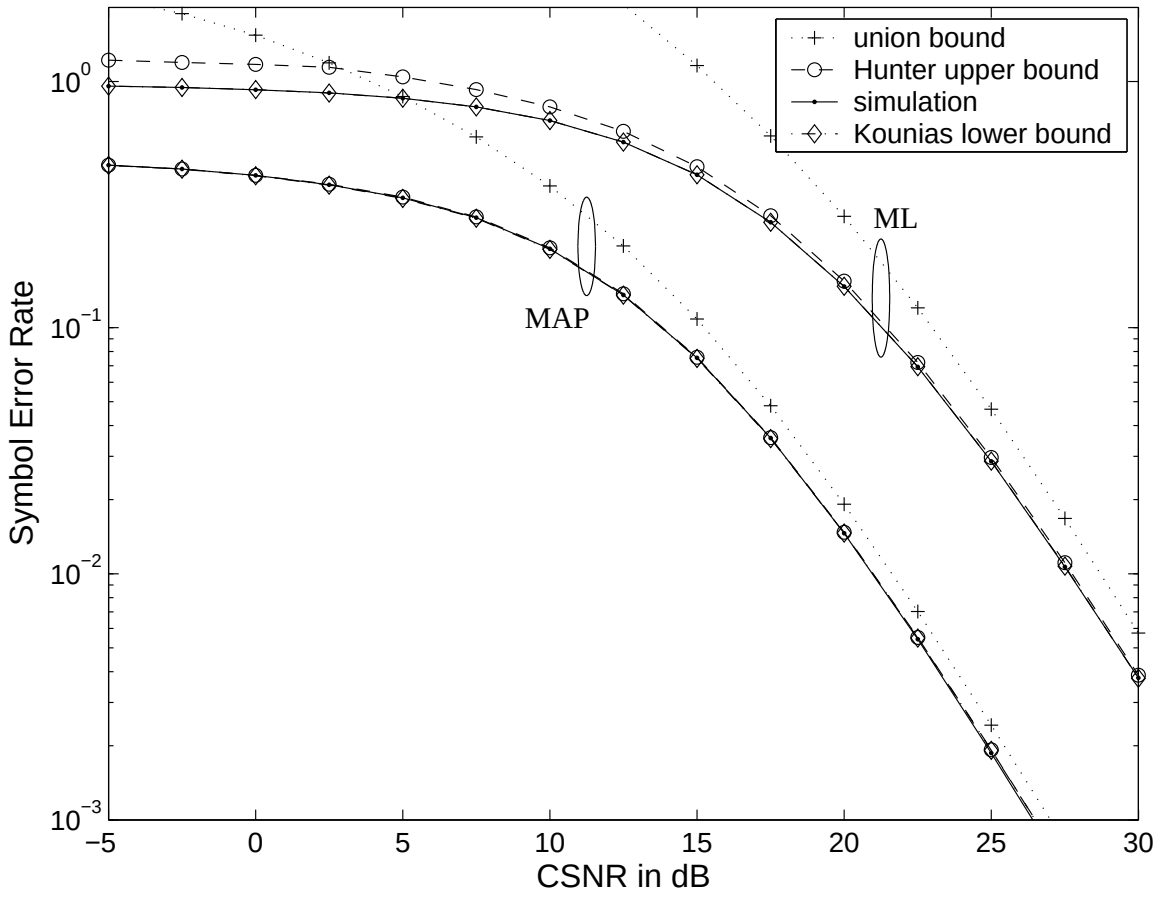

Figure 6.11: SER curves for 64-QAM signaling with Gray mapping, $K = 2$, and $L = 1$.

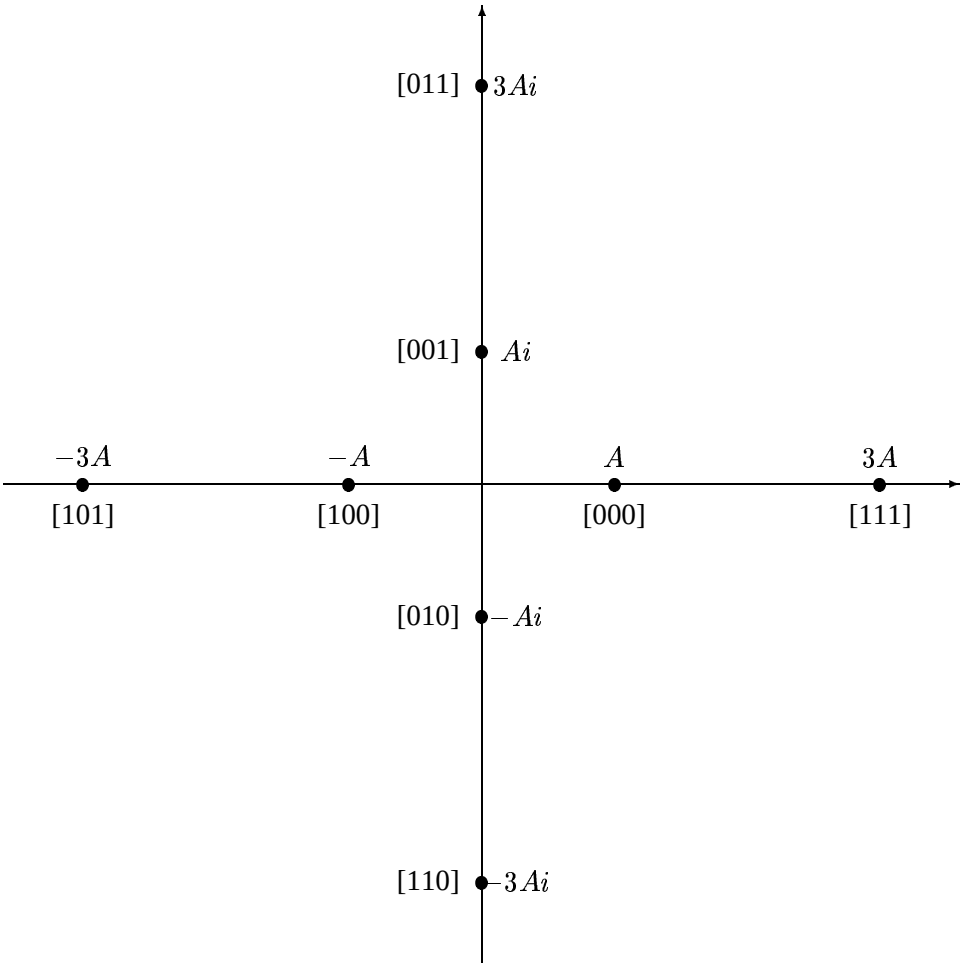

Figure 6.12: The star-QAM signaling scheme with M1 mapping.

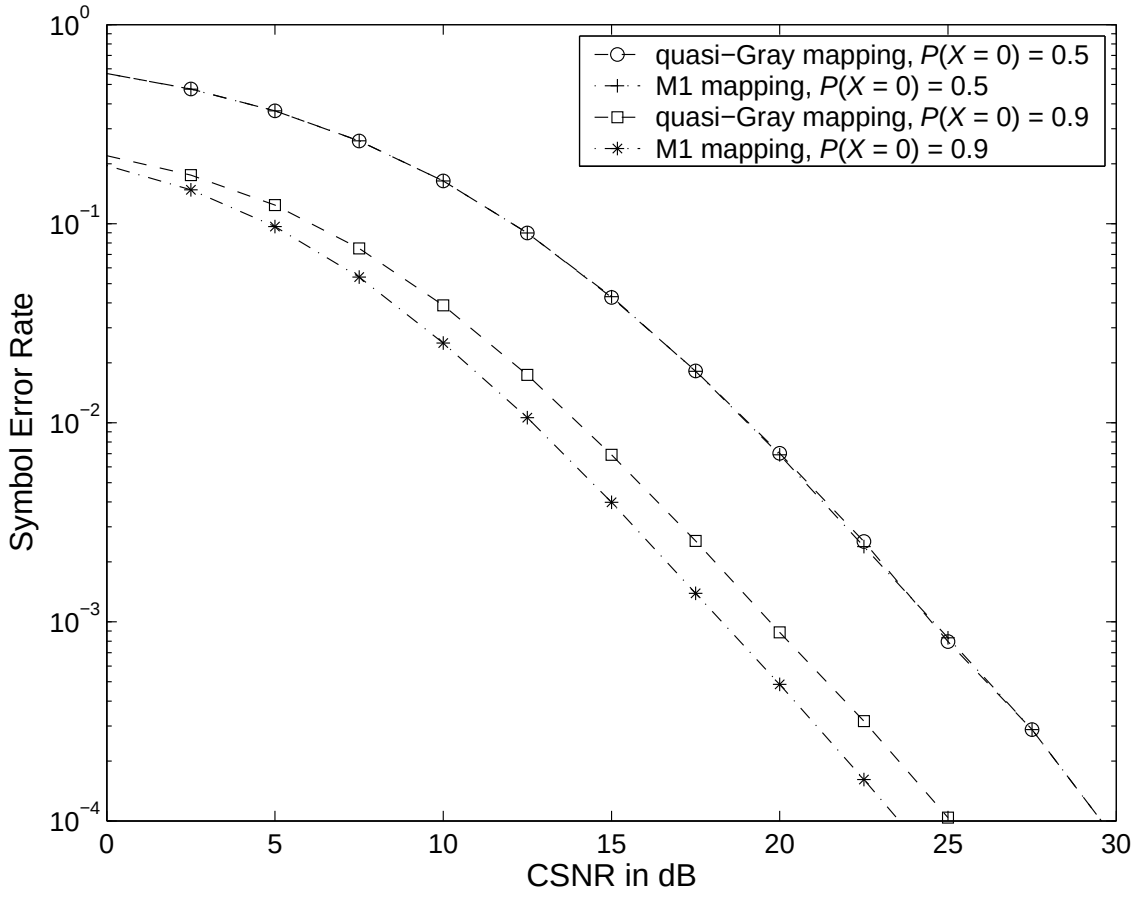

Figure 6.13: Comparison between the quasi-Gray and the M1 mappings with Star QAM for a system with $K = 2$, and $L = 1$.

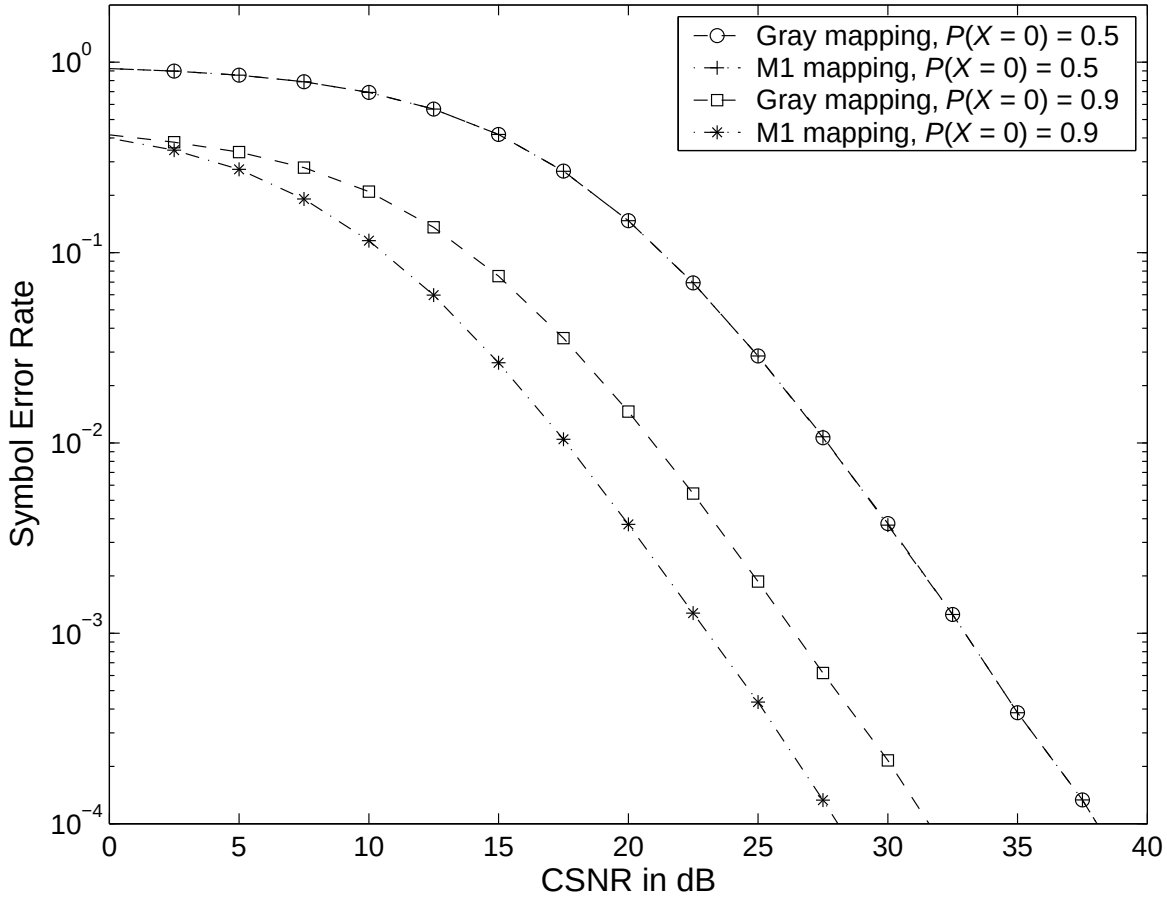

Figure 6.14: Comparison between the M1 and Gray mappings for 64-QAM signaling, $K = 2$, and $L = 1$.

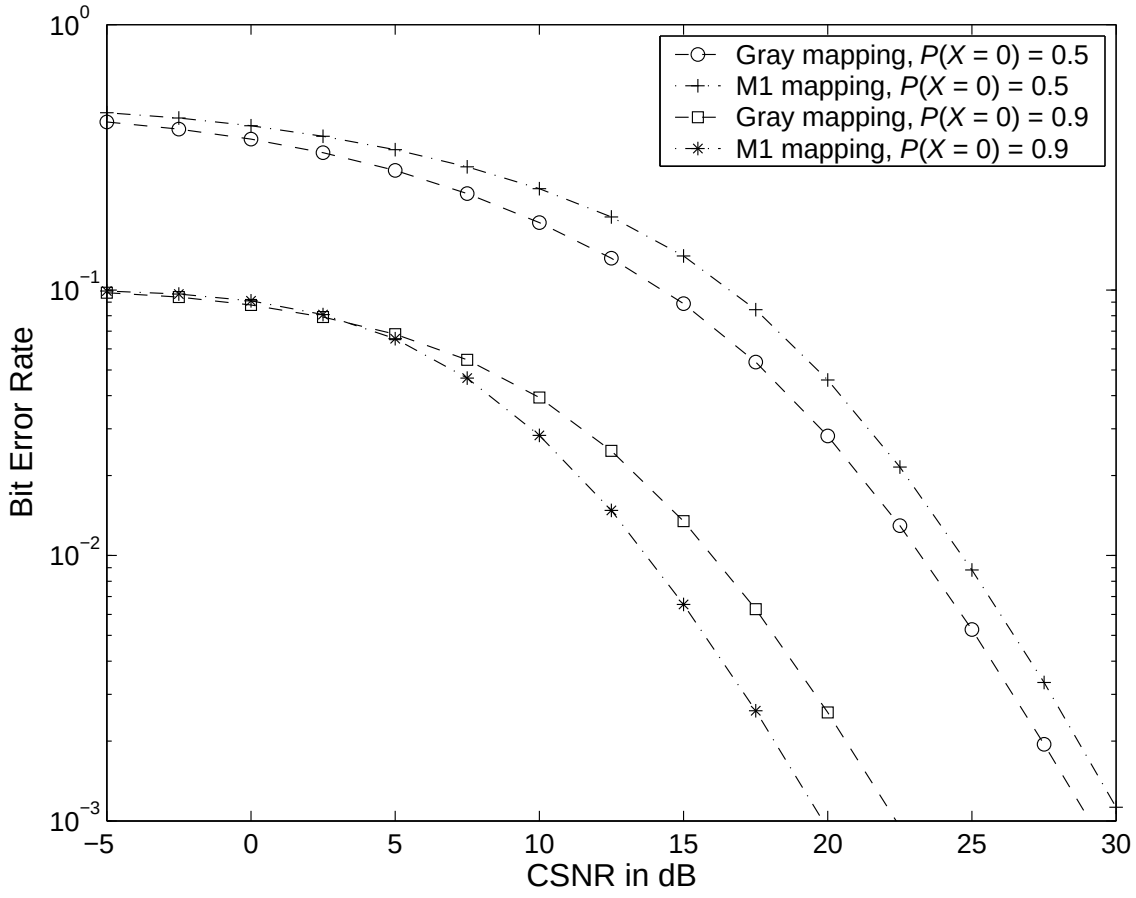

Figure 6.15: Comparison between the BER performance of the M1 and Gray mappings for 64-QAM signaling, $K = 2$, and $L = 1$.

Chapter 7

Quantization with Soft-decision Decoding for MIMO Channels

7.1 Introduction

Like many other error protection schemes that are designed in the spirit of Shannon's separation theorem [160, 161], space-time codes are designed to operate on uniform independent and identically distributed bit-streams. As explained in Subsection 1.3.1, Shannon's separation theorem does not take into consideration constraints on system complexity and delay. Since real-world communication systems are constrained, systems with independent source and channel codes, known as tandem coding systems, may have inferior performance compared with systems which perform source and channel coding jointly.

In this chapter, we consider the transmission of continuous-alphabet (analog) sources over MIMO channels. Our proposed system adds only two blocks, with modest compu-

tational needs, to a conventional space-time coded system. As the system may have multiple receive antennas, an important task is the proper processing of the received signals from the different antennas. We propose to address this problem by performing space-time soft-decoding followed by linear combining at the receiver. The linear combiner has the following key advantages: i) it has a very simple structure, ii) its design criterion allows the COVQ index transition probabilities to be determined in closed form, and iii) its output is continuous, making soft-decision decoding possible. Inspired by the work in [6, 146], we use soft-decision decoding as opposed to soft-decoding methods such as the work in [179], to exploit the soft information available at the output of the linear combiner. Our choice is motivated by two factors. First, soft-decision decoding may be implemented via a q-bit uniform quantizer at the receiver (not to be confused with the COVQ blocks at the transmitter and the receiver) which makes the task of decoding computationally simple. In contrast, the first version of soft-decoding in [179] needs the computation of trigonometric functions and matrix multiplication and the second version also requires matrix inversion. Second, as discussed in [6], the performance of soft-decision decoding can be close to that of soft-decoding and requires less computational complexity (although its storage complexity may be higher).

We show that the concatenation of the space-time encoder, the MIMO channel, the space-time soft-decoder, the combiner, and the uniform scalar quantizer is equivalent to a binary-input, 2^q-output discrete memoryless channel (DMC) used kr times, where k and r are the quantizer dimension and rate, respectively. The step-size of the uniform quantizer used for soft-decision decoding is numerically selected, so that the capacity of the equivalent DMC is maximized for each value of the channel signal-to-noise ratio (CSNR). This is

a heuristic (sub-optimal) criterion, but as the simulation results of [146] demonstrate, there is a substantial correlation between maximizing channel capacity and minimizing distortion. We show that the transition probabilities of this equivalent DMC can be expressed in terms of the symbol pairwise error probability of the ML-decoded space-time orthogonal block coded channel. Hence, these probabilities can be determined using (3.18).

We design three soft-decision decoding COVQs for the equivalent DMC. The first COVQ is the classical COVQ which assumes that the index transition probabilities are known at both the transmitter and the receiver. The COVQ codebook is determined iteratively using the modified generalized Lloyd algorithm [66]. As the CSNR is not always available at the transmitter, we consider the design of two fixed-encoder adaptive-decoder (FEAD) COVQs. In a FEAD COVQ, the encoder is designed for a fixed CSNR and the decoder, which can estimate the channel fading coefficients and the CSNR, adapts itself to the channel conditions. Our first FEAD COVQ uses only the knowledge of the CSNR at the receiver (as in [180]), while the second one, which we call the On-line FEAD COVQ, employs also the knowledge of the channel fading coefficients at the receiver and, as a result, it outperforms the FEAD COVQ. An important feature of FEAD COVQ is that its decoder codebooks are *computed* in terms of the transmitter parameters, and not through a training process as for classical COVQ. Therefore, this method does not need a large memory at the receiver to store a different codebook for each value of the CSNR. We demonstrate that with a proper choice of the design CSNR, the performance loss of FEAD COVQ can be significantly reduced as compared with the classical COVQ.

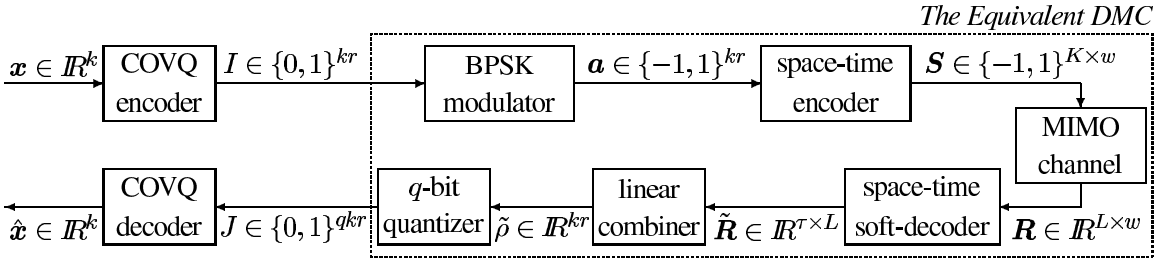

Figure 7.1: System block diagram, where every τ bits in a kr-bit index I is transmitted via a space-time codeword $\boldsymbol{S} = (\boldsymbol{s}_1, ..., \boldsymbol{s}_w)$ (with orthogonal columns $\boldsymbol{s}_i, i = 1, ..., w = g\tau$), received as $\boldsymbol{R} = (\boldsymbol{r}_1, ..., \boldsymbol{r}_w)$, and space-time soft-decoded as $\tilde{\boldsymbol{R}} = (\tilde{\boldsymbol{r}}^1, ..., \tilde{\boldsymbol{r}}^L)$. For simplicity, we have assumed that $\tau = kr$.

7.2 System Components

The system block diagram is shown in Figure 7.1. A COVQ encoder forms a vector $\boldsymbol{x}$ of dimension k from the incoming scalar source samples. It then encodes $\boldsymbol{x}$ at a rate of r bits per sample (bps) into a binary index I of length kr bits, whose bits are each mapped to a signal in the BPSK signaling scheme consisting of $c_{(1)}$ and $c_{(2)}$. Encoding is specified by the decision regions $\{S_i\}_{i=0}^{N_e}$ ($N_e = 2^{kr}$), which form a partition of the k-dimensional space, using the rule that $I = i$ if $\boldsymbol{x} \in S_i$. Index I is then sent over the channel and received as index J. The COVQ decoder simply uses $\boldsymbol{v}_J$, the J^{th} element in the codebook, to reconstruct $\boldsymbol{x}$ as $\hat{\boldsymbol{x}} = \boldsymbol{v}_J$. The goal in COVQ design is to minimize the expected value of $\|\boldsymbol{x} - \hat{\boldsymbol{x}}\|^2$ through finding the optimal partition and codebook.

Our objective is to model the concatenation of the blocks between the encoder and the decoder of the vector quantizer by a discrete channel and then design efficient vector quantization systems for this channel. The system is designed so that the channel judiciously

incorporates the soft-information of the STOB-coded channel and admits a closed-form expression for its transition probabilities. This is achieved by designing a soft-decision decoding space-time receiver which consists of a space-time soft detector, followed by a linear combiner (with optimized weight coefficients), and a simple q-bit scalar uniform quantizer (whose cell size is chosen so the capacity of the equivalent discrete channel is maximized). As a result of the simple memoryless structure of our receiver and due to the orthogonality of the space-time code, we obtain that the equivalent discrete channel is indeed a binary-input 2^q-output memoryless channel whose distribution can be easily determined analytically in terms of the system parameters. In the following, we describe the system components in detail.

7.2.1 The Channel

From (3.12), the output of the STOB soft-decoder is given by

$$\tilde{\boldsymbol{r}}^j = g' Y_j \boldsymbol{c} + \tilde{\boldsymbol{n}}^j,$$

where $g' = g\sqrt{\gamma_s / K}$. We remember that each entry $\tilde{R}_t^j$ of $\tilde{\boldsymbol{r}}^j$ is associated with only one transmitted symbol in $\boldsymbol{c}$. From (6.3), we know that

$$\tilde{N}_t^j \sim \text{i.i.d. } \mathcal{N}(0, gY_j), \quad j = 1, ..., L, t = 1, ..., \tau, \tag{7.1}$$

and hence symbol i can be detected by only considering the i^{th} entry of the vectors $\tilde{\boldsymbol{r}}^j$, $1 \leq j \leq L$. For our application, this will imply that the bits corresponding to a COVQ index can be detected independently. The pairwise error probability between a pair of ML

decoded STOB coded BPSK symbols $c_{(i)}$ and $c_{(j)}$ was given in (3.18) as

$$\begin{aligned}\Lambda(\delta) \stackrel{\triangle}{=} P(c_{(i)} \to c_{(j)}) &= E_Y\left[Q\left(\delta\sqrt{Y}\right)\right] \\ &= \frac{1}{2}\left(1 - \frac{\delta}{\sqrt{2+\delta^2}}\sum_{k=0}^{KL-1}\binom{2k}{k}\frac{1}{(2\delta^2+4)^k}\right), \end{aligned} \quad (7.2)$$

where $\delta = \sqrt{2g\gamma_s/K}$.

7.2.2 Soft-Decision Decoding and the Equivalent DMC

Soft-Decision Decoding: Linear Combining and Scalar Quantization

Many communication systems employ hard decoding in processing the received signals of space-time coded systems and so do not exploit the soft information available at the space-time soft-decoder outputs $\tilde{\boldsymbol{r}}^1, ..., \tilde{\boldsymbol{r}}^L$. Methods that exploit soft information can provide significant performance gains. In our case, in addition to using the soft information efficiently, the solution should allow the COVQ index transition probabilities to be determined in closed form, since this is required for the COVQ design and encoding phases. As we illustrate below and in Section 7.4, linear combining has both of the above properties.

This design problem is a variation of the classical maximum ratio combining (MRC) setup [150] in which the signals to be combined (the space-time soft-decoded signals) have different noise variances (see (7.1)). Letting $\tilde{\rho}_i^j \stackrel{\triangle}{=} \tilde{R}_i^j/(g'Y_j)$, we can write the output of the linear combiner as (see Figure 7.2)

$$\tilde{\rho}_i = \sum_{j=1}^{L}\alpha_j\frac{\tilde{R}_i^j}{g'Y_j} = \sum_{j=1}^{L}\alpha_j(c_i + \tilde{\eta}_i^j), \quad i = 1, ..., \tau, \quad (7.3)$$

where c_i is the i^{th} transmitted symbol and the α_j's are weighting coefficients to be determined. From (7.1), we know that the distribution of $\tilde{\eta}_i^j$, the noise component of $\tilde{\rho}_i^j$, is $\mathcal{N}(0, g/(g'^2 Y_j))$. Therefore, the SNR at the output of the linear combiner is

$$\text{SNR}_{\text{CO}} = \frac{\left(\sum_{j=1}^{L} \alpha_j\right)^2}{\sum_{j=1}^{L} \frac{g}{g'^2 Y_j} \alpha_j^2} \cdot \tag{7.4}$$

In linear combining, the objective is then to choose the weights $\{\alpha_j\}_{j=1}^{L}$ so that SNR_{CO} is maximized by enforcing the constraint $\sum_{j=1}^{L} \alpha_j = 1$. Therefore, the problem is to minimize the denominator of (7.4), i.e., finding

$$\min \sum_{j=1}^{L} \frac{g}{g'^2 Y_j} \alpha_j^2,$$

subject to $\sum_{j=1}^{L} \alpha_j = 1$. Minimizing the Lagrangian

$$D_\lambda = \sum_j \frac{g}{g'^2 Y_j} \alpha_j^2 + \lambda \left(\sum_j \alpha_j - 1 \right),$$

we obtain that $\lambda = -2g/(g'^2 Y)$, and $\alpha_j = Y_j/Y$. Therefore, the output of the combiner can be written from (7.3) as

$$\tilde{\rho}_i = c_i + \tilde{\eta}_i, \tag{7.5}$$

where $\tilde{\eta}_i = \sum_{j=1}^{L} \alpha_j \tilde{\eta}_i^j$. We note that $E\left[\tilde{\eta}_i^2\right] = (g'Y)^{-2} \sum_{j=1}^{L} E\left[\tilde{\eta}_i^{j2}\right]$, and therefore,

$$\tilde{\eta}_i \sim \mathcal{N}\left(0, \frac{K}{g\gamma_s Y}\right), \quad i = 1, ..., \tau. \tag{7.6}$$

It is easy to verify that when $q = 1$ (i.e., hard decoding), the concatenation of the linear combining and decision blocks is equivalent to ML decoding.

The linear combiner output, $\tilde{\rho}_i$, is next fed into a "uniform" scalar quantizer which acts as the soft-decision decoder. Let us indicate the decision levels of this quantizer by

$\{u_k\}_{k=-1}^{N-1}$ and its codepoints by $\{w_k\}_{k=0}^{N-1}$, where $N = 2^q$ is the number of the codewords. As $\tilde{\rho}_i$ can take any real value, the quantizer should have two unbounded decision regions. The decision regions of the uniform quantizer are given by

$$u_k = \begin{cases} -\infty, & \text{if } k = -1 \\ (k + 1 - N/2)\Delta, & \text{if } k = 0, \cdots, N-2 \\ +\infty, & \text{if } k = N-1, \end{cases}$$

and the quantization rule $f(\cdot)$ is simply

$$f(\tilde{\rho}) = k, \quad \text{if } \tilde{\rho} \in (u_{k-1}, u_k], \quad k = 0, \cdots, N-1.$$

Transition Probabilities of the Equivalent DMC

For COVQ design, we need to derive the transition probabilities of the 2^{kr}-input 2^{qkr}-output discrete channel represented by the concatenation of the space-time encoder, the MIMO channel, the space-time soft-decoder, the linear combiner, and the uniform quantizer. Since the detection of bits which correspond to each quantizer index is decoupled, we note that the transmission and decoding of COVQ indices are independent of one another, and also the discrete channel is equivalent to a binary-input 2^q-output DMC used kr times. We shall refer to this discrete channel as the "equivalent DMC".

The required set of the transition probabilities are $P(w_k|c_{(1)})$ and $P(w_k|c_{(2)})$ for all w_k, where $c_{(1)}$ and $c_{(2)}$ are the BPSK constellation points which, without loss of generality, are assumed to correspond to 1 and 0, respectively. Decision is made in favor of the k^{th} codepoint if the output of the linear combiner falls into the $(u_{k-1}, u_k]$ interval of length Δ.

Using (7.5) and (7.6) we can write

$$\begin{aligned} P(w_k|c_{(i)}, \boldsymbol{H}) &= P(u_{k-1} \leq c_{(i)} + \tilde{\eta}_i < u_k|\boldsymbol{H}) \\ &= Q\left((u_{k-1} - c_{(i)})\delta\sqrt{Y}\right) - Q\left((u_k - c_{(i)})\delta\sqrt{Y}\right). \end{aligned} \tag{7.7}$$

The expectation over $\boldsymbol{H}$ of each of the above $Q(\cdot)$ functions can be determined using (7.2) to yield

$$P(w_k|c_{(i)}) = \Lambda\left(\left(u_{k-1} - c_{(i)}\right)\delta\right) - \Lambda\left(\left(u_k - c_{(i)}\right)\delta\right), \tag{7.8}$$

where $\Lambda(\cdot)$ is defined in (7.2). Note that the DMC transition probability matrix is symmetric in the sense of [63].

For our k-dimensional COVQ with rate r shown in Figure 7.1, we denote the natural binary representation of the index of decision region S_i by $\{b_l\}_{l=1}^{kr}$ and that of codevector w_j by $\{B_l\}_{l=1}^{kr}$, where B_l is a binary q-tuple. As the DMC is memoryless, the COVQ index transition probabilities can easily be computed as

$$P_{J|I}(j|i) = \prod_{l=1}^{kr} P\left(w_{B_l}|c_{(2-b_l)}\right). \tag{7.9}$$

7.2.3 The Step-Size of the Uniform Quantizer at the Decoder

The final design parameter of the system is Δ, the step-size of the uniform quantizer at the receiver. For a given CSNR, we numerically select the Δ which maximizes the capacity of the equivalent DMC. This is a sub-optimal criterion since our ultimate goal is minimizing the MSE, not maximizing the capacity, but as the simulation results of [146] demonstrate, there is a strong correlation between having a high channel capacity and reduced mean-squared error distortion.

For a given soft-decision resolution q and CSNR γ_s, we determine the step-size Δ which maximizes the capacity of the DMC by maximizing the mutual information between the DMC input and output. Because the channel transition probability matrix is symmetric, a uniform input distribution achieves channel capacity [63]. Note that the step-size does not depend on the rate or dimension of the COVQ (used to quantize the source), and is only a function of q and the CSNR. As a typical set of results, we list, in Table 7.1, the capacity of the equivalent DMC versus the "optimal" step-size of the uniform quantizer for Alamouti's [9] dual transmit single receive setup. Similar results can be derived for systems with a different number of transmit antennas, receive antennas, or space-time codes. As shown in Figure 7.3, when the step-size is very small (close to zero) or very large, soft-decision decoding does not significantly increase channel capacity. We also note that if the CSNR is high, soft-decision decoding is not very beneficial in terms of improving channel capacity. However, for moderate and low CSNRs, and with the optimal choice of Δ, soft-decision decoding significantly increases channel capacity. For example, at CSNR $= -2$ dB in Table 7.1, there is a 15% benefit in using soft-decision decoding with $q = 5$ bits. Also note that the channel capacity increases less than 1% from $q = 3$ to $q = 5$ even for severe channel conditions. This shows that typically $q = 3$ achieves most of the capacity gain offered by soft-decision decoding.

7.3 Quantization with Soft-Decision Decoding

7.3.1 Soft-Decision Decoding COVQ

The transition probability given in (7.9) can be used in the modified generalized GLA algorithm [66] to design a soft-decision decoding COVQ for space-time coded MIMO channels as explained below. Every input k-tuple is encoded at a rate of r bits per sample. Therefore, the input space is partitioned into $N_e = 2^{kr}$ subsets. As we use BPSK modulation, a vector of kr real-valued signals is received for every transmitted index. This vector is soft-decision decoded at a rate of q bits per dimension. Therefore, each k-dimensional source vector is decoded to one of the $N_d = 2^{qkr}$ codevectors. The input space partitioning and the codebook are optimized based on two necessary conditions for optimality using training data $\{\boldsymbol{x}_l, l = 0, ..., M-1\}$ as follows.

- *The nearest neighbor condition*: for a fixed codebook and $i = 0, \cdots, N_e - 1$, the optimal partition $\mathcal{P}^* = \{S_i^*\}$ is

$$S_i^* = \left\{ \boldsymbol{x} : \sum_{j=0}^{N_d-1} P_{J|I}(j|i) d(\boldsymbol{x}, \boldsymbol{v}_j) \leq \sum_{j=0}^{N_d-1} P_{J|I}(j|l) d(\boldsymbol{x}, \boldsymbol{v}_j), \forall l \right\} \tag{7.10}$$

  where $\boldsymbol{x}$ is a training vector, $\{\boldsymbol{v}_j, j = 0, ..., N_d - 1\}$ is the codebook, $d(\boldsymbol{x}, \boldsymbol{v})$ is the squared Euclidean distance between $\boldsymbol{x}$ and $\boldsymbol{v}$, and ties are broken according to a preset rule.

- *The centroid condition*: given a partition $\mathcal{P} = \{S_i, i = 0, ..., N_e - 1\}$, the optimal codebook $\mathcal{C}^* = \{\boldsymbol{v}_j^*\}$ is

$$\boldsymbol{v}_j^* = \frac{\sum_{i=0}^{N_e-1} P_{J|I}(j|i) \sum_{l:\boldsymbol{x}_l \in S_i} \boldsymbol{x}_l}{\sum_{i=0}^{N_e-1} P_{J|I}(j|i)|S_i|}, \qquad j = 0, \cdots, N_d - 1. \tag{7.11}$$

  where $|S_i|$ is the number of the training vectors in S_i.

Training consists of using the above conditions iteratively to update the codebook until the average training distortion given by

$$D = \frac{1}{kM} \sum_{l=0}^{M-1} \sum_{j=0}^{N_d-1} P_{J|I}(j|\mathcal{I}(\boldsymbol{x}_l)) d(\boldsymbol{x}_l, \boldsymbol{v}_j)$$

converges, where $\mathcal{I}(\boldsymbol{x})$ is the index of the partition cell to which $\boldsymbol{x}$ belongs.

7.3.2 Fixed-Encoder Adaptive-Decoder Soft-Decision Decoding COVQ

Equations (7.2), (7.7)-(7.9) show that the CSNR should be known at both the transmitter and the receiver to compute the COVQ index transition probabilities. The CSNR can be estimated at the receiver and then fed back to the transmitter. As the feedback path may not always be available, it is of particular interest to consider the case where no information about the channel state is available to the transmitter. In [180], a fixed-encoder adaptive-decoder (FEAD) COVQ is proposed which addresses this issue for a different setup involving hybrid digital-analog SISO transmission systems. In the following, we show how to design a FEAD COVQ for the soft-decision decoded STOB coded channel. In addition to having multiple antennas, our FEAD COVQ differs from the one in [180]

in that we have a digital channel (instead of a hybrid digital-analog channel). The block diagram of the FEAD COVQ looks the same as in Figure 7.1. The key difference is that here the encoder partition matches a "design CSNR" and the receiver codebook is adapted to the actual CSNR. The encoder uses a design codebook $\{\boldsymbol{z}_i\}_{i=0}^{N_e-1}$ to find its partition via

$$S_i^* = \left\{ \boldsymbol{x} : \sum_{j=0}^{N_e-1} P_{J|I}(j|i) d(\boldsymbol{x}, \boldsymbol{z}_j) \leq \sum_{j=0}^{N_e-1} P_{J|I}(j|l) d(\boldsymbol{x}, \boldsymbol{z}_j), \forall l \right\}.$$

Because we assume complete lack of information at the transmitter, the encoder codebook $\{\boldsymbol{z}_i\}$ is designed assuming the channel is hard decoded (i.e, that $q = 1$).

The problem is then to adapt the decoder codebook according to the actual CSNR value, while the encoder codebook remains fixed. Let us denote the encoder index by I and the decoder index by J. The average distortion per dimension is given by

$$\begin{aligned} D &= \frac{1}{k} E\left[\|\boldsymbol{x} - \boldsymbol{v}\|^2\right] = \frac{1}{k} \sum_{j=0}^{N_d-1} E\left[\|\boldsymbol{x} - \boldsymbol{v}\|^2 | J = j\right] P_J(j) \\ &= \frac{1}{k} \sum_{j=0}^{N_d-1} E\left[\|\boldsymbol{x} - \boldsymbol{v}_j\|^2 | J = j\right] P_J(j). \end{aligned} \tag{7.12}$$

The goal in quantizer design is to derive the $\boldsymbol{v}_j$ which minimize (7.12). This gives the optimal $\boldsymbol{v}_j$ in the minimum MSE sense as

$$\begin{aligned} \boldsymbol{v}_j^* &= E\left[\boldsymbol{x} | J = j\right] = \sum_{i=0}^{N_e-1} E\left[\boldsymbol{x} | I = i, J = j\right] P_{I|J}(i|j) \\ &= \sum_{i=0}^{N_e-1} \boldsymbol{m}_i P_{I|J}(i|j), \quad j = 0, \cdots, N_d - 1. \end{aligned} \tag{7.13}$$

where $\boldsymbol{m}_i = \int_{S_i} \boldsymbol{x} p(\boldsymbol{x}) d\boldsymbol{x}$ denotes the mean of the samples in S_i and (7.13) follows because $E\left[\boldsymbol{x} | I = i, J = j\right] = E\left[\boldsymbol{x} | I = i\right] = \boldsymbol{m}_i$. Note that the decoder can simply determine $P_{I|J}(i|j)$ as

$$P_{I|J}(i|j) = \frac{P_{J|I}(j|i) P_I(i)}{\sum_{l=0}^{N_e-1} P_{J|I}(j|l) P_I(l)}, \tag{7.14}$$

where $P_I(i) = P(I = i) = P(\boldsymbol{x} \in S_i)$. Also note that $P_I(i)$ and $\boldsymbol{m}_i$ can be approximated in the training phase of the encoder as follows

$$P_I(i) \approx \frac{|S_i|}{M}, \qquad \boldsymbol{m}_i \approx \frac{1}{|S_i|} \sum_{l:\boldsymbol{x}_l \in S_i} \boldsymbol{x}_l. \tag{7.15}$$

From (7.13), we observe that unlike COVQ, given the encoder means $\{\boldsymbol{m}_i\}_{i=0}^{N_e-1}$, the FEAD-COVQ does not require a training phase to determine $\{\boldsymbol{v}_j\}$. In other words, the decoder codebook is *computed* from the channel transition probabilities and the encoder means via (7.13) and (7.14).

7.3.3 On-line FEAD Soft-Decision Decoding COVQ

One of our assumptions is that the receiver has perfect knowledge of the channel fading coefficients without error. In light of this assumption, we observe in equation (7.5) that the output of the linear combiner has an identical form to the output of an additive white Gaussian noise channel with the variance of the additive noise $\tilde{\eta}_i$ known at the receiver and given by (7.6). This motivates us to apply soft-decision decoding directly on $\tilde{\rho}_i$ using the step-size Δ derived in [146, Section II]) for AWGN channels. The channel transition probabilities, given the path gains matrix $\boldsymbol{H}$, are given by

$$\begin{aligned} P(w_k|c_{(j)}, \boldsymbol{H}) &= P(u_{k-1} \leq c_{(j)} + \tilde{\eta}_i < u_k|\boldsymbol{H}) \\ &= Q\left((u_{k-1} - c_{(j)})\delta\sqrt{Y}\right) - Q\left((u_k - c_{(j)})\delta\sqrt{Y}\right), \end{aligned}$$

Note that the above derivation is valid if the channel fading coefficients remain constant during the transmission time of an index.

7.4 Numerical Results and Discussion

7.4.1 Implementation Issues

We consider the transmission of zero-mean unit-variance i.i.d. Gaussian and Gauss-Markov sources over MIMO channels. 500,000 training vectors and 850,000 test vectors are employed. Each test is performed 5 times and the average signal-to-distortion ratio (SDR) in dB is reported. MIMO systems with K transmit and L receive antennas are referred to as $(K$-$L)$ systems. Alamouti's code [9] is used for the dual transmit-antenna systems. The real (rate 1) code of [192] is employed for the quad-transmit system because our constellation is real.

Several training strategies were examined, and the best one in terms of having consistent results and high training SDR was used as follows. For any given COVQ rate r, dimension k, and number of soft-decision decoding bits q, we first train a k-dimensional rate-qr VQ with the Split algorithm [66]. We next use the Simulated Annealing algorithm [49] which aims to minimize the average end-to-end distortion for a given VQ codebook through optimizing the assignment of indices of the VQ codevectors. The average overall distortion can be written as

$$\begin{aligned} D &= \frac{1}{k}E\left[d(\boldsymbol{x},\boldsymbol{v})\right] = \frac{1}{k}\sum_{i=0}^{N_e-1}\sum_{j=0}^{N_d-1} E\left[d(\boldsymbol{x},\boldsymbol{v})|I=i,J=j\right] P_{I,J}(I=i,J=j) \\ &= \frac{1}{k}\sum_{i} P_I(i)\sum_{j} P_{J|I}(j|i)\int_{S_i}\|\boldsymbol{x}-\boldsymbol{v}_{\pi(j)}\|^2 p(\boldsymbol{x})d\boldsymbol{x} \\ &= \frac{1}{k}E\left[\|\boldsymbol{x}\|^2\right] + \frac{1}{k}\sum_{i} P_I(i)\sum_{j} P_{J|I}(j|i)\langle \boldsymbol{v}_{\pi(j)}, (\boldsymbol{v}_{\pi(j)}-2\boldsymbol{m}_i)\rangle, \end{aligned} \tag{7.16}$$

where $\langle\boldsymbol{\alpha},\boldsymbol{\beta}\rangle = \sum_i \alpha_i\beta_i$ is the standard inner product and $\pi : \{0,\cdots,N_d-1\} \rightarrow$

$\{0, \cdots, N_d - 1\}$ is the one-to-one mapping function to be optimized. It follows that the cost function to be minimized equals

$$\sum_{i=0}^{N_e-1} P_I(i) \sum_{j=0}^{N_d-1} P_{J|I}(j|i) \langle \boldsymbol{v}_{\pi(j)}, (\boldsymbol{v}_{\pi(j)} - 2\boldsymbol{m}_i) \rangle.$$

Simulated Annealing is used only at the highest CSNR. We then use an approach similar to the one in [50]; namely, we use the modified generalized Lloyd algorithm to derive the COVQ codebooks starting from the highest CSNR to the lowest and vice-versa. This method is referred to as the "decrease-increase" (DI) method. Another way to obtain the codebooks could be starting from the highest CSNR down to the lowest, which we refer to as the "decreasing" method.

Table 7.2 compares the results of the DI and descending methods for various STOB coded systems. It is observed that the DI method is mostly beneficial at low CSNR values. This is because at low CSNR some encoder cells are empty. Empirical results show that these cells are optimized more efficiently through the CSNR-increasing loop.

7.4.2 COVQ for Various MIMO Channels

Figure 7.4 plots the SDR curves of various COVQ-based space-time coded systems as a function of the CSNR. Even at the low COVQ dimension and rate considered here, the gain of using MIMO channels over the SISO channel is obvious. For example, at SDR = 5 dB, the (2-1) system outperforms the SISO system by 6 dB (for hard-decoding) and is outperformed by the (2-2) system by 4.3 dB. This figure also demonstrates the effectiveness of our linear combiner. Note that as the signal power collected by the (2-2) system is twice

that of the (4-1) system, the former has a better performance, although the diversity gain of both of the systems is the same and equals $KL = 4$.

We observe in Table 7.1 that soft-decision decoding becomes less beneficial as the CSNR grows. Increasing the number of transmit or receive antennas results in a CSNR gain due to space diversity. Therefore, we expect that increasing the number of transmit or receive antennas would leave little room for further enhancement through soft-decision decoding. It follows from (7.6) that between two systems with the same diversity gain, coding gain g, and CSNR γ_s, the one with fewer transmit antennas has a higher SNR at its linear combiner output. In other words, given two systems with the same diversity gain, the one with more transmit antennas obtains a larger soft-decision decoding gain. This result can be stated more intuitively: systems with more receive branches collect more signal power. Hence, the SNR at their linear combiner would be higher, making soft-decision decoding less effective. This observation is supported by the simulations of Figure 7.4: at CSNR = 4 dB, the soft-decision decoding gain in SDR is 0.29 dB for both of the (2-1) and (4-1) systems; this gain reduces to 0.12 dB for the (2-2) system.

7.4.3 COVQ versus Tandem Coding

We next compare our COVQ-based system with traditional tandem coding schemes which use separate source coding and channel coding blocks with VQ and convolutional coding (CC), respectively. We consider, in Figure 7.5, a (2-1) system and quantization with dimension $k = 2$. The overall rate is 3.0 bps and hence there are six choices for the (VQ, CC) code rates; namely, (0.5, $1/6$), (1.0 , $1/3$), (1.5, $1/2$), (2.0, $2/3$), (2.5 , $5/6$), and (3.0,

0). The first four convolutional codes have 64 states and are non-systematic with free distances of 27 [116], 14, 10, and 5 [101]. For rate $5/6$, we use a rate-compatible punctured convolutional (RCPC) code with a rate-$1/2$ mother code. The generator polynomials of the rate-$1/6$, $1/3$, $1/2$, and $2/3$ convolutional codes are given by (754, 644, 564, 564, 714, 574), (574, 664, 744), (634, 564), and (3, 4, 5; 4 3 7). They are the strongest codes given in [101, 150] for the given number of states. The generator polynomials are defined as in [101]. The generator polynomials of the mother code for the rate-$5/6$ code are (554, 744) and its puncturing matrix is given by $\binom{11010}{10101}$ [150]. Figure 7.5 shows a typical behavior: the jointly designed COVQ outperforms the substantially more complex tandem systems almost everywhere. Further tests with i.i.d. sources yield even more supportive results towards COVQ.

Note that if one aims to design an unequal error protection (UEP) joint source-channel coder with the above separate coders (i.e., select the best tandem coder at each CSNR), one needs to design an algorithm to allocate the source and channel code rates for each given CSNR, thus increasing the complexity of the UEP system. COVQ does not have this problem since error protection in COVQ is built-in.

7.4.4 COVQ, FEAD COVQ, and On-line FEAD COVQ

Figure 7.6 demonstrates the performance of a (2-1) system quantizing an i.i.d. $\mathcal{N}(0,1)$ source with various rate-2 bps FEAD COVQs with dimension $k = 2$. A FEAD$_\gamma$ COVQ is one whose design CSNR is γ dB. The FEAD VQ assumes that the channel is noiseless; hence it has a lower computational complexity at the encoder. The figure shows that such an

assumption will lead to a significant SDR loss at low to medium CSNRs. FEAD_0 COVQ also suffers from a considerable performance degradation at high CSNRs. It seems that assuming a mid-range CSNR of 8 dB (for the given MIMO system) will lead to reasonable performance everywhere.

The three quantizers presented in this chapter are compared in Figure 7.7, where a unit-variance Gauss-Markov source is quantized with dimension 2 and rate 1 bps and sent over a (2-1) system. The FEAD VQs are designed assuming a noiseless channel, hence the SDR of the three systems become closer as the CSNR grows because the channel mismatch of the VQs decreases. The On-line FEAD VQ maintains its gain over the FEAD VQ when soft-decision decoding is employed. It is also observed that although the On-line FEAD VQ encoder assumes the channel is noiseless (CSNR $\rightarrow \infty$), it slightly outperforms the COVQ, which is designed for the exact CSNR, at high CSNRs.

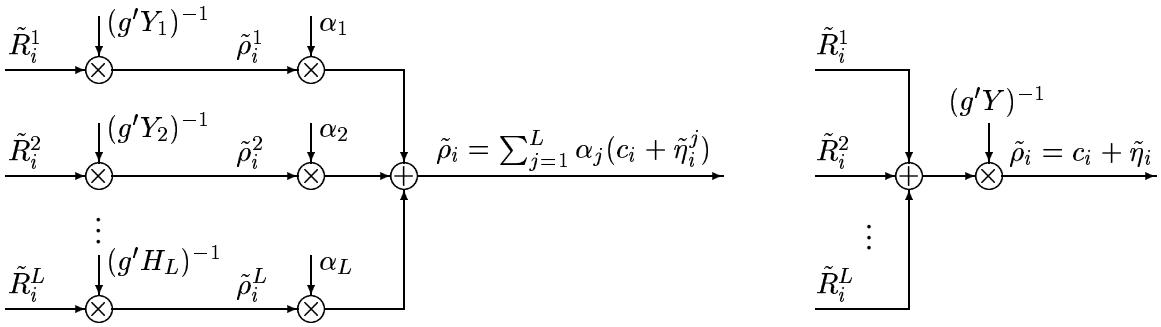

Figure 7.2: Linear combiner which follows the space-time soft decoder at the receiver. Left: problem statement, right: solution to the problem.

CSNR	$q=1$	$q=2$		$q=3$		$q=4$		$q=5$	
(dB)	C	C	Δ	C	Δ	C	Δ	C	Δ
16.0	0.9945	0.9969	0.414	0.9973	0.219	0.9974	0.183	0.9974	0.108
14.0	0.9881	0.9929	0.403	0.9937	0.214	0.9939	0.109	0.9940	0.109
12.0	0.9752	0.9842	0.394	0.9858	0.209	0.9862	0.107	0.9864	0.111
10.0	0.9506	0.9660	0.390	0.9695	0.207	0.9702	0.107	0.9705	0.113
8.0	0.9070	0.9333	0.393	0.9381	0.208	0.9392	0.108	0.9397	0.116
6.0	0.8374	0.8760	0.405	0.8833	0.214	0.8849	0.111	0.8855	0.120
4.0	0.7386	0.7891	0.430	0.7987	0.226	0.8009	0.118	0.8015	0.128
2.0	0.6164	0.6741	0.472	0.6852	0.248	0.6877	0.129	0.6884	0.139
0.0	0.4849	0.5427	0.536	0.5540	0.280	0.5565	0.146	0.5572	0.157
-2.0	0.3608	0.4142	0.627	0.4223	0.327	0.4246	0.170	0.4252	0.183
-4.0	0.2560	0.2974	0.751	0.3057	0.390	0.3076	0.203	0.3081	0.219

Table 7.1: Capacity (in bits/channel use) of the DMC derived from q-bit soft-decision decoding of BPSK-modulated space-time coded MIMO channel with $K = 2$ and $L = 1$. Δ is the step-size which maximizes the capacity and q is number of soft-decision decoding bits.

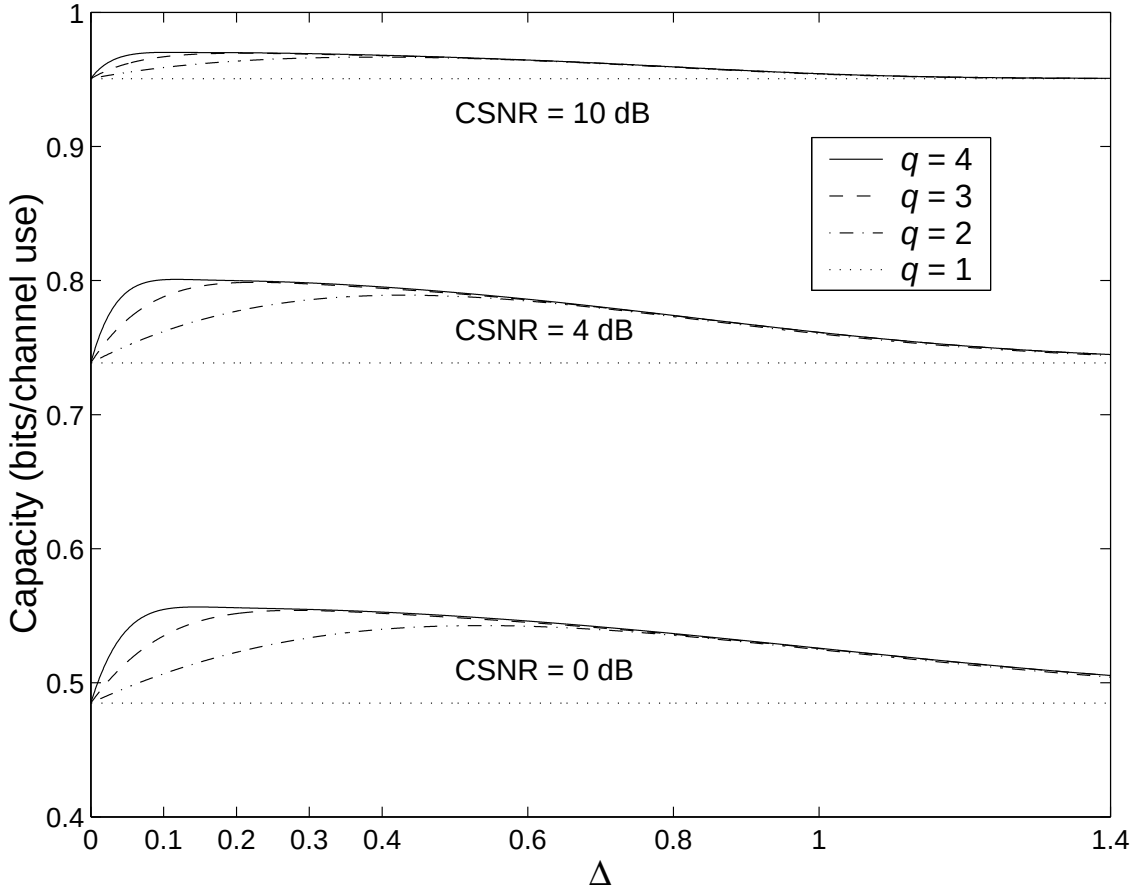

Figure 7.3: DMC capacity versus the step-size of the uniform quantizer, $K = 2$, $L = 1$.

CSNR	(2-1)		(4-1)		(2-2)	
in dB	DI	decreasing	DI	decreasing	DI	decreasing
10	7.385	7.368	7.809	7.795	7.899	7.876
8	6.886	6.845	7.551	7.536	7.867	7.839
6	6.119	6.026	6.949	6.908	7.712	7.691
4	5.167	4.968	5.948	5.832	7.288	7.272
2	4.178	3.830	4.781	4.508	6.477	6.416
0	3.315	2.783	3.714	3.245	5.353	5.179
-1	2.916	2.329	3.266	2.700	4.772	4.508
-2	2.546	1.930	2.830	2.224	4.217	3.853
-3	2.202	1.578	2.436	1.818	3.713	3.245

Table 7.2: Comparison between the training SDR (in dB) of two COVQ training methods for a unit-variance Gauss-Markov source ($\rho = 0.9$) channel-optimized vector quantized at rate $r = 1.0$ bps. Quantization dimension is $k = 2$. Three MIMO systems are considered with $(K\text{-}L) = (2\text{-}1)$, $(4\text{-}1)$, and $(2\text{-}2)$.

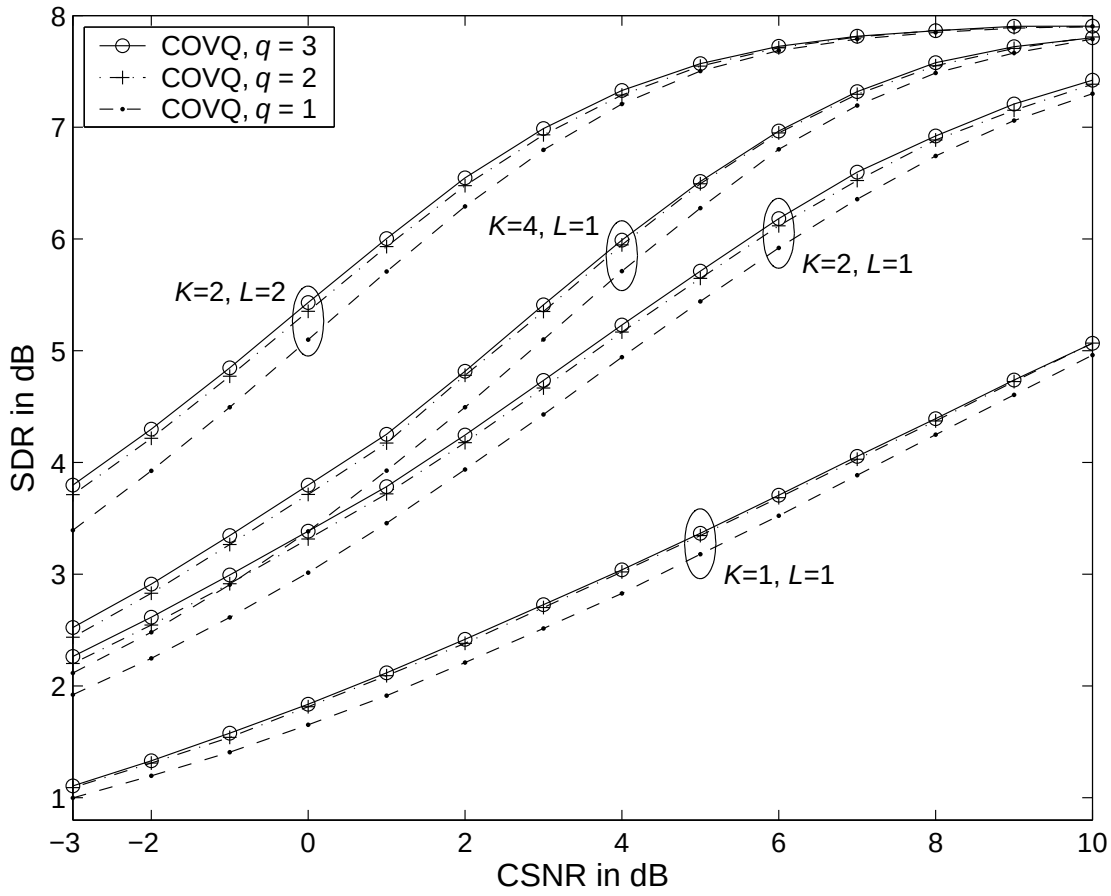

Figure 7.4: Simulated SDR in dB for a zero-mean unit-variance Gauss-Markov source ($\rho = 0.9$) vector quantized at rate $r = 1.0$ bps and soft-decision decoded with q bits. Quantization dimension is $k = 2$.

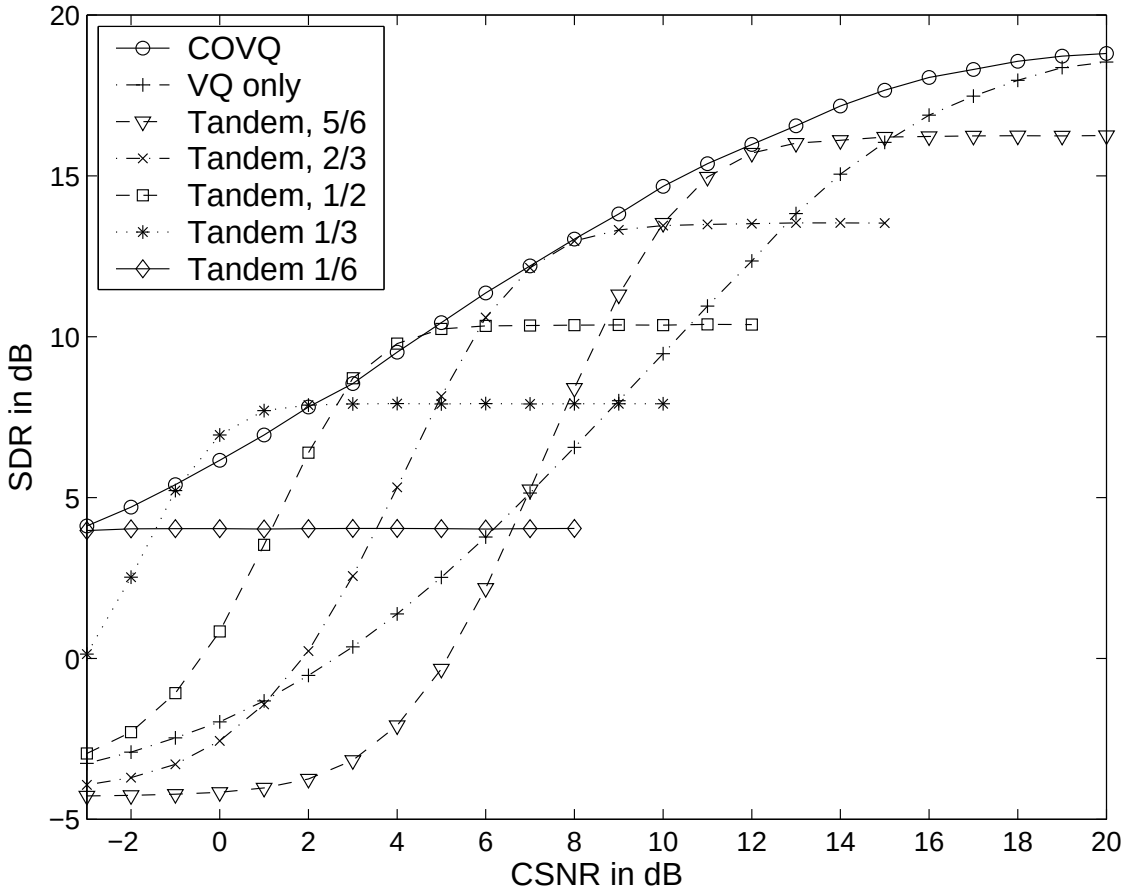

Figure 7.5: Jointly designed versus tandem coding schemes for a zero-mean unit-variance Gauss-Markov source ($\rho = 0.9$). Quantization dimension is $k = 2$ and the overall rate is $r = 3.0$ bps. $K = 2$ and $L = 1$.

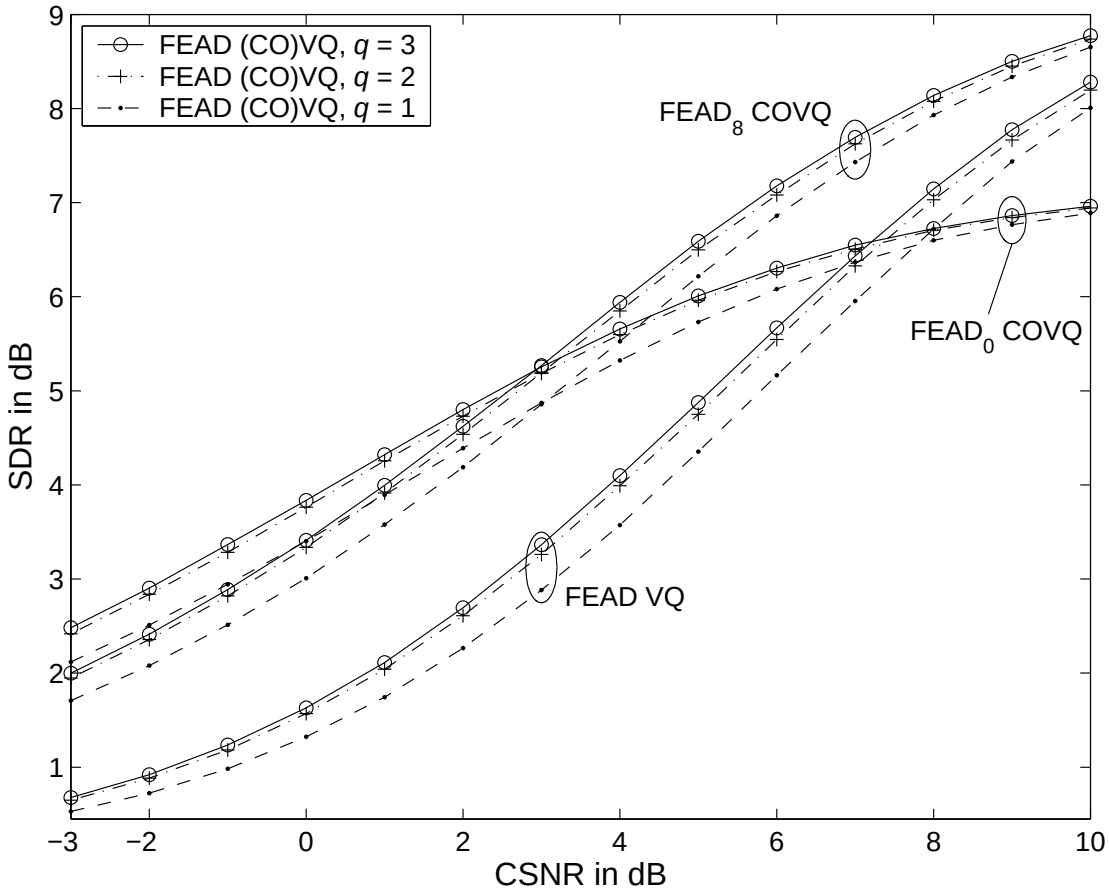

Figure 7.6: Simulated SDR in dB for an i.i.d. $\mathcal{N}(0,1)$ source vector quantized at rate $r = 2.0$ bps and soft-decoded with q bits. Quantization dimension is $k = 2$. $K = 2$ and $L = 1$.

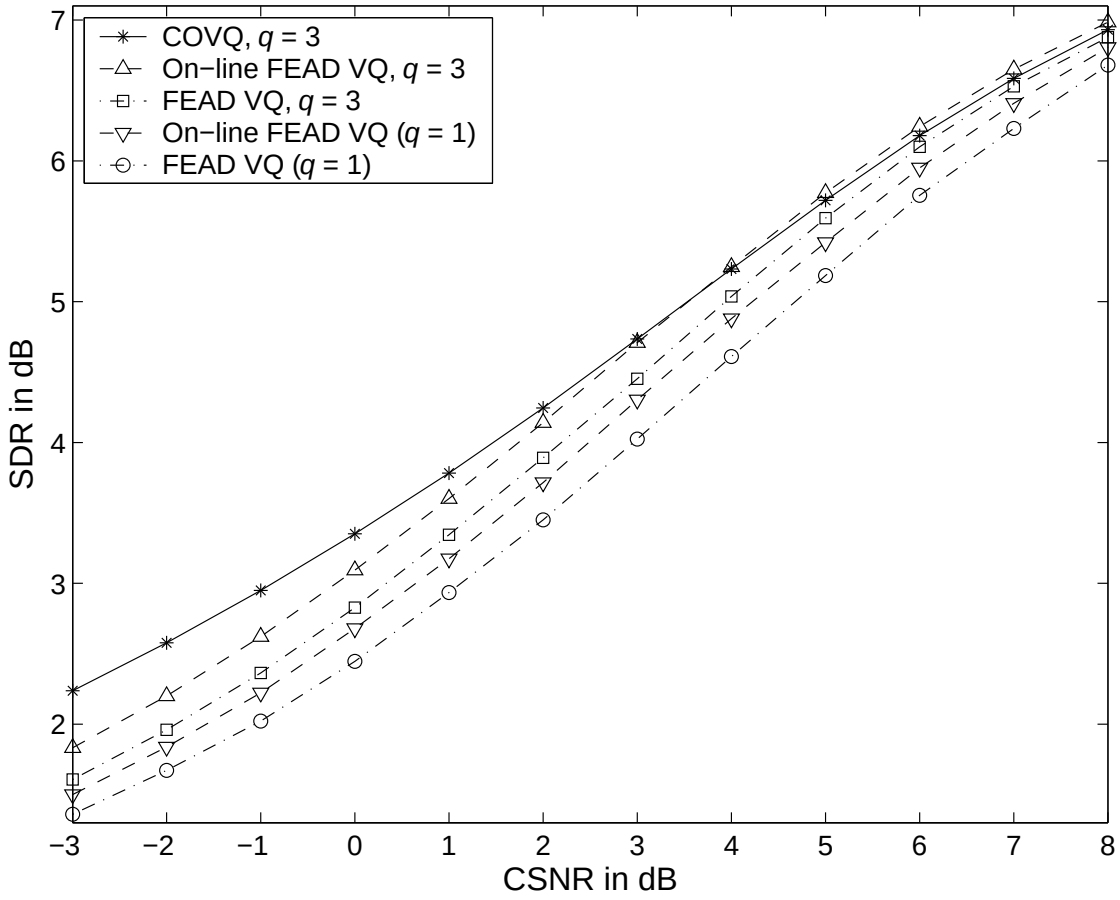

Figure 7.7: Comparison among the COVQ, FEAD VQ, and On-line FEAD VQ for a $\mathcal{N}(0,1)$ Gauss-Markov source vector quantized at rate $r = 1.0$ bps and hard decoded. Quantization dimension is $k = 2$, $K = 2$, and $L = 1$.

Chapter 8

Summary

In this thesis, we studied the analysis of the error rates of coded SISO channels and uncoded MIMO channels with both uniform and non-uniform sources. We also designed a soft-decision decoding COVQ for the transmission of analog sources over MIMO channels. The contributions of this thesis are summarized in the following.

- We presented an alternative derivation of the pairwise error probability of space-time codes of arbitrary structure under quasi-static fading. Our method, which is based on a moment generating function approach, is very simple and can be applied to many scenarios in single or multiple antenna systems. It can also be specialized to exploit the structure of certain codes to simplify the derivation, as was done in [176].

- We established upper and lower Bonferroni-type bounds on the block and bit error rates of single-antenna communication systems. The KAT lower bound was also studied. The AWGN as well as the block Rayleigh fading channels were considered.

We derived closed-form formulas for the pairwise error probability and also for the probability of the intersection of two pairwise error events. These quantities are required for the computation of the Bonferroni and KAT bounds. We also proposed to use a subset of the codebook and suggested a good initial set for the computation of the bounds for the case where the number of bits input to the channel coder is large (that is, for large k, where $r_c = k/n$ is the channel code rate). The bounds were often identical up to four significant digits for the AWGN channel.

- For MIMO channels with a uniform i.i.d. binary input, we considered the case where space-time orthogonal block coding is used and established tight Bonferroni-type upper and lower bounds on the symbol and bit error rates of the system. We derived the probability of the intersection of two pairwise error events in closed form. The bounds, which can be applied to any kind of signaling geometry and arbitrary symbol mapping, are often the same up to six significant digits. In the case of PSK signaling (with any size), the bounds are identical up to ten significant digits even at negative channel signal-to-noise ratios.

- We developed a new approach to derive the symbol pairwise error probability of space-time orthogonal block codes under MAP detection for non-uniform inputs. With the pairwise error probability in hand, we computed tight upper and lower bounds on the symbol and bit error rates of the system. It was shown that gains up to 10 dB can be obtained via MAP decoding and using symbol mappings better than Gray coding. Furthermore, we derived the optimal binary signaling scheme and demonstrated that very large gains exist in using this scheme instead of BPSK sig-

naling. Moreover, it was shown that MAP decoding can significantly outperform a typical tandem coding system which is much more complex. In fact, it was shown that MAP decoding is superior to tandem coding for the bit error rates of interest.

- In addition to MAP decoding, which is a form of joint source-channel coding, we considered the case where the input to the MIMO system is a continuous-alphabet (analog) signal. We designed a soft-decision decoding COVQ for robust compression and communication of the analog source. We also considered the case where the transmitter does not have the channel signal-to-noise ratio and designed two COVQs for the system one of which exploits the knowledge of the channel gains at the receiver to gain better performance. Comparisons with typical tandem systems were also presented and it was shown that the COVQ can not only outperform tandem systems, but also it can beat unequal error protection systems which use another approach to joint source-channel coding.

Bibliography

[1] M. Abramowitz and I. Stegun, *Handbook of Mathematical Functions with Formulas, Graphs, and Mathematical Tables*. New York, NY: Dover Publications, fifth ed., 1966.

[2] A. Abdi and M. Kaveh, "A space-time correlation model for multielement antenna systems in mobile fading channels," *IEEE J. Select. Areas Commun.*, vol. 20, pp. 550-560, Apr. 2002.

[3] R. K. Ahuja, T. L. Magnanti, and J. B. Orlin, *Network Flows.* Englewood Cliffs, NJ: Prentice Hall, 1993.

[4] F. Alajaji, S. A. Al-Semari, and P. Burlina, "Visual communication via trellis coding and transmission energy allocation," *IEEE Trans. Commun.*, vol. 47, pp. 1722-1728, Nov. 1999.

[5] F. Alajaji and T. Fuja, "A communication channel modeled on contagion," *IEEE Trans. Inform. Theory*, vol. 40, pp. 2035-2041, Nov. 1994.

[6] F. Alajaji and N. C. Phamdo, “Soft-decision COVQ for Rayleigh-fading channels,” *IEEE Commun. Let.*, vol. 2, pp. 162-164, June 1998.

[7] F. Alajaji, N. Phamdo, N. Farvardin, and T. Fuja, “Detection of binary Markov sources over channels with additive Markov noise,” *IEEE Trans. Inform. Theory*, vol. 42, pp. 230-239, Jan. 1996.

[8] F. Alajaji, N. Phamdo and T. Fuja, “Channel codes that exploit the residual redundancy in CELP-encoded speech,” *IEEE Trans. Speech Audio Processing*, vol. 4, pp. 325-336, Sept. 1996.

[9] S. M. Alamouti, “A simple transmit diversity technique for wireless communications,” *IEEE J. Select. Areas Commun.*, vol. 16, pp. 1451-1458, Oct. 1998.

[10] S. M. Alamouti, V. Tarokh, and P. Poon, “Trellis-coded modulation and transmit diversity: design criteria and performance evaluation,” in *Proc. IEEE Int’l Conf. Universal Personal Commun.*, Florence, Italy, Oct. 5-9, 1998, pp. 703-707.

[11] N. Al-Dhahir, “Overview and comparison of equalization schemes for space-time-coded signals with application to EDGE,” *IEEE Trans. Signal Processing*, vol. 50, pp. 2477-2488, Oct. 2002.

[12] N. Al-Dhahir, “A new high-rate differential space-time block coding scheme,” *IEEE Commun. Let.*, vol. 7, pp. 540-542, Nov. 2003.

[13] S. Al-Semari, F. Alajaji, and T. Fuja, “Sequence MAP decoding of trellis codes for Gaussian and Rayleigh channels,” *IEEE Trans. Veh. Technol.*, vol. 48, pp. 1130-1140, July 1999.

[14] E. Ayanoglu and R. M. Gray, “The design of joint source and channel trellis waveform coders,” *IEEE Trans. Inform. Theory*, vol. 33, pp. 855-865, Nov. 1987.

[15] I. Bahceci, and T. M. Duman, “Combined turbo coding and unitary space-time modulation,” *IEEE Trans. Commun.*, vol. 50, pp. 1244-1249, Aug. 2002.

[16] P. Balaban and J. Salz, “Optimum diversity combining and equalization in digital data transmission with application to cellular mobile radio,” *IEEE Trans. Veh. Technol.*, vol. 40, pp. 342-354, May. 1991.

[17] I. Barhumi, G. Leus, and M. Moonen, “Optimal training design for MIMO OFDM systems in mobile wireless channels,” *IEEE Trans. Signal Processing*, vol. 51, pp. 1615-1624, June 2003.

[18] S. Baro, G. Bauch, and A. Hansmann, “Improved codes for space-time trellis-coded modulation,” *IEEE Commun. Let.*, vol. 4, pp. 20-22, Jan. 2000.

[19] G. Bauch, J. Hagenauer, and N. Seshadri, “Turbo processing in transmit antenna diversity systems,” *Annals Telecommun.*, vol. 56, pp. 455-471, Aug. 2001.

[20] F. Behnamfar, F. Alajaji and T. Linder, “Progressive image communication over binary channels with additive bursty noise,” in *Proc. IEEE Data Compression Conf.*, Snowbird, UT, Apr. 2002.

[21] F. Behnamfar, F. Alajaji and T. Linder, “Image coding for binary bursty noise channels,” in *Proc. 21st Biennial Symp. Commun.*, Kingston, ON, June 2002.

[22] F. Behnamfar, F. Alajaji, and T. Linder, “Image transmission over the Polya channel via channel-optimized quantization,” *IEEE Trans. Signal Processing*, to appear.

[23] R. S. Blum, “Some analytical tools for the design of space-time convolutional codes,” *IEEE Trans. Commun.*, vol. 50, pp. 1593-1599, Oct. 2002.

[24] C. Budianu and L. Tong, “Channel estimation for space-time orthogonal block codes,” *IEEE Trans. Signal Processing*, vol. 50, pp. 2515-2528, Oct. 2002.

[25] Q. Chen and T. R. Fisher, “Image coding using robust quantization for noisy digital transmission,” *IEEE Trans. Image Processing*, vol. 7, pp. 496-505, Apr. 1998.

[26] M. Chiani, M. Z. Win, and A. Zanella, “On the capacity of spatially correlated MIMO Rayleigh-fading channels,” *IEEE Trans. Inform. Theory*, vol. 49, pp. 2363-2371, Oct. 2003.

[27] D. Chizhik, G. J. Foschini, M. J. Gans, and R. A. Valenzuela, “Keyholes, correlations, and capacities of multielement transmit and receive antennas,” *IEEE Trans. Wireless Commun.*, vol. 1, pp. 361-368, Apr. 2002.

[28] D. Chizhik, J. Ling, P. W. Wolniansky, R. A. Valenzuela, N. Costa, and K. Huber, “Multiple-input-multiple-output measurements and modeling in Manhattan,” *IEEE J. Select. Areas Commun.*, vol. 21, pp. 321-331, Apr. 2003.

[29] S.-Y. Chung, J. G. D. Forney, T. Richardson, and R. Urbanke, “On the design of low-density parity-check codes within 0.0045 dB of the Shannon limit,” *IEEE Commun. Lett.*, vol. 5, pp. 58-60, Feb. 2001.

[30] A. Cohen and N. Merhav, "Lower bounds on the error probability of block codes based on improvements on de Caen's inequality," *IEEE Trans. Inform. Theory*, vol. 50, pp. 290-310, Feb. 2004.

[31] T. M. Cover and J. A. Thomas, *Elements of Information Theory*. New York: Wiley, 1991.

[32] C. Cozzo and B. L. Hughes, "Joint channel estimation and data detection in space-time communications," *IEEE Trans. Commun.*, vol. 51, pp. 1266-1270, Aug. 2003.

[33] J. W. Craig, "A new, simple, and exact result for calculating the probability of error for two-dimensional signal constellations," in *Proc. IEEE Military Commun. Conf. (MilCom)*, McLean, VA, Nov. 1991, pp. 571-575.

[34] D. Cui and A. M. Haimovich, "A new bandwidth efficient antenna diversity scheme using turbo codes," in *Proc. 34th Annual Conf. Inform. Sci. Syst.*, Princeton, NJ, Mar. 2000, vol. 1, pp. 24-29.

[35] M. O. Damen, K. Abed-Meraim, and J. C. Belfiore, "Diagonal algebraic space-time block codes," *IEEE Trans. Inform. Theory*, vol. 48, pp. 628-636, Mar. 2002.

[36] M. O. Damen and N. C. Beaulieu, "On two high-rate algebraic space-time codes," *IEEE Trans. Inform. Theory*, vol. 49, pp. 1059-1063, Apr. 2003.

[37] M. O. Damen, A. Chkeif, and J. C. Belfiore, "Lattice code decoder for space-time codes," *IEEE Commun. Let.*, vol. 4, pp. 161-163, May 2000.

[38] M. O. Damen, H. El Gamal, and N. C. Beaulieu, "Linear threaded algebraic space-time constellations," *IEEE Trans. Inform. Theory*, vol. 49, pp. 2372-2388, Oct. 2003.

[39] D. de Caen, "A lower bound on the probability of a union," *Discr. Math.*, vol. 169, pp. 217-220, 1997.

[40] A. Dembo, unpublished notes, communicated by I. Sason, 2000.

[41] A. Dogandzic, "Chernoff bounds on pairwise error probabilities of space-time codes," *IEEE Trans. Inform. Theory*, vol. 49, pp. 1327-1336, May 2003.

[42] T. G. Donnelly, "Bivariate normal distribution," *Commun. ACM*, vol. 16, pp. 636, 1973, Algorithm 462.

[43] J. G. Dunham and R. M. Gray, "Joint source and noisy channel encoding," *IEEE Trans. Inform. Theory*, vol. 27, pp. 516-519, July 1981.

[44] H. El Gamal and M. O. Damen, "Universal space-time coding," *IEEE Trans. Inform. Theory*, vol. 49, pp. 1097-1119, May 2003.

[45] H. El Gamal and A. R. Hammons, "A new approach to layered space-time coding and signal processing," *IEEE Trans. Inform. Theory*, vol. 47, pp. 2321-2334, Sept. 2001.

[46] H. El Gamal and A. R. Hammons, "On the design and performance of algebraic space-time codes for BPSK and QPSK modulation," *IEEE Trans. Commun.*, vol. 50, pp. 907-913, June 2002.

[47] H. El Gamal and A. R. Hammons, “On the design of algebraic space-time codes for MIMO block-fading channels,” *IEEE Trans. Inform. Theory*, vol. 49, pp. 151-163, Jan. 2003.

[48] E. O. Elliott, “Estimates of error rates for codes on burst-noise channels,” *Bell Syst. Tech. J.*, vol. 42, pp. 1977-1997, Sept. 1963.

[49] N. Farvardin, “A study of vector quantization for noisy channels,” *IEEE Trans. Inform. Theory*, vol. 36, pp. 799-809, July 1990.

[50] N. Farvardin and V. Vaishampayan, “Optimal quantizer design for noisy channels: an approach to combined source-channel coding,” *IEEE Trans. Inform. Theory*, vol. 33, pp. 827-838, Nov. 1987.

[51] N. Farvardin and V. Vaishampayan, “On the performance and complexity of channel optimized vector quantizers,” *IEEE Trans. Inform. Theory*, vol. 37, pp. 155-160, Jan. 1991.

[52] T. Fazel and T. Fuja, “Robust transmission of MELP-compressed speech: an illustrative example of joint source-channel decoding,” *IEEE Trans. Commun.*, vol. 51, pp. 973-982, June 2003.

[53] G. Femenias, “BER performance of linear STBC from orthogonal designs over MIMO correlated Nakagami-m fading channels,” *IEEE Trans. Veh. Technol.*, vol. 53, pp. 307-317, Mar. 2004.

[54] T. Fine, “Properties of an optimal digital system and applications,” *IEEE Trans. Inform. Theory*, vol. 10, pp. 443-457, Oct. 1964.

[55] G. D. Forney, Jr., "Geometrically uniform codes," *IEEE Trans. Inform. Theory*, vol. 37, pp. 1241-1260, Sept. 1991.

[56] G. J. Foschini, "Layered space-time architecture for wireless communication over a fading environment when using multiple antennas," *Bell Labs Tech. J.*, vol. 1, pp. 41-59, Autumn 1996.

[57] G. J. Foschini and M. J. Gans, "On limits of wireless communications in a fading environment when using multiple antennas," *Wireless Pers. Commun.*, vol. 6, pp. 311-335, Mar. 1998.

[58] G. J. Foschini, G. D. Golden, R. A. Valenzuela, and P. W. Wolniansky, "Simplified processing for high spectral efficiency wireless communication employing multi-element arrays," *IEEE J. Select. Areas Commun.*, vol. 17, pp. 1841-1852, Nov. 1999.

[59] M. Fozunbal, S. W. McLaughlin, and R. W. Schafer, "On performance limits of space-time codes: a sphere-packing bound approach," *IEEE Trans. Inform. Theory*, vol. 49, pp. 2681-2687, Oct. 2003.

[60] S. Gadkari and K. Rose, "Robust vector quantizer design by noisy channel relaxation," *IEEE Trans. Commun.*, vol. 47, pp. 1113-1116, Aug. 1999.

[61] S. Gadkari and K. Rose, "Corrections to "robust vector quantizer design by noisy channel relaxation"," *IEEE Trans. Commun.*, vol. 48, pp. 176-176, Jan. 2000.

[62] J. Galambos and I. Simonelli, *Bonferroni-Type Inequalities with Appications.* New York: Springer-Verlag, 1996.

[63] R. G. Gallager, *Information Theory and Reliable Communication.* New York: Wiley, 1968.

[64] R. G. Gallager, "Claude E. Shannon: a retrospective on his life, work, and impact," *IEEE Trans. Inform. Theory*, vol. 47, pp. 2681-2695, Nov. 2001.

[65] D. Gesbert, H. Bolcskei, D. A. Gore, and A. J. Paulraj, "Outdoor MIMO wireless channels: models and performance prediction," *IEEE Trans. Commun.*, vol. 50, pp. 1926-1934, Dec. 2002.

[66] A. Gersho, and R. M. Gray, *Vector Quantization and signal compression*. Kluwer Academic Publishers, 1992.

[67] M. Gharavi-Alkhansari and A. B. Gershman, "Fast antenna subset selection in MIMO systems," *IEEE Trans. Signal Processing*, vol. 52, pp. 339-347, Feb. 2004.

[68] E. N. Gilbert, "Capacity of a burst-noise channel," *Bell Syst. Tech. J.*, vol. 39, pp. 1253-1265, Sept. 1960.

[69] A. Gorokhov, D. Gore, and A. J. Paulraj, "Receive antenna selection for MIMO flat-fading channels: theory and algorithms," *IEEE Trans. Inform. Theory*, vol. 49, pp. 2687-2696, Oct. 2003.

[70] L. Goulet and H. Leib, "Serially concatenated space-time codes with iterative decoding and performance limits of block-fading channels," *IEEE J. Select. Areas Commun.*, vol. 21, pp. 765-773, June 2003.

[71] I. Gradstein and I. Ryshik, *Tables of Integrals, Series, and Products*. San Diego, CA: Academic Press, fifth ed., 1994.

[72] A. Grant, "Rayleigh fading multiple-antenna channels," *EURASIP J. Applied Signal Processing*, vol. 2002, pp. 316-322, Mar. 2002.

[73] J. Grimm, M. P. Fitz, and J. V. Krogmeier, "Further results in space-time coding for Rayleigh fading," *IEEE Trans. Commun.*, vol. 51, pp. 1093-1101, July 2003.

[74] J. C. Guey, M. P. Fitz, M. R. Bell, and W. Y. Kuo, "Signal design for transmitter diversity wireless communication systems over Rayleigh fading channels," *IEEE Trans. Commun.*, vol. 47, pp. 527-537, Apr. 1999.

[75] A. Guyader, E. Fabre, C. Guillemot, and M. Robert, "Joint source-channel turbo decoding of entropy-coded sources," *IEEE J. Select. Areas Commun.*, vol. 19, pp. 1680-1696, Sept. 2001.

[76] J. Hagenauer, "Rate-compatible punctured convolutional codes (RCPC codes) and their applications," *IEEE Trans. Commun.*, vol. 36, pp. 389-400, Apr. 1988.

[77] A. R. Hammons and H. El Gamal, "On the theory of space-time codes for PSK modulation," *IEEE Trans. Inform. Theory*, vol. 46, pp. 524-542, Mar. 2000.

[78] B. Hassibi, "A fast square-root implementation for BLAST," in *Proc. 34th Asilomar Conf. Signals Syst. Computers*, Pacific Grove, CA, Oct.-Nov. 2000, pp. 1255-1259.

[79] B. Hassibi and B. M. Hochwald, "Cayley differential unitary space-time codes," *IEEE Trans. Inform. Theory*, vol. 48, pp. 1485-1503, June 2002.

[80] B. Hassibi and B. M. Hochwald, "High-rate codes that are linear in space and time," *IEEE Trans. Inform. Theory*, vol. 48, pp. 1804-1824, June 2002.

[81] B. Hassibi and M. Khorrami, "Fully-diverse multiple-antenna signal constellations and fixed-point-free Lie groups," *Proc. IEEE Int'l Symp. Inform. Theory*, Washington, DC, June 2001, p. 199.

[82] L. He and H. Ge, "A new full-rate full-diversity orthogonal space-time block coding scheme," *IEEE Commun. Let.*, vol. 7, pp. 590-592, Dec. 2003.

[83] R. W. Heath, Jr. and A. J. Paulraj, "Linear dispersion codes for MIMO systems based on frame theory," *IEEE Trans. Signal Processing*, vol. 50, pp. 2429-2441, Oct. 2002.

[84] H. Herzberg and G. Poltyrev, "The error probability of M-ary PSK block coded modulation schemes," *IEEE Trans. Commun.*, vol. 44, pp. 427-433, Apr. 1996.

[85] B. M. Hochwald and W. Sweldens, "Differential unitary space-time modulation," *IEEE Trans. Commun.*, vol. 48, pp. 2041-2052, Dec. 2000.

[86] B. M. Hochwald and T. L. Marzetta, "Unitary space-time modulation for multiple-antenna communications in Rayleigh flat fading," *IEEE Trans. Inform. Theory*, vol. 46, pp. 543-564, Mar. 2000.

[87] B. M. Hochwald, T. L. Marzetta, and B. Hassibi, "Space-time autocoding," *IEEE Trans. Inform. Theory*, vol. 48, pp. 2761-2781, Nov. 2001.

[88] B. M. Hochwald, T. L. Marzetta, T. J. Richardson, W. Sweldens, and R. Urbanke, "Systematic design of unitary space-time constellations," *IEEE Trans. Inform. Theory*, vol. 46, pp. 1962-1973, sept. 2000.

[89] B. L. Hughes, "Differential space-time modulation," *IEEE Trans. Inform. Theory*, vol. 46, pp. 2567-2578, Nov. 2000.

[90] B. L. Hughes, "Optimal space-time constellations from groups," *IEEE Trans. Inform. Theory*, vol. 49, pp. 401-410, Feb. 2003.

[91] D. Hunter, "An upper bound for the probability of a union," *J. Appl. Probab.*, vol. 13, pp. 597-603, 1976.

[92] W. J. Hwang, F. J. Lin, and C. T. Lin, "Fuzzy channel-optimized vector quantization," *IEEE Commun. Let.*, vol. 4, pp. 408-410, Dec. 2000.

[93] T. M. Ivrlac, W. Utschick, and J. A. Nossek, "Fading Correlations in Wireless MIMO Communication Systems," *IEEE Trans. Wireless Commun.*, vol. 2, pp. 819-824, May 2003.

[94] H. Jafarkhani, P. Ligdas and N. Farvardin, "Adaptive rate allocation in a joint source/channel coding framework for wireless channels," in *Proc. IEEE Veh. Technol. Conf.,* Atlanta, GA, pp. 492-296, 1996.

[95] H. Jafarkhani and N. Seshadri, "Super-orthogonal space-time trellis codes," *IEEE Trans. Inform. Theory*, vol. 49, pp. 937-950, Apr. 2003.

[96] H. Jafarkhani and V. Tarokh, "Multiple transmit antenna differential detection from generalized orthogonal designs," *IEEE Trans. Inform. Theory*, vol. 47, pp. 2626-2631, Sept. 2001.

[97] J. Jaldén and B. Ottersten, "An exponential lower bound on the expected complexity of sphere decoding," in *Proc. IEEE Int. Conf. Acoustics, Speech and Signal Processing (ICASSP)*, Montreal, QC, May 2004.

[98] S. Jiang and R. Kohno, "A new space-time multiple trellis coded modulation scheme for flat fading channels," *Inst. Electron. Inf. Commun. Eng. (IEICE) Trans.*, vol. E87-A, pp. 640-647, Mar. 2004.

[99] Y. Jing and B. Hassibi, "Fully-diverse $Sp(2)$ code design," *Proc. IEEE Int'l Symp. Inform. Theory*, Yokohama, Japan, June-July 2003, p. 299.

[100] Y. Jing and B. Hassibi, "Unitary space-time modulation via Cayley transform," *IEEE Trans. Signal Processing*, vol. 51, pp. 2891-2904, Nov. 2003.

[101] R. Johannesson and K. Zigangirov, *Fundamentals of Convolutional Coding*. New York, NY: IEEE Press, 1999.

[102] J. P. Kermoal, L. Schumacher, K. I. Pedersen, P. E. Mogensen, and F. Frederiksen, "A stochastic MIMO radio channel model with experimental validation," *IEEE J. Select. Areas Commun.*, vol. 20, pp. 1211-1226, Aug. 2002.

[103] M. A. Khojastepour, A. Sabharwal, and B. Aazhang, "Improved achievable rates for user cooperation and relay channels," in *Proc. IEEE Int'l Symp. Inform. Theory (ISIT)*, Chicago, IL, June-July 2004.

[104] Y. J. Kim and H. S. Lee, "Generalized principal ratio combining for space-time codes in slowly fading channels," *IEEE Commun. Let.*, vol. 4, pp. 343-345, Nov. 2000.

[105] I. M. Kim and V. Tarokh, "Variable-rate space-time block codes in M-ary PSK systems," *IEEE J. Select. Areas Commun.*, vol. 21, pp. 362-373, Apr. 2003.

[106] P. Knagenhjelm and E. Agrell, "The Hadamard transform – a tool for index assignment," *IEEE Trans. Inform. Theory.*, vol. 42, pp. 1139-1151, July 1996.

[107] I. Korn, J. P. Fonseka, and S. Xing, "Optimal binary communication with nonequal probabilities," *IEEE Trans. Commun.*, vol. 51, pp. 1435-1438, Sept. 2003.

[108] E. G. Kounias, "Bounds on the probability of a union, with applications," *Ann. Math. Statist.*, vol. 39, pp. 2154-2158, 1968.

[109] H. Kuai, F. Alajaji, and G. Takahara, "A lower bound on the probability of a finite union of events," *Discr. Math.*, vol. 215, pp. 147-158, 2000.

[110] H. Kuai, F. Alajaji, and G. Takahara, "Tight error bounds for nonuniform signaling over AWGN channels," *IEEE Trans. Inform. Theory*, vol. 46, pp. 2712-2718, Nov. 2000.

[111] H. Kumazawa, M. Kasahara, and T. Namekawa, "A construction of vector quantizers for noisy channels," *Electronics Eng. in Japan*, vol. 67-B, pp. 39-47, Jan. 1984.

[112] B. C. Kuo, *Automatic Control Systems*. Englewood Cliffs, NJ: Prentice Hall, seventh ed., 1995.

[113] A. Kurtenbach and P. Wintz, "Quantizing for noisy channels," *IEEE Trans. Commun. Technol.*, vol. 17, pp. 291-302, Apr. 1969.

[114] J. N. Laneman, G. W. Wornell, and D. N. C. Tse, "An efficient protocol for realizing cooperative diversity in wireless networks," in *Proc. IEEE Int'l Symp. Inform. Theory (ISIT)*, Washington, DC, June 2001.

[115] E. G. Larsson, "Unitary nonuniform space-time constellations for the broadcast channel," *IEEE Commun. Let.*, vol. 7, pp. 21-23, Jan. 2003.

[116] L. H. C. Lee, *Convolutional Coding: Fundamentals and Applications*, Norwood: Artech House, Inc., 1997.

[117] G. Leus, W. Zhao, G. B. Giannakis, and H. Delic, "Space-time frequency-shift keying," *IEEE Trans. Commun.*, vol. 52, pp. 346-349, Mar. 2004.

[118] Y. Li, C. N. Georghiades, and G. Huang, "Transmit diversity over quasi-static fading channels using multiple antennas and random signal mapping," *IEEE Trans. Commun.*, vol. 51, pp. 1918-1926, Nov. 2003.

[119] Y. Li, J. H. Winter, and N. R. Sollenberger, "MIMO-OFDM for wireless communications: signal detection and enhanced channel estimation," *IEEE Trans. Commun.*, vol. 50, pp. 1471-1477, Sept. 2002.

[120] X. B. Liang, "A high-rate orthogonal space-time block code," *IEEE Commun. Let.*, vol. 7, pp. 222-223, May 2003.

[121] X. B. Liang, “Orthogonal designs with maximal rates,” *IEEE Trans. Inform. Theory*, vol. 49, pp. 2468-2503, Oct. 2003.

[122] M. Lienard, P. Degauque, J. Baudet, and D. Degardin, “Investigation on MIMO channels in subway tunnels,” *IEEE J. Select. Areas Commun.*, vol. 21, pp. 332-339, Apr. 2003.

[123] J. Lim and D. L. Neuhoff, “Joint and tandem source-channel coding with complexity and delay constraints,” *IEEE Trans. Commun.*, vol. 51, pp. 757-766, May 2003.

[124] X. Lin and R. S. Blum, “Improved space-time codes using serial concatenation,” *IEEE Commun. Let.*, vol. 4, pp. 221-223, July 2000.

[125] T. Linder, G. Lugosi, and K. Zeger, “Rates of convergence in the source coding theorem, in empirical quantizer design, and in universal lossy source coding,” *IEEE Trans. Inform. Theory*, vol. 40, pp. 1728-1740, Nov 1994.

[126] T. Linder, G. Lugosi, and K. Zeger, “Empirical quantizer design in the presence of source noise or channel noise,” *IEEE Trans. Inform. Theory*, vol. 43, pp. 612-623, Mar. 1997.

[127] Y. Liu, M. P. Fitz, and O. Y. Takeshita, “Full rate space-time turbo codes,” *IEEE J. Select. Areas Commun.*, vol. 19, pp. 969-980, May 2001.

[128] H. A. Loeliger, “Signal sets matched to groups,” *IEEE Trans. Inform. Theory*, vol. 37, pp. 1675-1682, Nov. 1991.

[129] A. Lozano and C. Papadias, “Layered space-time receivers for frequency-selective wireless channels,” *IEEE Trans. Commun.*, vol. 50, pp. 65-73, Jan. 2002.

[130] B. Lu and X. Wang, “Iterative receivers for multiuser space-time coding systems,” *IEEE J. Select. Areas Commun.*, vol. 18, pp. 2322-2335, Nov. 2000.

[131] H. F. Lu, Y. Wang, P. V. Kumar, and K. M. Chugg, “Remarks on space-time codes including a new lower bound and an improved code,” *IEEE Trans. Inform. Theory*, vol. 49, pp. 2752-2757, Oct. 2003.

[132] X. Ma and G. B. Giannakis, “Full-diversity full-rate complex-field space-time coding,” *IEEE Trans. Signal Processing*, vol. 51, pp. 2917-2930, Nov. 2003.

[133] A. Manikas and M. Sethi, “A space-time channel estimator and single-user receiver for code-reuse DS-CDMA systems,” *IEEE Trans. Signal Processing*, vol. 51, pp. 39-51, Jan. 2003.

[134] T. L. Marzetta and B. M. Hochwald, “Capacity of a mobile multiple-antenna communication link in Rayleigh flat fading,” *IEEE Trans. Inform. Theory*, vol. 45, pp. 139-157, Jan. 1999.

[135] J. L. Massey, “Joint source and channel coding,” in *Commun. Syst. and random process theory*, pp. 279-293, The Netherlands: Noordhoff, 1978.

[136] D. Miller and K. Rose, “Combined source-channel vector quantization using deterministic annealing,” *IEEE Trans. Commun.*, vol. 42, pp. 347-356, Feb./Mar./Apr. 1994.

[137] A. F. Molisch, "A generic model for MIMO wireless propagation channels in macro- and microcells," *IEEE Trans. Signal Processing*, vol. 52, pp. 61-71, Jan. 2004.

[138] A. L. Moustakas, S. H. Simon, and A. M. Sengupta, "MIMO capacity through correlated channels in the presence of correlated interferers and noise: a (not so) large N analysis," *IEEE Trans. Inform. Theory*, vol. 49, pp. 2545-2561, Oct. 2003.

[139] S. H. Muller-Weinfurtner, "Coding approaches for multiple antenna transmission in fast fading and OFDM," *IEEE Trans. Signal Processing*, vol. 50, pp. 2442-2450, Oct. 2002.

[140] A. Naguib, N. Seshadri, and A. Calderbank, "Increasing data rate over wireless channels," *IEEE Signal Processing Magazine*, vol. 46, pp. 76-92, May 2000.

[141] B. K. Ng and E. S. Sousa, "On bandwidth-efficient multiuser-space-time signal design and detection," *IEEE J. Select. Areas Commun.*, vol. 20, pp. 320-329, Feb. 2002.

[142] A. Nosratinia, J. Lu, and B. Aazhang, "Source-channel rate allocation for progressive transmission of images," *IEEE Trans. Commun.*, vol. 51, pp. 186-196, Feb. 2003.

[143] H. Nyquist, "Certain topics in telegraph transmission theory," *Trans. AIEE*, vol. 47, p. 617, 1928.

[144] O. Oyman, R. U. Nabar, H. Bolcskei, and A. J. Paulraj, "Characterizing the statistical properties of mutual information in MIMO channels," *IEEE Trans. Signal Processing*, vol. 51, pp. 2784-2795, Nov. 2003.

[145] B. D. Pettijohn, M. W. Hoffman, and K. Sayood, "Joint source/channel coding using arithmetic codes," *IEEE Trans. Commun.*, vol. 49, pp. 826-836, May 2001.

[146] N. Phamdo and F. Alajaji, "Soft-decision demodulation design for COVQ over white, colored, and ISI Gaussian channels," *IEEE Trans. Commun.*, vol. 48, pp. 1499-1506, Sept. 2000.

[147] N. Phamdo, F. Alajaji, and N. Farvardin, "Quantization of memoryless and Gauss-Markov sources over binary Markov channels," *IEEE Trans. Commun.*, vol. 45, pp. 668-675, June 1997.

[148] N. Phamdo and N. Farvardin, "Optimal detection of discrete Markov sources over discrete memoryless channels - Applications to combined source-channel coding," *IEEE Trans. Inform. Theory*, vol. 40, pp. 186-193, Jan. 1994.

[149] G. Poltyrev, "Bounds on the decoding error probability of binary linear codes via their spectra," *IEEE Trans. Inform. Theory*, vol. 40, pp. 1284-1292, July 1994.

[150] J. G. Proakis, *Digital Communications*. New York: McGraw-Hill, 4th ed., 2001.

[151] T. J. Richardson, M. A. Shokrollahi, and R. L. Urbanke, "Design of capacity-approaching irregular low-density parity-check codes," *IEEE Trans. Inform. Theory*, vol. 47, pp. 619-637, Feb. 2001.

[152] A. Said and W. A. Pearlman, "A new, fast and efficient image codec based on set partitioning in hierarchical trees," *IEEE Trans. Circuits Syst. Video Technol.*, vol. 6, pp. 243-250, June 1996.

[153] D. Samardzija and N. Mandayam, "Pilot-assisted estimation of MIMO fading channel response and achievable data rates," *IEEE Trans. Signal Processing*, vol. 51, pp. 2882-2890, Nov. 2003.

[154] K. Sayood and J. C. Borkenhagen, "Use of residual redundancy in the design of joint source/channel coders," *IEEE Trans. Commun.*, vol. 39, pp. 838-846, June 1991.

[155] C. Schlegel and A. Grant, "Differential space-time turbo codes," *IEEE Trans. Inform. Theory*, vol. 49, pp. 2298-2306, Sept. 2003.

[156] G. Séguin, "A lower bound on the error probability for signals in white Gaussian noise," *IEEE Trans. Inform. Theory*, vol. 44, pp. 3168-3175, Nov. 1998.

[157] M. Sellathurai and S. Haykin, "Turbo-BLAST for wireless communications: theory and experiments," *IEEE Trans. Signal Processing*, vol. 50, pp. 2538-2546, Oct. 2002.

[158] A. Sendonaris, E. Erkip, and B. Aazhang, "Increasing uplink capacity via user cooperation diversity," in *Proc. IEEE Int'l Symp. Inform. Theory (ISIT)*, Camberidge, MA, Aug. 1998.

[159] M. Shafi and P. J. Smith, "On a Gaussian approximation to the capacity of wireless MIMO systems," in *Proc. IEEE Int'l Conf. Commun.*, New York, NY, Apr.-May 2002, pp. 406-410.

[160] C. E. Shannon, "A mathematical theory of communication (Part 1)," *Bell Syst. Tech. J.*, vol. 27, pp. 379-423, 1948.

[161] C. E. Shannon, “A mathematical theory of communication (Part 2),” *Bell Syst. Tech. J.*, vol. 27, pp. 623-656, 1948.

[162] C. E. Shannon, “Communication in the presence of noise,” in *Proc. IRE*, vol. 37, pp. 10-21, 1949.

[163] C. E. Shannon, “Coding theorems for a discrete source with a fidelity criterion,” in *IRE Nat. Conv. Rec.*, pp. 142-163, 1959.

[164] C. E. Shannon, “Probability of error for optimal codes in a Gaussian channel,” *Bell Syst. Tech. J.*, vol. 38, pp. 611-656, May 1959.

[165] P. G. Sherwood and K. Zeger, “Error protection for progressive image transmission over memoryless and fading channels,” *IEEE Trans. Commun.*, vol. 46, pp. 1555-1559, Dec. 1998.

[166] H. Shin and J. H. Lee, “Performance analysis of space-time block codes over keyhole Nakagami-m fading channels,” *IEEE Trans. Veh. Technol.*, vol. 53, pp. 351-362, Mar. 2004.

[167] H. Shin and J. H. Lee, “Exact symbol error probability of orthogonal space-time block codes,” *Proc. IEEE Global Telecom. Conf.*, Taipei, Taiwan, Nov. 2002, vol. 2, pp. 1197-1201.

[168] H. Shin and J. H. Lee, “Capacity of multiple-antenna fading channels: spatial fading correlation, double scattering, and keyhole,” *IEEE Trans. Inform. Theory*, vol. 49, pp. 2636-2647, Oct. 2003.

[169] D. S. Shiu, G .J. Foschini, M. J. Gans, and J. M. Kahn, "Fading correlation and its effect on the capacity of multielement antenna systems," *IEEE Trans. Commun.*, vol. 48, pp. 502-513, Mar. 2000.

[170] A. Shokrollahi, "Computing the performance of unitary space-time group codes from their character table," *IEEE Trans. Inform. Theory*, vol. 48, pp. 1355-1371, June 2002.

[171] A. Shokrollahi, B. Hassibi, B. M. Hochwald, and W. Sweldens, "Representation theory for high-rate multiple-antenna code design," *IEEE Trans. Inform. Theory*, vol. 47, pp. 2335-2367, Sept. 2001.

[172] M. A. Shokrollahi, "Design of unitary space-time codes from representations of $SU(2)$," in *Proc. IEEE Int'l Symp. Inform. Theory*, Washington, DC, May 2001, p. 241.

[173] M. K. Simon, "Evaluation of the average bit error probability for space-time coding based on a simpler exact evaluation of pairwise error probabillity," *J. Commun. Net.*, vol. 3, pp. 257-264, Sept. 2001.

[174] M. K. Simon, "A simpler form of the Craig representation for the two-dimensional joint Gaussian Q-Function," *IEEE Commun. Let.*, vol. 6, pp. 49-51, Feb. 2002.

[175] M. K. Simon and M. S. Alouini, *Digital Communications over Fading Channels: a Unified Approach.* New York, NY: John Wiley, 2000.

[176] M. K. Simon and H. Jafarkhani, "Performance evaluation of super-orthogonal space-time trellis codes using a moment generating function-based approach," *IEEE Trans. Signal Processing*, vol. 51, pp. 2739-2751, Nov. 2003.

[177] M. Skoglund, "A soft decoder vector quantizer for a Rayleigh fading channel-Application to image transmission," in *Proc. IEEE Int. Conf. Acoustics, Speech and Signal Processing (ICASSP)*, pp. 2507-2510, May 1995.

[178] M. Skoglund, "Soft decoding for vector quantization over noisy channels with memory," *IEEE Trans. Inform. Theory*, vol. 45, pp. 1293-1307, May 1999.

[179] M. Skoglund and P. Hedelin, "Hadamard-based soft decoding for vector quantization over noisy channels," *IEEE Trans. Inform. Theory*, vol. 45, pp. 515-532, Mar. 1999.

[180] M. Skoglund, N. Phamdo, and F. Alajaji, "Design and performance of VQ-based hybrid digital-analog joint source-channel codes," *IEEE Trans. Inform. Theory*, vol. 48, pp. 708-720, Mar. 2002.

[181] F. K. Soong and B. H. Juang, "Line spectrum pair (LSP) and speech data compression," in *Proc. IEEE Int'l Conf. Acoustics, Speech, and Signal Processing*, 1984, pp. 1.10.1-1.10.4.

[182] B. Srinivas, R. Ladner, M. Azizoğlu and E. Riskin, "Progressive transmission of images using MAP detection over channels with memory," *IEEE Trans. Image Processing*, vol. 8, pp. 462-475, Apr. 1999.

[183] A. Stefanov and T. M. Duman, "Turbo-coded modulation for systems with transmit and receive antenna diversity over block fading channels: system model, decoding

approaches, and practical considerations," *IEEE J. Select. Areas Commun.*, vol. 19, pp. 958-968, May 2001.

[184] H. J. Su and E. Geraniotis, "Space-time turbo codes with full antenna diversity," *IEEE Trans. Commun.*, vol. 49, pp. 47-57, Jan. 2001.

[185] W. Su and X. G. Xia, "Two generalized complex orthogonal space-time block codes of rates 7/11 and 3/5 for 5 and 6 transmit antennas," *IEEE Trans. Inform. Theory*, vol. 49, pp. 313-316, Jan. 2003.

[186] G. Takahara, F. Alajaji, N. C. Beaulieu, and H. Kuai, "Constellation mappings for two-dimensional signaling of nonuniform sources," *IEEE Trans. Commun.*, vol. 51, pp. 400-408, Mar. 2003.

[187] N. Tanabe and N. Farvardin, "Subband image coding using entropy-coded quantization over noisy channels," *IEEE J. Select. Areas Commun.*, vol. 10, pp. 926-943, June 1992.

[188] M. Tao and R. S. Cheng, "Trellis-coded differential unitary space-time modulation over flat fading channels," *IEEE Trans. Commun.*, vol. 51, pp. 587-596, Apr. 2003.

[189] M. Tao and R. S. Cheng, "Improved design criteria and new trellis codes for space-time coded modulation in slow flat fading channels," *IEEE Commun. Let.*, vol. 5, pp. 313-315, July 2001.

[190] G. Taricco and E. Biglieri, "Exact pairwise error probability of space-time codes," *IEEE Trans. Inform. Theory*, vol. 48, pp. 510-513, Feb. 2002.

[191] V. Tarokh and H. Jafarkhani, "A differential detection scheme for transmit diversity," *IEEE J. Select. Areas Commun.*, vol. 18, pp. 1169-1174, July 2000.

[192] V. Tarokh, H. Jafarkhani, and A. R. Calderbank, "Space-time block codes from orthogonal designs," *IEEE Trans. Inform. Theory*, vol. 45, pp. 1456-1467, July 1999.

[193] V. Tarokh and T. K. Y. Lo, "Principal ratio combining for fixed wireless applications when transmitter diversity is employed," *IEEE Commun. Let.*, vol. 2, pp. 223-225, Aug. 1998.

[194] V. Tarokh, N. Seshadri, and A. R. Calderbank, "Space-time codes for high data rate wireless communication: performance criterion and code construction," *IEEE Trans. Inform. Theory*, vol. 44, pp. 744-765, Mar. 1998.

[195] V. Tarokh, N. Seshadri, and A. R. Calderbank, "Combined array processing and space-time coding," *IEEE Trans. Inform. Theory*, vol. 45, pp. 1121-1128, May 1999.

[196] E. Telatar, "Capacity of multi-antenna Gaussian channels," *European Trans. Telecom.*, vol. 10, pp. 585-595, Nov.-Dec. 1999.

[197] M. Uysal, "Effect of shadowing on the performance of space-time trellis codes," *IEEE Trans. Wireless Commun.*, to appear.

[198] M. Uysal, "Pairwise error probability of space-time codes in Rician-Nakagami channels," *IEEE Commun. Let.*, vol. 8, pp. 132-134, Mar. 2004.

[199] M. Uysal and C. N. Georghiades, "Error performance analysis of space-time codes over Rayleigh fading channels," *J. Commun. Networks*, vol. 2, pp. 351-356, Dec. 2000.

[200] V. Vaishampayan, "Combined source-channel coding for bandlimited waveform channels," Ph.D. Thesis, University of Maryland, College Park, MD, 1989.

[201] V. Vaishampayan and N. Farvardin, "Joint design of block source codes and modulation signal sets," *IEEE Trans. Inform. Theory*, vol. 36, pp. 1230-1248, July 1992.

[202] E. Viterbo and J. Boutros, "A universal lattice code decoder for fading channel," *IEEE Trans. Inform. Theory*, vol. 45, pp. 1639-1642, July 1999.

[203] U. Wachsmann, J. Thielecke, and H. Schotten, "Capacity-achieving coding for MIMO channels: multi-stratum space-time coding," *IEEE Veh. Technol. Conf.*, Rhodes, Greece, May 2001, vol. 1, pp. 199-203.

[204] X. Wang and H. V. Poor, "Space-time multiuser detection in multipath CDMA channels," *IEEE Trans. Signal Processing*, vol. 47, pp. 2356-2374, Sept. 1999.

[205] S. Wicker, *Error Control Systems for Digital Communication and Storage.* Prentice Hall, 1995.

[206] J. H. Winters, "On the capacity of radio communication systems with diversity in Rayleigh fading environment," *IEEE J. Select. Areas Commun.*, vol. 5, pp. 871-878, June 1987.

[207] J. H. Winters, "The diversity gain of transmit diversity in wireless systems with Rayleigh fading," *IEEE Trans. Veh. Technol.*, vol. 47, pp. 119-123, Feb. 1998.

[208] J. H. Winters, J. Salz, and R. D. Gitlin, "The impact of antenna diversity on the capacity of wireless communication systems," *IEEE Trans. Commun.*, vol. 42, pp. 1740-1751, Feb.-Apr. 1994.

[209] A. Wittneben, "A new bandwidth efficient transmit antenna modulation diversity scheme for linear digital modulation," *Proc. IEEE Int'l Conf. Commun.*, vol. 3, pp. 1630-1634, May 1993.

[210] W. Xu, J. Hagenauer and J. Hollmann, "Joint source-channel coding using the residual redundancy in compressed images," in *Proc. IEEE Int'l COnf. Commun.*, Dallas, TX., June 1996.

[211] S. Yousefi, "Bounds on the performance of maximum-likelihood decoded binary block codes in AWGN interference," Ph.D. Dissertation, Department of Electrical and Computer Engineering, University of Waterloo, Ontario, Canada.

[212] K. Zeger and A. Gersho, "Pseudo-Gray coding," *IEEE Trans. Commun.*, vol. 38, pp. 2147-2158, Dec. 1990.

[213] K. Zeger and V. Manzella "Asymptotic bounds on optimal noisy channel quantization via random coding," *IEEE Trans. Inform. Theory*, vol. 40, pp. 1926-1938, Nov. 1994.

[214] K. Zeger, J. Vaisey, and A. Gersho, "Globally optimal vector quantizer design by stochastic relaxation," *IEEE Trans. Signal Processing*, vol. 40, pp. 310-322, Feb. 1992.

[215] L. Zheng and D. N. C. Tse, "Communication on the Grassmann manifold: a geometric approach to the noncoherent multiple-antenna channel," *IEEE Trans. Inform. Theory*, vol. 48, pp. 359-383, Feb. 2002.

[216] Y. Zhong, F. Alajaji, and L. Campbell, "When is joint source-channel coding worthwhile: an information theoretic perspective," in *Proc. 22nd Biennial Symp. Commun.*, Kingston, ON, June 2004.

[217] L. Zhong, F. Alajaji, and G. Takahara, "Error analysis for nonuniform signaling over Rayleigh fading channels," *IEEE Trans. Commun.*, accepted.

[218] S. Zhou and G. B. Giannakis, "Optimal transmitter eigen-beamforming and space-time block coding based on channel mean feadback," *IEEE Trans. Signal Processing*, vol. 50, pp. 2599-2613, Oct. 2002.

[219] S. Zhou and G. B. Giannakis, "Space-time coding with maximum diversity gains over frequency-selective fading channels," *IEEE Signal Processing Let.*, vol. 8, pp. 269-272, Oct. 2001.

[220] G. C. Zhu and F. Alajaji, "Turbo codes for nonuniform memoryless sources over noisy channels," *IEEE Commun. Let.*, vol. 6, pp. 64-66, Feb. 2002.

[221] G.-C. Zhu, F. Alajaji, J. Bajcsy and P. Mitran, “Transmission of non-uniform memoryless sources via non-systematic turbo codes,” *IEEE Trans. Commun.*, vol. 52, Aug. 2004.

[222] X. Zhu and R. D. Murch, “Performance analysis of maximum likelihood detection in a MIMO antenna system,” *IEEE Trans. Commun.*, vol. 50, pp. 187-191, Feb. 2002.

[223] S. A. Zummo and S. A. Al-Semari, “A tight bound on the error probability of space-time codes for rapid fading channels,” *Proc. IEEE Wireless Commun. Networking Conf.*, Chicago, IL, Sept. 2000, vol. 3, pp. 1086-1089.